International
Progress Report

IPR-05-41

Äspö Hard Rock Laboratory

Petrographic and mineral-chemical evaluation of the distribution and conditions of alterations around deformation zones in granitic bedrock, Äspö HRL, Sweden

Sadoon Morad
Ala Aldahan

Uppsala University

October 2005

Svensk Kärnbränslehantering AB
Swedish Nuclear Fuel
and Waste Management Co
Box 5864
SE-102 40 Stockholm Sweden
Tel 08-459 84 00
+46 8 459 84 00
Fax 08-661 57 19
+46 8 661 57 19

Äspö Hard Rock
Laboratory

Report no.
IPR-05-41

No.
F48K

Author
Sadoon Morad
Ala Aldahan

Date
October 2005

Checked by
Carljohan Hardenby

Date
2009-09-16

Approved
Mats Ohlsson

Date
2009-10-15

Äspö Hard Rock Laboratory

Petrographic and mineral-chemical evaluation of the distribution and conditions of alterations around deformation zones in granitic bedrock, Äspö HRL, Sweden

Sadoon Morad
Ala Aldahan

Uppsala University

October 2005

Keywords: KAS09, KAS14, Petrographic, Minerals, Mineral-chemical, Alterations, Deformation zones, Granitic bedrock

Abstract

Unravelling the types, degree and relative timing of mineral alterations about deformation zones in crystalline basement rocks is of profound importance for: (i) elucidation of fluid flow and pressure-temperature histories prevailed during uplift and cooling of the bedrock, and (ii) modelling physical and chemical properties, and hence of the suitability of bedrocks for the disposal of spent nuclear fuel.

This study of two drill cores (KAS09 and KAS14) from the ca 1800 Ma old granitic bedrock at Äspö Hard Rock Laboratory, SE Sweden aimed to unravel: (i) the spatial and temporal distribution of mineral alterations in dominantly seemingly un-deformed samples collected at various distances from major and minor, brittle deformation zones, and (ii) the physical and chemical conditions during major alteration episodes. Various analytical methods have been used, including core observations, petrographic examinations (optical as well as secondary and backscattered electron imaging), mineral-chemical analyses using an electron microprobe, stable isotopes, and equilibrium thermodynamic methods.

The mineral alterations include mainly extensive plagioclase saussuritisation, replacement of plagioclase by K-feldspar, and replacement of biotite by chloritic and illitic clays. The alteration processes, which are interpreted to have occurred at < 350ºC and conducted by hydrothermal fluids that circulated in the basement, have resulted in concomitant formation of Al-rich titanite, epidote, calcite, pumpellyite, prehnite, and iron oxides. The mineral alterations are most common in fractured rocks, but occur also in smaller amounts in the seemingly unaltered rocks. The distribution patterns are thus not systematic in the whole core length in relation to the main deformation zones, but are, instead, rather strongly controlled by the presence of local fracture zones of various dimensions. Thus, the distribution pattern of mineral alteration reflects mainly the complex deformation and related fracture-formation and fluid flow histories.

Sammanfattning

Kartläggning av mineralomvandlingar kring deformationszoner i kristallin berggrund är av stor betydelse: (i) för förståelse av fluidrörelse och tryck-temperatur förhållanden under uplyftning och nedkylning, och (ii) för att kunna modellera fysikaliska och kemiska egenskaper av bergrunden, med avseende på lämplighet som förvaringsplats för använt kärnbränsle.

Denna studie på två borrkärnor (KAS09 och KAS14) från den ca 1800 miljoner år gamla berggrunden i Äspö Hard Rock Laboratory, sydöstra Sverige syftar till att klargöra: (i) fördelningen av mineral omvandlingar i tid och rum i till synes icke omvandlade bergarter kring spröda deformationszoner, och (ii) de fysikaliska och kemiska förhållandena som rådde under bildningen av mineralassociationerna. Metoderna som använts för att beskriva borrkärnorna inkluderar: petrografiska (inklusive elektron mikroskopering), mineralkemiska (elektronmikrosond) samt analys av stabila isotoper i kalcit. Stabilitetsdiagram för relevanta faser har tagits till hjälp för att studera mineraljämvikterna.

Mineral omvandlingen omfattar främst saussuritisering av plagioklas (d v s omvandling till albit, epidot och sericit), bildning av K-fältspat och albit på bekostnad av plagioklas, samt omvandling av biotit till klorit. Vår tolkning är att omvandlingarna har skett vid temperaturer som är lägre än 350ºC under påverkan av cirkulerande hydrotermala lösningar. Omvandlingarna har resulterat i bildning av Al-rik titanit, epidot, kalcit, pumpellyit, prehnit och Fe-oxider. Mineralomvandling och mineralbildning är mest omfattande i sprickor, men förekommer även i tillsynes icke omvandlade/spruckna bergarter. Det finns dock ingen systematisk fördelning av nybildning och omvandling av mineral i förhållande till huvudsprickzonerna i berggrunden, vilket tyder på ett komplext cirkulationsmönster av hydrotermala lösningar, som är sin tur kan relateras till en komplex historia av deformation och sprickbildning.

Contents

1 Introduction

The physical and chemical properties of crystalline rocks are strongly influenced by the extent and distribution pattern of fractures, fracture mineralisation, and degree of mineral alteration in the host rock. Rock alteration occurs owing to reactions at mineral-fluid interface that result in mineral dissolution and/or precipitation, and hence records the history of fluid flow in the rocks. Fractures are structures that vary widely in length (< 1 mm to 100's of km) and develop at any depths within the uppermost 10 km (T < ca 300ºC; P < ca 4 kb) of the Earth's crust by forces that induce brittle deformation of the bedrock. Bedrock fracturing is usually recursive (but not continuous over geological times) owing to changes in local and regional direction and intensity of stress regimes with time. Forces that induce fracturing to bedrocks include plate motion, loading and unloading of the crust (e.g., during glacier advance and retreat and during erosion of overburden rocks), emplacement of magmas, changes in temperature and humidity, increase in fluid pressure, and impact by asteroids.

Fractures in crystalline bedrock act as the major conduits for fluid flow, and hence are major zones of mass and heat flux and healing/sealing by precipitation of wide variety of secondary minerals. Conversely, granite matrix permeability is poorly developed, and hence has little bearing on fluid flow. However, mass flux and related mineral alteration occur also along grain boundaries as well as along twinning, cleavage and dislocation planes (cf. Johansson et al., 1998). The presence of microscopic fluid-inclusion trails in minerals of granite has been suggested to witness large and durable fluid percolation pathways (Cathelineau et al., 1994). The presence of water films within micro-pores and micro-fractures in individual mineral and rock matrix are also of decisive importance for rock mechanical stability (e.g., Holl et al., 1997).

Repeated fracturing, fluid flow, and mineralogical/geochemical modification of the bedrock occur along old and newly formed rupture planes. Therefore, the resulting mineral alteration and dissolution reactions encountered in the rock usually have complex paragenetic relationships (O'Reilly et al., 1977; Parry, 1998; Zulauf et al., 1999; Morad and Aldahan, 2002). Alteration reactions in crystalline basements may occur during various episodes of fluid circulation, prior to, during and subsequent to tectonic deformation of the bedrock, as well as during weathering (Morad and Aldahan, 2002).

Fluids that circulate in crystalline basement rocks have various origins, chemical compositions and temperatures, including hydrothermal, metamorphic, sedimentary and meteoric waters. High-temperature, fluids include those expelled from magma during migration to shallow depths and during crystallization and heating of meteoric and marine waters that have descended to magmatic regimes. Metamorphic fluids, which have high temperatures, are released mainly from dehydration reactions during prograde metamorphism of mudstones to amphibolites facies. Low-temperature (< 100ºC) fluids in crystalline basement include surface waters (marine, meteoric and brackish) that often aid rock weathering and formation of secondary minerals at shallow depths (< ca 3 km).

The type and extent of secondary mineralisation in the fracture zone and in the host-rocks are controlled by temperature, pressure, fluid/rock ratio, chemical composition of the fluids, organic matter and bacterial activities, width of the main deformation zone, and by the mineralogical composition of the host rocks. Careful mineralogical and geochemical studies of the spatial and temporal distribution of mineral alteration can shed light on the timing, pattern of fluid circulation as well on the chemical and physical conditions encountered during the history of bedrock deformation and fluid flow. Unravelling these mineralogical modifications play a significant role in determining the chemical and mechanical stability of deformed bedrock (Kirby and Kronenberg, 1987; Janecke and Evans, 1988; Wintsch et al., 1995), including anticipated changes in the retention properties (Landström et al., 2001), and hence suitability for disposal of spent nuclear fuels.

Petrographic and geochemical studies of mineral-alteration reactions in crystalline basement, which commonly induce considerable modifications to the primary mineralogical composition as well as the porosity-permeability of granitic bedrock, are, therefore, considered to be important pre-requisite step for the selection of suitable sites for the disposal of spent nuclear fuel (Eliasson, 1993).

2 Aims of study

This report aims at highlighting the types, extent, and distribution patterns of hydrothermal mineral alterations in fractured and seemingly unaltered rocks located at various distances from major and minor, brittle deformation zones in two drill cores (KAS09 and KAS14) obtained from Proterozoic crystalline basement of the Äspö Hard Rock Laboratory (Äspö HRL), SE Sweden (Figure 2-1). Additionally, the secondary-mineral assemblages are used to unravel the conditions encountered during cooling and fracturing of the rocks. For these purposes, core samples were collected at various distances from such deformation zones that are up to 30 m wide. Data obtained in this study compliment to data obtained from an earlier, twin study performed on four drill cores from this area (Morad and Aldahan, 2002).

Earlier work dealing with the propagation of mineral alteration has focused on major reactions and mainly in the immediate vicinity (i.e., distances of centimetres) of fracture zones (Eliasson, 1993; Banwart et al., 1994). However, Morad and Aldahan (2002) performed detailed modal and mineral-chemical analyses of minor and major alteration reactions, and not merely of primary minerals and of a few major alteration features. Drill core KAS09 was included in a similar study by Morad and Aldahan (2002). The previously obtained data from four boreholes were used in order to further highlight the conditions encountered during various stages of mineral paragenesis based on detailed petrographic as well as on chemical further analyses of various chemical as well as carbon, oxygen and strontium isotopic analyses of secondary minerals.

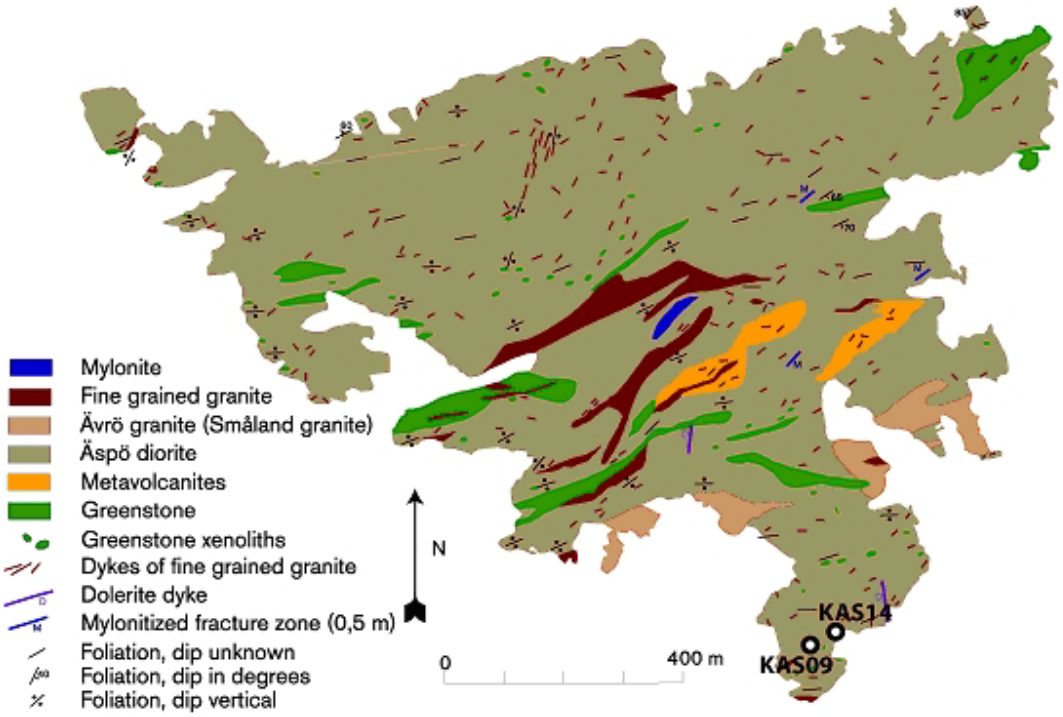

Figure 2-1. *Location and bedrock map of the Äspö HRL (Rhén et al., 1997; Stanfors et al., 1997).*

3 Geological setting

The Äspö Hard Rock Laboratory (HRL), which was selected in 1986 by the Swedish Nuclear Fuel and Waste Management Company (SKB) with the aim of establishing a natural analogue scale test laboratory for nuclear waste disposal activities, is located on the island of Äspö on the Baltic east cost of Sweden (Figure 2-1). The construction of the laboratory, which included excavation and tunnelling, has been accompanied by a large variety of geotechnical and engineering drilling activities, which resulted in huge amount of research results that cover a wide front of knowledge (e.g., Markström and Erlström, 1996). These operations targeted bedrock and related structures and were particularly designed to generate information of importance to the evaluation of natural habitat of the bedrock and expected man made impact.

Geologically, the Äspö bedrock comprises greyish to reddish grey granitic to quartz monzodioritic rocks (Figure2-1) as well as dikes, sills and lenses of fine-grained (aplitic) granites, dolerites and mylonites of the Precambrian basement of south-eastern Sweden, (Kornfält and Wikman, 1988; Wikman and Kornfält, 1995; Stanfors et al., 1999). The whole suite of igneous rocks in Äspö represents part of the Trans-Scandinavian Igneous Belt (TSIB) that has been evolved about 1850-1400 Ma and was episodically rejuvenated by intrusive bodies dating as early as 1000 Ma (Stanfors et al., 1999). The Äspö bedrock has been affected by structural deformation events encountered during the Gothian (≈ 1500-1400 Ma), Sveconorwegain (≈ 1000-900 Ma) and Caledonian (≈ 400 Ma) orogenies, and more recently during glacio-tectonic activity. These processes have resulted in a complex suit of ductile and brittle deformation, which have affected almost all rock types on the island (for more details see, e.g., Stanfors, 1996; Munier, 1993; Milnes et al., 1998; Stanfors et al., 1999). Among the prominent tectonic features are mylonitic, NE-SW deformation belts (up to 100 m wide). These features and other less extensive fracture zones (up to 50 m wide) form orthogonal geometry with dips varying from vertical to sub-horizontal (Munier, 1993).

4 Sampling sites and analytical methods

The investigated boreholes KAS09 and KAS14 were drilled from the surface and aimed to provide details about steeply dipping fracture zones trending EW-NE (Table 4-1; Figure 4-1), in particular NE-1 in the tunnel. The main lithology penetrated by KAS09 is the Äspö diorite with occurrence of some fine-grained granite. Fracture density fluctuates between zero and more than 40 per metre. Sealed fractures are common in most parts of the section, but a major fracture zone is encountered at a cored length of about 128-147 m and we have sampled within and outside this fracture zone. For details of the lithological section, see Sehlstedt et al. (1990). A total of 190 samples, which are strongly dominated by seemingly unaltered rocks, have been collected from the two drill cores (KAS09 and KAS14).

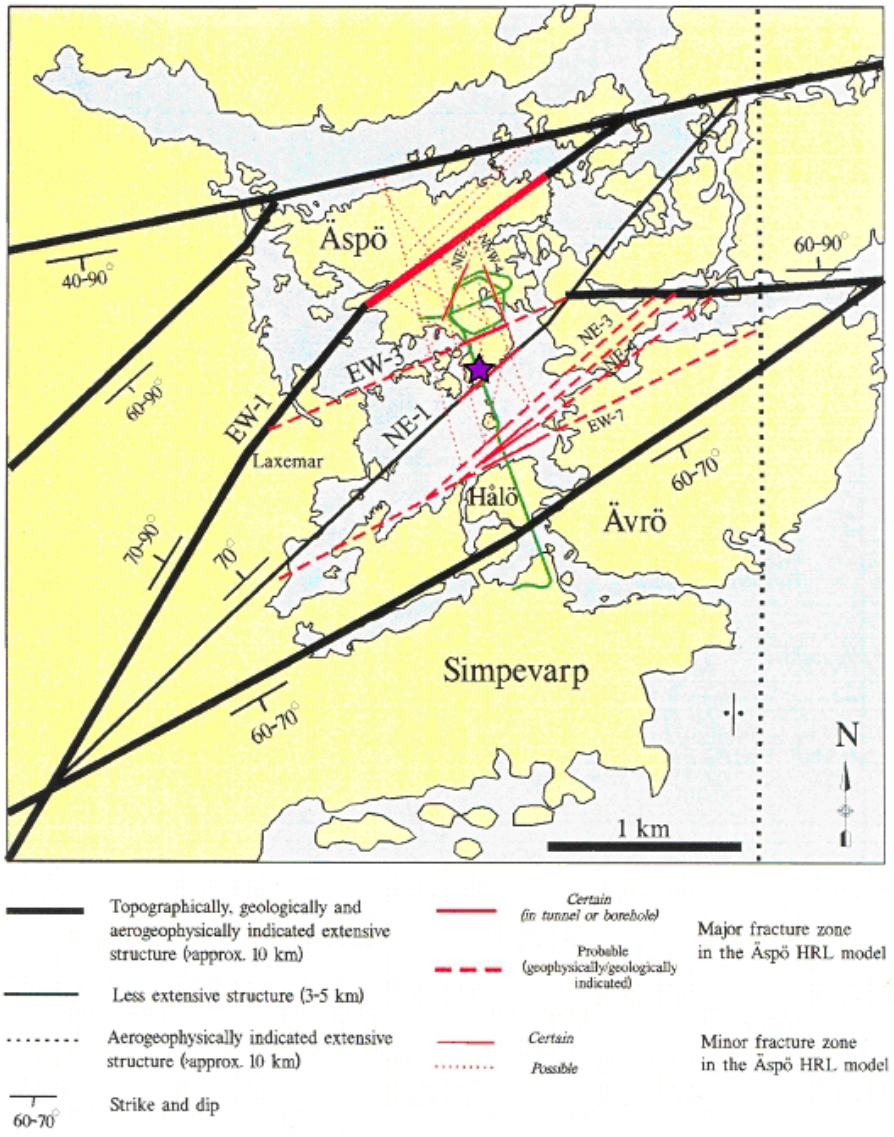

Figure 4-1. *Map showing major deformation and fracture zones in the vicinity of the Äspö HRL (Rhén et al., 1997; Stanfors et al., 1997).Star indicates location of the bore holes sampled for the purpose of this study.*

Table 4-1. Technical and geological details of the investigated boreholes.

KAS09	
Location (local system)	X = 6925.190, Y = 2091.110, Z = 4.080
Initial azimuth	dir = 169°, inclination (from horizontal) = 60°
Borehole length	450 m
Rock types %	82% ÄD, 14% FG, 2% GS, 1% M
Number of fractures	2869
Fracture density /metre	6.3
Major fracture	
Deformation zones	100-110 m, 128-147 m (NE-1), 249-255 m, 391-420 m
KAS14	
Location (local system)	X = 6948.540, Y = 2138.800, Z = 3.700
Initial azimuth	dir = 137°, inclination (from horizontal) = 60°
Borehole length	212 m
Rock types %	75% ÄD, 18% FG, 6% SG, 1% GS
Number of fractures	1638
Fracture density /meter	7.7
Major fracture	
(deformation) zones	51-57 m, 81-89 m, 98-129 (NE-1), 154-166 m, 183-202 m

ÄD= Äspö diorite, FG= Fine-grained granite, GS=Greenstone, SG= Småland granite and M= Mylonite/Cataclasite

Data from Sehlstedt et al. (1990), Carlsten (1990), Stanfors et al. (1997)

Thin sections were prepared for all samples and subjected to modal mineralogical compositions were obtained by counting 400 points in each thin section. Crystal habits and paragenetic relationships were examined in 61 small gold-coated chips, using a JEOL JSM-T330 scanning electron microscope (SEM) with an acceleration voltage of 10 kV. The chemical composition of minerals was determined in polished, carbon-coated thin sections using a Cameca Camebax BX50 microprobe equipped with three spectrometers and a back-scattered electron detector (BSE). Operating conditions were: 20 kV acceleration voltage, 8 nA (for carbonates) to 12 nA (for silicates) measured beam current, and a 1 μm beam diametre. Standards and count times were: wollastonite (Ca, 10 seconds), orthoclase (K, 5 s), albite (Na, Si, 5 and 10 s, respectively), corundum (Al, 20 s), MgO (Mg, 10 s), $MnTiO_3$ (Mn, 10 s) and haematite (Fe, 10 s). Precision of analyses was better than 0.1 mole%, and the detection limit was 50 ppm. Representative analyses of mineral phases are tabulated in the appendices.

For the purpose of carbon and oxygen isotope analyses of calcite, 15 calcite-containing samples were reacted with 100% phosphoric acid at 25°C for 4 hour. The evolved gas was analysed using a SIRA-12 mass spectrometer. The phosphoric acid fractionation factor used was 1.01025 (Friedman & O'Neil, 1977). Carbon and oxygen isotope data are presented in the normal δ notation relative to V-PDB and V-SMOW. Precision (1 σ) was monitored through daily analysis of the NBS-20 calcite standard and was better than ± 0.05‰ for both $\delta^{13}C$ and $\delta^{18}O$. Due to the common presence of more than one generation of calcite, the isotopic values should be considered as average for bulk calcite in the sample. The same, calcite samples were subjected to strontium isotope analyses. For this purpose, the samples were reacted with dilute acetic acid, and analysed using an automated Finnigan 261 mass-spectrometer equipped with 9 Faraday collectors. All analyses were performed in the static multi-collector mode using Re filaments. Correction for isotope fractionation during the analyses was made by normalisation to $^{86}Sr/^{88}Sr = 0.1194$. The mean standard error of mass spectrometer performance was ±0.00003 for NBS-987.

5 Petrology of bedrock

The mineralogical modal analyses of core samples from KAS09 and KAS14 (appendix 5-1 and 5-2) show that the present-day composition (Figures 5-1A and 5-1B) is considerably poorer in plagioclase, which was subjected to extensive sassuritisation and/or albitisation, compared to the original, magmatic composition (Figure 5-2A and 5-2B). The original composition is based on texture and occurrence habit of the minerals which are quite different from the secondary (hydrothermal) minerals. However, both the original and present-day composition indicates that the studied rocks are dominantly syenogranite, monzogranite to granodiorite. The primary magmatic minerals include plagioclase, K-feldspar, quartz, biotite, amphibole, muscovite, titanite, epidote, magnetite, and trace amounts of zircon, apatite, and monazite. Mineral abundances provided are given in volume%. The petrographic and mineral-chemical characteristics of primary and secondary minerals encountered in both borehole samples have been outlined by Morad and Aldahan (2002), but additional data and new insights into the data base are included in the descriptions below.

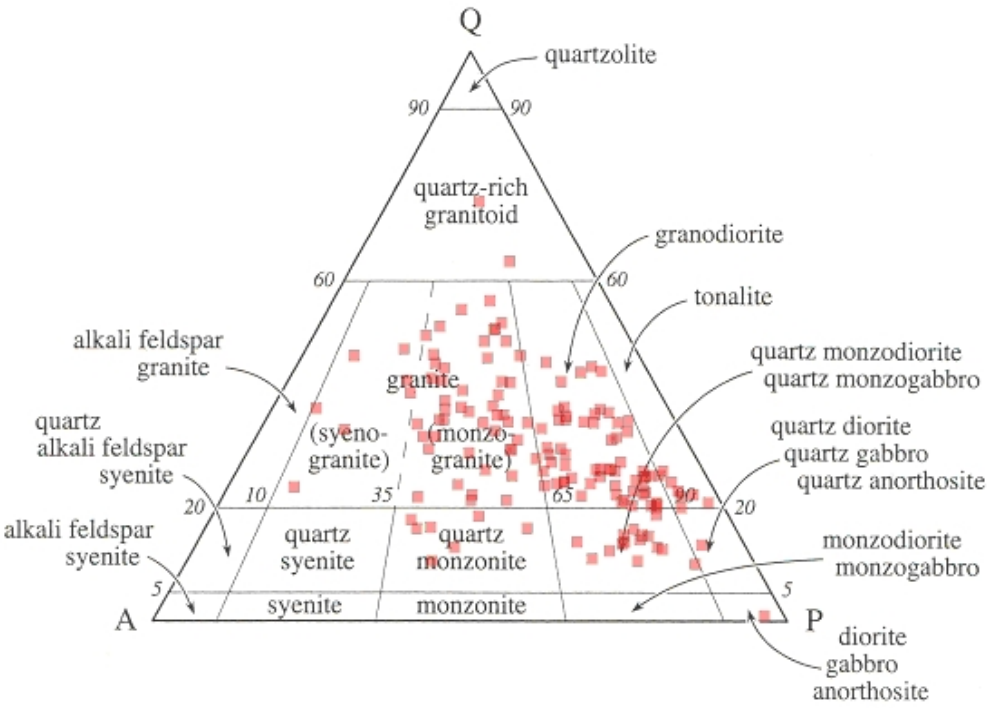

Figure 5-1. A.

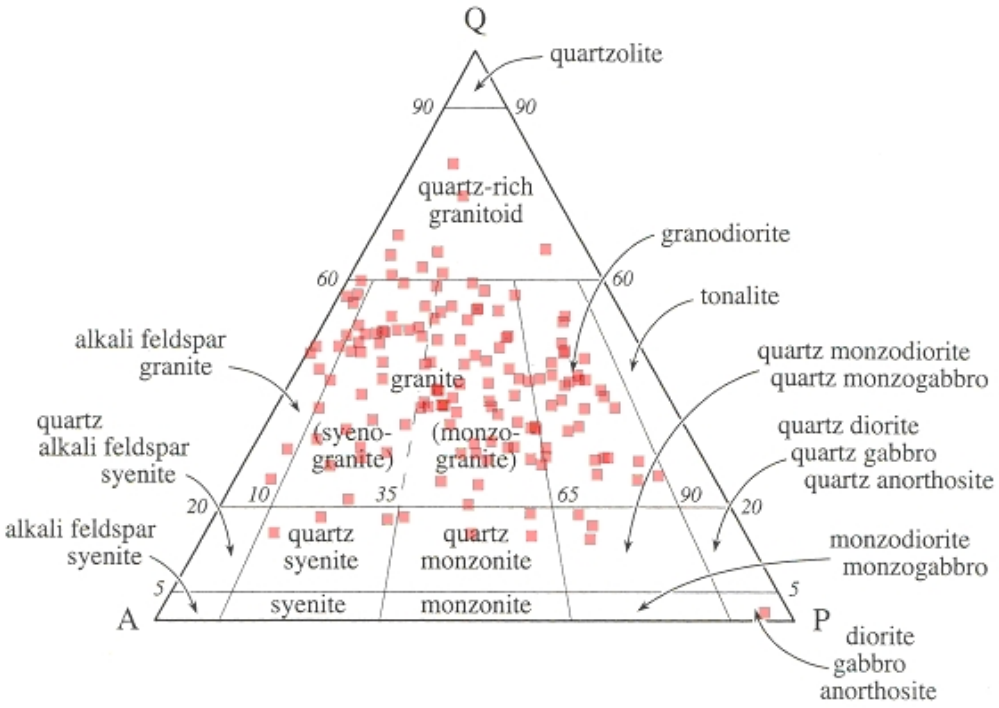

Figure 5-1. B.

Figure 5-1 A and B. *Present-day modal composition of the studied rocks from boreholes KAS09 and KAS14, respectively, obtained by counting 400 points in each thin section (IUGS, 1973 classification).*

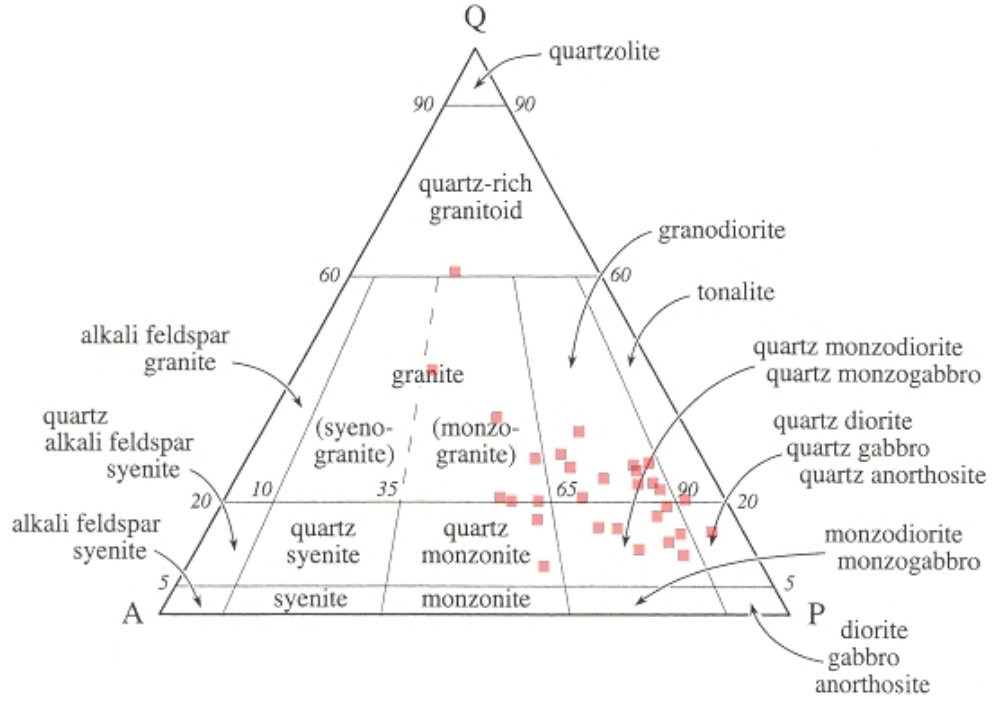

Figure 5-2. A.

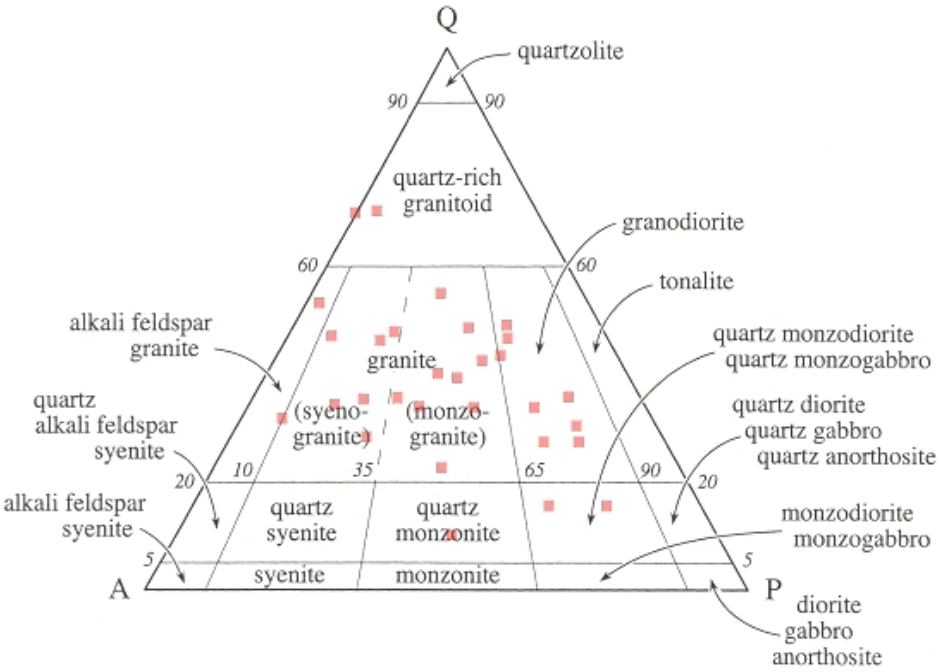

***Figure 5-2. B**.*

***Figure 5-2 A and B.** Original modal composition of the studied rocks from boreholes KAS09 and KAS14, respectively, obtained by counting 400 points in each thin section (IUGS, 1973 Classification).*

5.1 Magmatic minerals: petrography and mineral chemistry

Feldspars: Magmatic feldspars include plagioclase and K-feldspar. The K-feldspar occurs mainly as microcline perthite, which varies in abundance from 1.4-51% (appendix 5-1 and 5-2). Microcline is mainly fresh but, in some cases, contains dissolution voids filled with secondary minerals, including calcite and silicates, such as chlorite. Plagioclase crystals show evidence of pervasive saussuritisation (i.e., replacement by sericite, albite and epidote; Figure 5-3) or merely albitisation (± illitisation). Fresh plagioclase crystals are either untwinned or display albite twinning. The twinning planes of saussuritised and albitised plagioclase are dislocated in samples that are occur in the vicinity of the deformation zones (Figure 5-3). Typically, the merely albitised plagioclase crystals have indistinct or no twinning planes and riddled with Fe-oxides pigment (Figure 5-3). In some cases, the plagioclase is replaced by illite (Figure 5-3). Albitisation is most pervasive in plagioclase crystals containing micro-fractures formed by brittle deformation. The total amounts of saussuritised and albitised plagioclase vary between trace and 50 %, whereas the amounts of fresh plagioclase vary from trace to 44% (appendix 5-1 and 5-2).

Electron microprobe analysis of plagioclase crystals was difficult because most crystals are replaced to various extents by albite and/or K-feldspar. However, analyses aided by backscattered electron imaging revealed that the amounts of CaO in plagioclase vary between 4.2% and 7.4% (An = 20 and 36 mole %), whereas albite replacing plagioclase has a nearly pure, end-member composition (Ab > 98 mole%; appendix 5-3). The average composition of plagioclase crystal is $An_{25}Ab_{74}Or_1$. The average chemical composition of magmatic K-feldspar is $Or_{92}Ab_8An_0$.

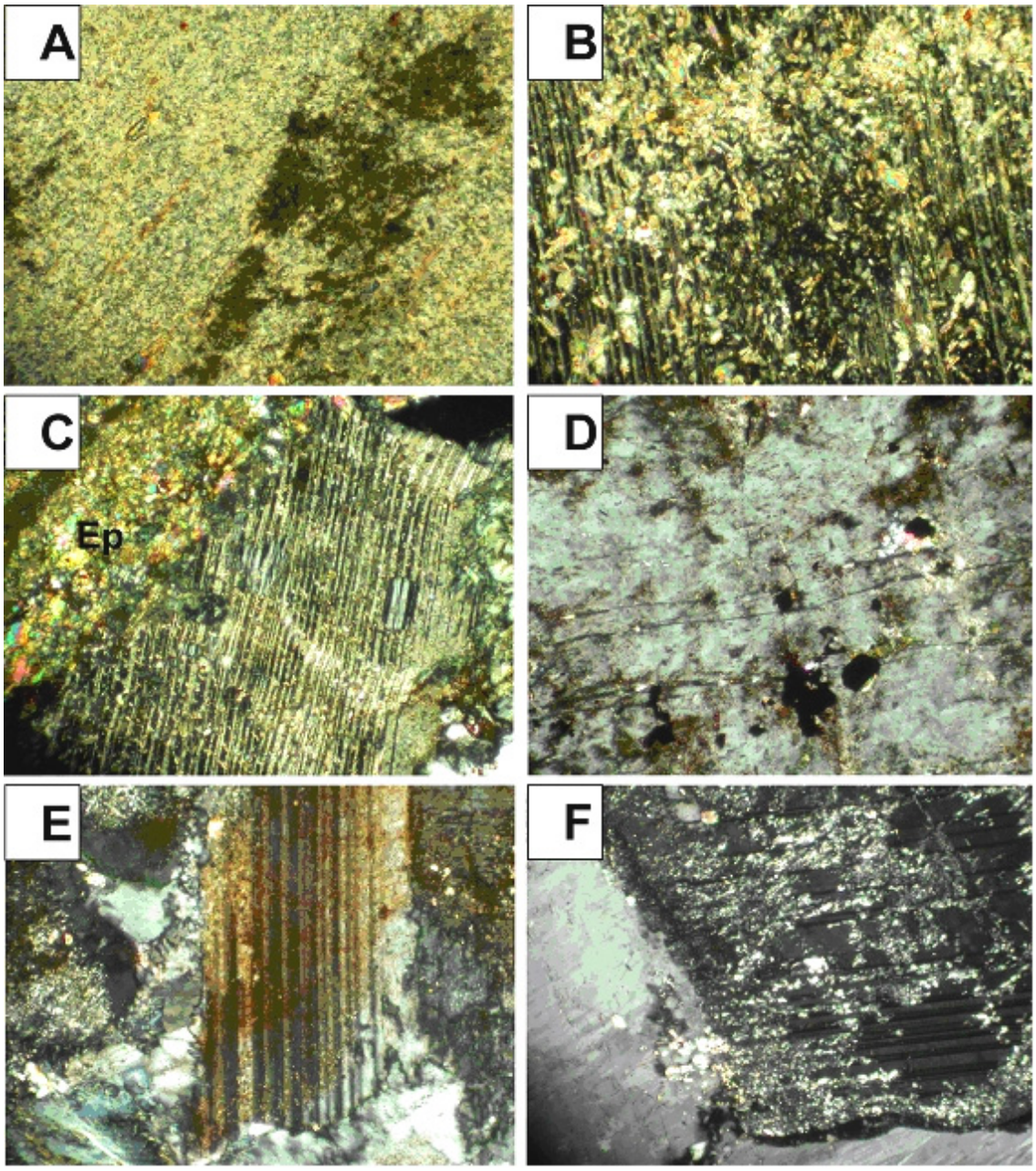

Figure 5-3. *Optical micrographs (X-nicols) showing saussuritised (i.e., replaced by albite, sericite and epidote) and albitised plagioclase. .Note that the twinning planes in the albitised plagioclase in figure* ***C*** *are bent due to deformation. In some cases, the twinning planes in albitised plagioclase are totally destroyed (Figure* ***D****). The albitised crystals are often riddled with tiny Fe-oxide pigment (Figure* ***E****). The merely albitised plagioclase often contains illite (Figure* ***F****) rather than sericite. Illite is finer crystalline than sericite but has similar chemical composition.*

Quartz. This mineral varies widely in crystal size and in abundance (0.5 to 54%). Most of the quartz crystals display straight to slightly undulous extinction, except in the vicinity of major deformation zones where quartz displays strong undulous extinction (cf. Morad and Aldahan, 2002).

Biotite: Biotite, which varies widely in the studied rock (trace to 34%), shows pleochroism from nearly colourless to yellowish brown to olive green, occurs mainly as large crystals (< 3 mm). The biotite crystals are unaltered or partly to extensively (trace to 18%) or completely chloritised (trace to 16%). The amount of chloritised biotite increases in the vicinity of minor and major fracture zones. Chloritised biotite is riddled with inclusions of secondary epidote and titanite and rarely pseudo-hexagonal crystals of hematite. Biotite is also replaced by mixed-layer illite/vermiculite. Chemically, the biotite is a Fe-Mg rich variety **(**Figure 5-4**)** characterized by moderate Fe/(Fe-Mg) ratio, extremely low (ca 0.01) to non-detectable amounts of Na, Ca and Ba, and relatively elevated amounts of Ti (TiO2 = 1.5-2.3%; 0.17-0.27 atoms per formula unit). Tetrahedral and octahedral Al range in abundance from 2.35 to 2.44 and from 0.15 to 0.28 atoms per formula unit, respectively (appendix 5-4).

Biotite is devoid of chemical zoning, shows little variation in composition among the samples collected from the two drill cores or within the same core, and has the following average formula: $K_{1.94}Na_{0.01}(Fe_{2.3}Mg_{3.1}Al_{0.3}Ti_{0.2})(Al_{2.4}Si_{5.6})O_{20}(OH)_4$. As biotite in most of the studied samples displays slight to pervasive alteration into chlorite and trioctahedral smectite/vermiculite, the chemical compositions obtained may have been contaminated by these secondary minerals, when occurring in sub-microscopic sizes. The amounts of interlayer K is usually less than ideal 2.0 in most of the biotite crystals owing to the sub-microscopic scale of chloritisation. Analyses encountering chloritised biotite are also characterised by elevated amounts of Al, whereas biotite partly replaced by illite/vermiculite has lower K, Fe and Mg but higher Si than unaltered biotite.

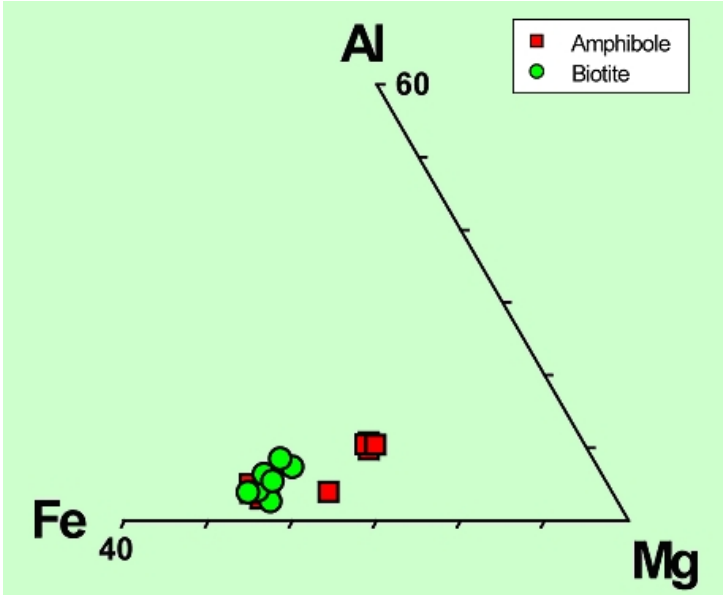

Figure 5-4. *Chemical composition (Al-Mg-Fe^{2+} triangular plot) of biotite and amphibole in the Äspö granitic basement rocks showing Fe-Mg rich composition; some of the analysed biotite and many of the amphiboles are more enriched in Fe. Data are based on this study and from Morad and Aldahan (2002).*

Muscovite: This mineral, which is rare (average < 1%) or absent in the majority of the studied samples, is < 100µm, colourless to slightly pleochroic from colourless to pale blue or bluish green. Electron microprobe analyses of muscovite (appendix 5-5) revealed a composition, which is typical for magmatic muscovite, i.e. the presence of low amounts of Mg (0.26-0.42 atoms per formula unit) and Fe (0.39-0.42 atoms per formula unit), and is hence only slightly phengitic in composition **(**Figure 5-5**)**. Tetrahedral and octahedral Al range in abundance from 1.66 to 1.74 and from 3.24 to 3.33 respectively. The interlayer sites are dominated by K (1.75-1.82 atoms per formula unit), whereas Na (i.e. paragonite solid solution) is low (< 0.1 atom). The average formula of muscovite is $K_{1.8}Na_{0.1}(Fe_{0.4}Mg_{0.3}Al_{3.3}Ti_{0.04})(Al_{1.7}Si_{6.3})\ O_{20}(OH)_4$).

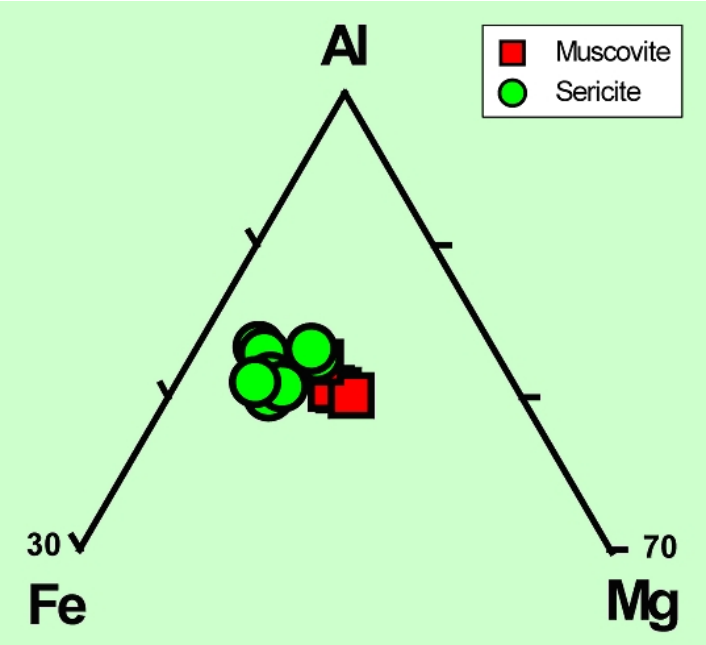

Figure 5-5. *Chemical composition (Al-Mg-Fe^{3+} triangular plot) of muscovite and sericite in the Äspö granitic basement rocks showing that the sericite contains more Fe, and are hence have more phengitic composition, than muscovite. Data are based on this study and from Morad and Aldahan (2002).*

Amphibole: This mineral occurs as prismatic crystals with two distinct types of optical habits one of which with pleochroism from nearly colourless to pale-green and another from pale green to dark-green colours. Amphibole is common in most of the samples, particularly in the dioritic rock, which contain up to 22%. Amphibole varies widely in crystal size (ca 200 µm to 2 mm), and is overall fresh or shows replacement by chlorite and mixed-layer chlorite/smectite (cf. Morad and Aldahan, 2002). Chemically, there are two varieties of amphibole (Figure 5-4, Figure 5-6, Figure 5-7; appendix 5-4):

- Type1 is a pale-green coloured variety that is enriched in Si (av. 7.7 atoms per formula unit), Mg (av. 3.1 atoms per formula unit) and, to a certain extent, in Na (av. 0.5 atoms per formula unit), but poorer in Al (av. total is 0.7 atoms per formula unit) and Fe (av. 1.2 atoms per formula unit), and has only trace amounts of Ti.

- Type2 is a dark-green coloured variety that is enriched in Al (total up to 1.4 atoms per formula unit), Fe (up to 2.1 atoms per formula unit), Ti (av. Ca 0.18 atoms per formula unit), and K (up to 0.2 atoms per formula unit).

The Mn content is fairly low in both amphibole types, being somewhat higher in Type2 (up to 0.06 atoms per formula unit) than in Type1 (< 0.03 atoms per formula unit). Differences in the chemical parameters and the correlation between inter-related elements are displayed in Figure 5-6. These plots reveal that Ti is positively correlated with Al, whereas there is a negative correlation, and hence considerable replacement, between (Na+K) ↔ Ca, Fe ↔ Mg and Na ↔ K. Plot of Mg/(Mg+Fe^{2+}) versus Si reveals that type 1 is actinolite whereas type 2 is magnesiohornblende (Figure 5-7).

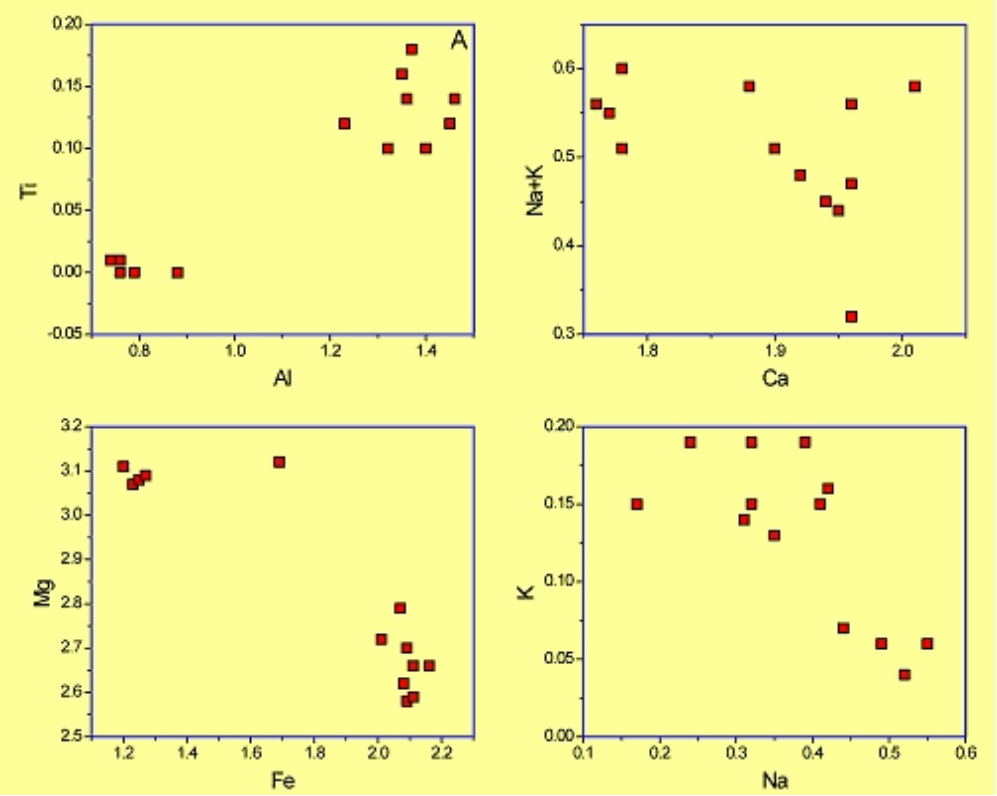

Figure 5-6. *Plots of several chemical parameters in amphiboles analysed showing that Ti has a positive correlation with Al (i.e., no replacement among them), whereas there is negative correlation between (Na+K) ↔ Ca, Fe ↔ Mg and Na ↔ K, and hence considerable replacement among these elements. Data are based on this study and from Morad and Aldahan (2002).*

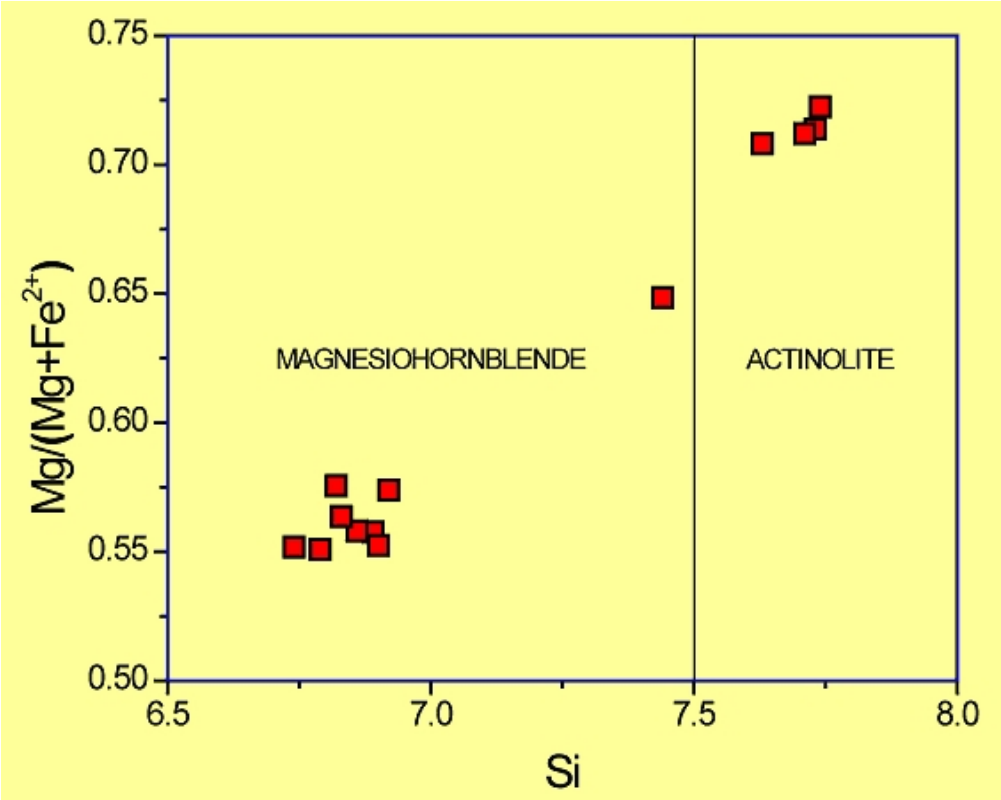

Figure 5-7. *Plot of Mg/(Mg+Fe^{2+}) versus Si analysed revealing that the amphiboles are actinolite and magnesiohornblende. Data are based on this study and from Morad and Aldahan (2002).*

The amphiboles show non-detectable or trace amounts of Ba and Sr. The average chemical formula of Type2 amphibole (actinolite) is $(Ca_{1.95}Na_{0.3}K_{0.3})(Fe_{2.0}Mg_{2.6}\ Al_{0.2})(Al_{1.0}Si_{7.0})O_{11}(OH)$, and of Type1 (magnesiohornblende) is $(Ca_{1.8}Na_{0.4}K_{0.3})(Fe_{1.2}Mg_{3.0}\ Al_{0.4})\ (Al_{0.3}Si_{7.7})O_{11}(OH)$. The greater amounts of total cations in X and Y sites than the stoichiometric sum of 5.0 is likely due to assuming all iron to be as Fe^{2+}. Simultaneous enrichment of Mg and Na in Type1 amphibole has been attributed to elevated f_{O2} under crystallisation (Hogarth, 1989).

Titanite: This mineral occurs usually in amounts less than 4%, as coarse (up to 800 μm), subhedral to euhedral crystals that contain small magnetite, apatite, epidote, allanite, and zircon inclusions. The magmatic titanite contains relatively low amounts of Al and Fe (< 1.2 wt. oxide%; appendix 5-6) and is zoned primarily in terms of variable degrees of enrichment in rare earth element (Morad and Aldahan, 2002). Magmatic titanite crystals are subjected to partial or pervasive alteration into leucoxene as well as replacement by fine-crystalline Fe-chlorite/berthierine and, in some cases, calcite and trace amounts of quartz (Figure 5-8). Alteration into leucoxene and replacement by clay mineral are most pervasive when the magmatic titanite crystals are fractured (Figure-5-9). Backscattered electron imaging revealed that alteration of magmatic titanite is accompanied by dissolution and formation of micro-pores (Figure 5-10).

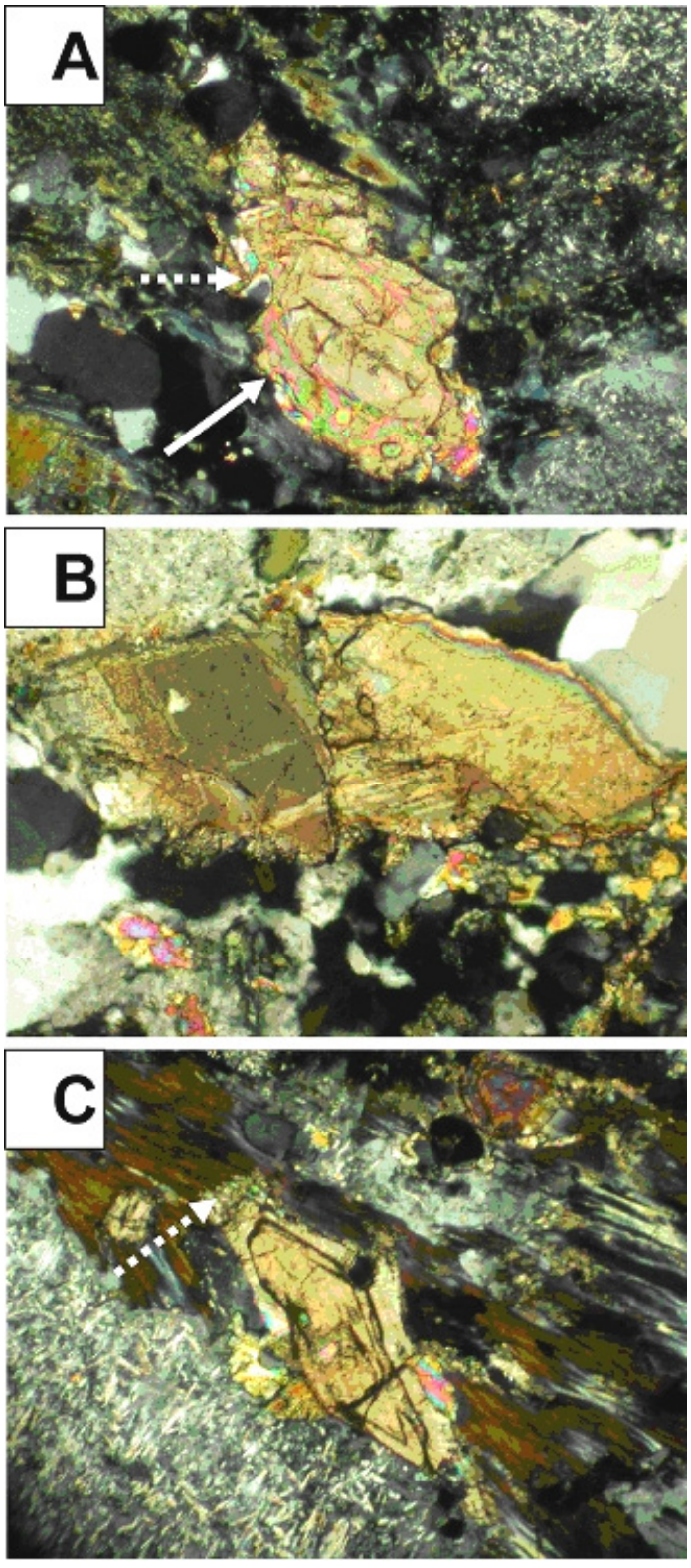

Figure 5-8. *Optical micrographs (X-nicols) showing slight alteration of zoned magmatic titanite and replacement by calcite and quartz (solid and dashed arrows, respectively in figure A) and dissolution (arrow in figure* ***C****).*

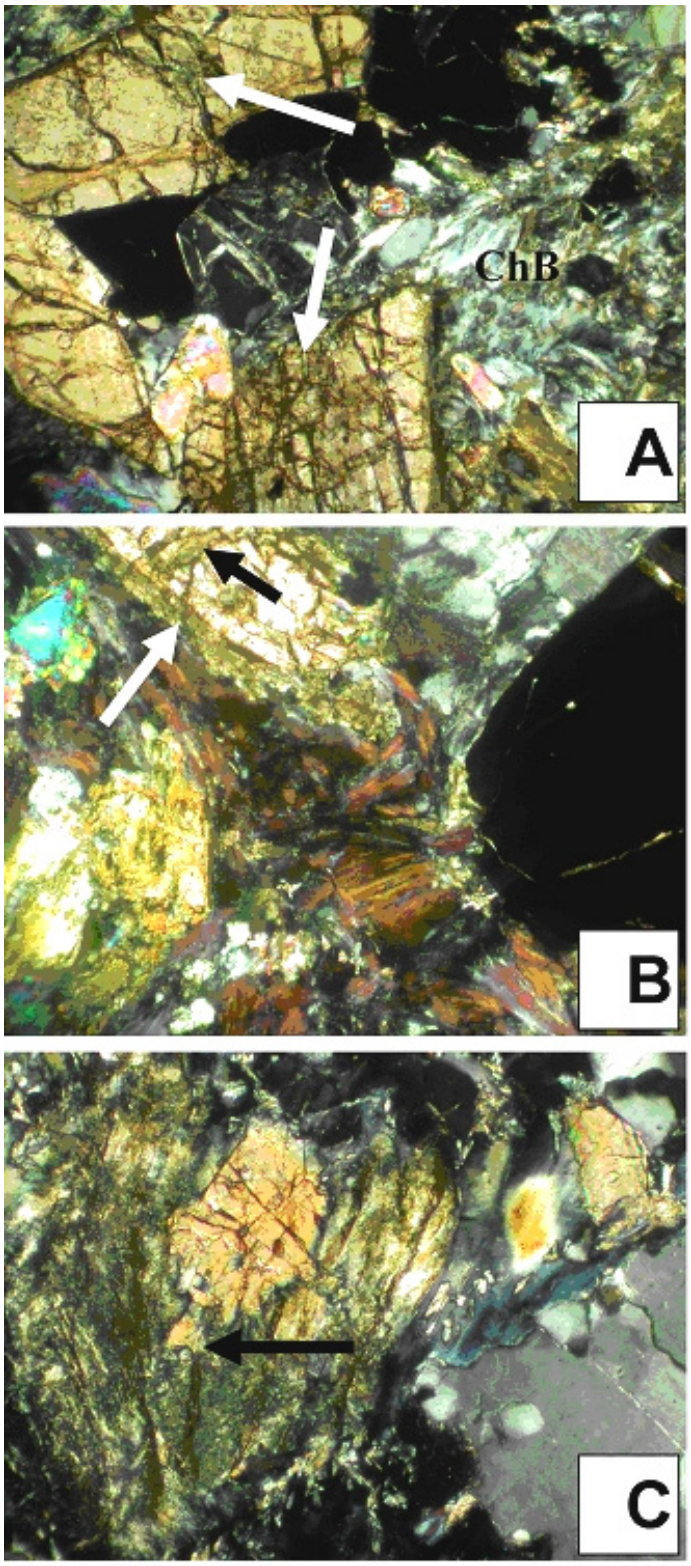

Figure 5-9. *Optical micrographs (X-nicols) showing that the alteration of magmatic titanite (arrows) is most pervasive in fractured crystals. Replacement by chlorite and leucoxene may in such case end up with tiny remnants of titanite (arrow in figure* ***C****).*

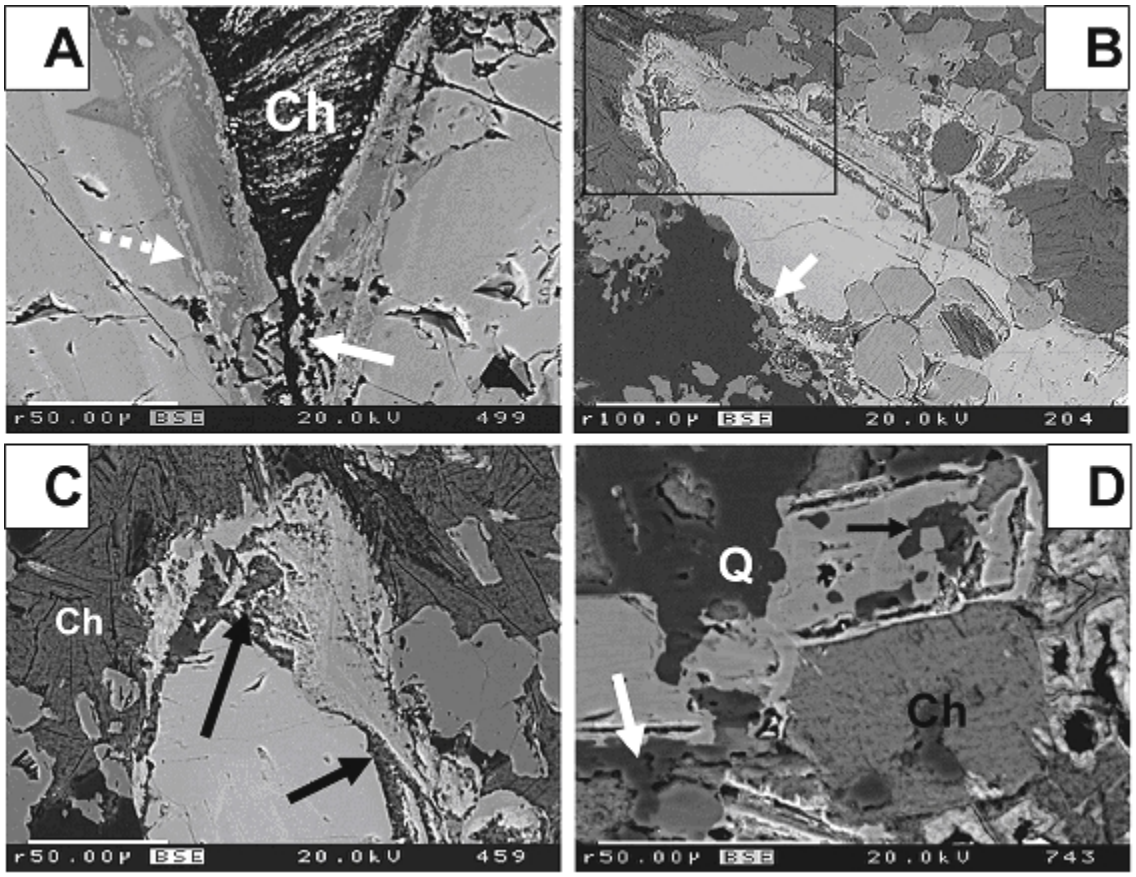

Figure 5-10. *Backscattered electron images showing that the formation of micro-porosity (arrows in Figure **A**) and replacement of magmatic titanite by chlorite affect mainly the outer zones of magmatic titanite. In figure **D** the titanite is partly replaced by microcrystalline quartz (Q and black arrow). Ch in figure **D** is chlorite that has completely replaced magnetite.*

Epidote: Total magmatic and secondary epidote (excluding fine crystals within saussuritised plagioclase) varies in abundance from trace to 42%, and occurs as coarse (100-600 µm), subhedral to euhedral crystals that are colourless or have slightly yellowish green colour. Electron microprobe analyses revealed that the epidote (appendix 5-7), which has the general chemical formula: $Ca_2(Fe^{3+}Al)_3Si_3O_{10}(OH)$, contains ca 20-30 mole% pistacite solid solution (Ps) [$Ps = Fe^{3+}/(Fe^{3+} + Al^{3+}) \times 100$]. The crystals reveal zones and scattered patches of Sr-rich epidote and/or enrichment with light REE and heavy REE (Morad and Aldahan, 2002).

Magnetite: Magnetite occurs in most samples as local patches made of several crystals. It usually does not exceed 1% in abundance, but in rare cases magnetite may form up to 13 % of the rock. Magnetite patches are intimately associated to magmatic epidote, titanite and apatite. Electron microprobe analyses of magnetite revealed a pure Fe_3O_4 composition with minor amounts (< 0.2 oxide wt.%) of Ti, Mg and Al. In dioritic rocks, the magnetite crystals are replaced by fine-crystalline, strongly Fe-rich chlorite/berthierine (Figure 5-11).

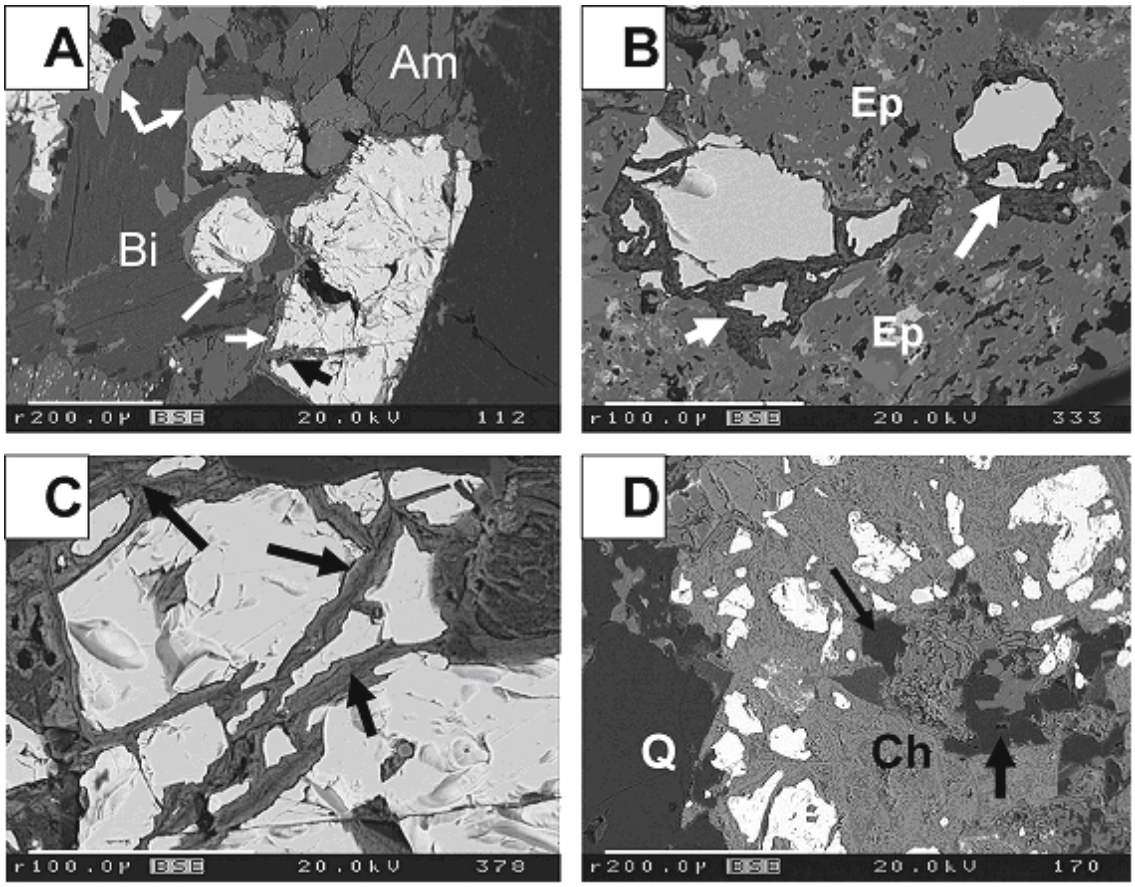

Figure 5-11. *Backscattered electron image showing the replacement of magnetite (bright) by Fe-chlorite/berthierine. In figure **A**, replacement of magnetite by Fe-chlorite/berthierine is slight and occurs along fractures (black arrow); Bi is biotite and Am is amphibole, and the arrows show slightly altered titanite rim around the magnetite. Magnetite that is replaced by Fe-chlorite/berthierine (arrows) in figure **B** is embedded in magmatic epidote crystal (Ep). Figure **C** display a greater replacement of magnetite along micro-fractures by Fe-chlorite/berthierine (arrows). Figure **D** displays scattered remnants of magnetite that is replaced by Fe-chlorite/berthierine (grey area). A titanite crystal embedded in magnetite was also severely replaced by Fe-chlorite/berthierine and quartz (arrows).*

5.2 Secondary minerals: petrography and mineral chemistry

Secondary minerals in the studied rocks occur in three forms: fracture-filling, void-filling and as alteration products of magmatic minerals. Intra-crystalline voids, which have resulted from mineral dissolution and alteration of the bedrock, and inter-crystalline micro-pores within fracture- and void-filling silicates (particularly chlorite and illite/vermiculite) vary greatly in size (< 1-15 µm). Argillised minerals refer to poorly-identified magmatic minerals that have been replaced by a fine-crystalline mixture of clay minerals. Secondary chlorite refers to chlorite that has completely replaced biotite and, to a small extent, magnetite and titanite.

Sericite: This mineral forms an important component of saussuritised magmatic plagioclase, i. e. together with epidote and albite. In some cases, however, saussuritised plagioclase does not contain epidote, but is merely albitised and replaced by sericite. Although the petrographic distinction between fine-crystalline, magmatic muscovite and hydrothermal sericite is not always straightforward, electron microprobe analyses of sericite (appendix 5-5) revealed the presence of higher amounts of total Fe (av. 0.53 atoms per formula unit), and are hence somewhat more phengitic in composition than a typical composition for magmatic muscovite (Figure 5-5). Tetrahedral and octahedral Al ranges in abundance from 1.69 to 1.77 and from 3.28 to 3.35 atoms per formula unit, respectively. The interlayer sites are strongly dominated by K, whereas Na (i.e. paragonite solid solution) is low (av. 0.1 atoms). The average formula of sericite is $K_{1.6}Na_{0.1}(Fe_{0.5}Mg_{0.2}Al_{3.3}Ti_{0.04}\ Al_{1.7}Si_{6.3})O_{20}(OH)_4$.

Titanite: This mineral forms < 3% of the bulk granitic rocks and usually occurs within biotite that is usually replaced pseudomorphically by sheet-like Fe-Mg chlorite and, less commonly by fine-crystalline Fe-chlorite/berthierine. (Figures 5-12 and 5-13). Titanite that occurs within chloritised biotite appears as small (2-15 μm), lenticular to elongated crystals with poorly defined outlines that are arranged along traces of the cleavage planes in biotite. Secondary titanite in chloritised biotite contains higher amounts of Fe (1.9 – 3.0 wt.% Fe_2O_3; 0.05 to 0.08 Fe^{3+} atoms per formula unit) and Al (5.4 – 8.4 wt.% Al_2O_3; 0.22 to 0.3 Al atoms per formula unit,), but similar amounts of Ca and lower Ti than magmatic titanite (Figures 5-14 and 5-15). The enrichment of titanite in Al, which is fairly typical for hydrothermal titanite (e.g., Tulloch, 1979), is usually attributed to the substitution of (Al, Fe^{3+}, OH, F) for (Ti, O) (Sahama, 1946). Titanite overgrowths or the outer zone of magmatic titanite are thin (< 25 μm) and have lower Al (4.2-5.2 wt% Al_2O_3; 0.17 to 0.21 atoms) and Fe (1.3-2.9 wt.% Fe_2O_3; 0.03-0.08 atoms) contents than titanite occurring within the chloritised biotite. Sr, Ba, Na, K, Mn and Mg occur in trace to non detectable amounts (appendix 5-6).

Secondary titanite contains considerably lower amounts of REE (Ce = 184 ppm, Nd 110 = ppm, Sm = 126 ppm, Yb = 92 ppm, and Y = 88 ppm) than magmatic titanite (Ce = 5884 ppm, Nd = 3140 ppm, Sm = 326 ppm, Yb = 402 ppm, and Y = 1638 ppm; Morad and Aldahan, 2002).

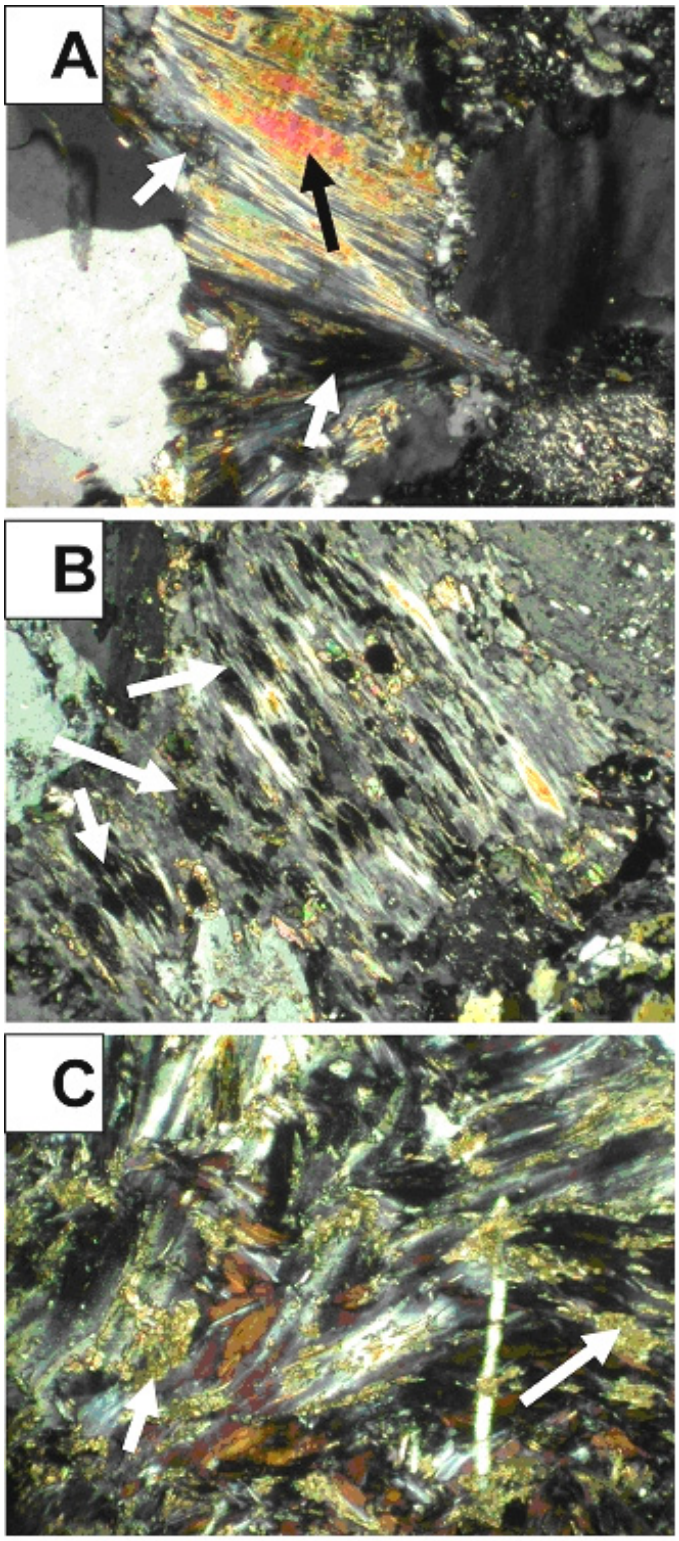

Figure 5-12. *Optical micrographs (X-nicols) showing that the amounts of secondary, lenticular titanite crystals (white arrows) are less abundant in partly chloritised biotite (Figure **A**; black arrow) than in severely to completely chloritised biotite (Figures **B** and **C**).*

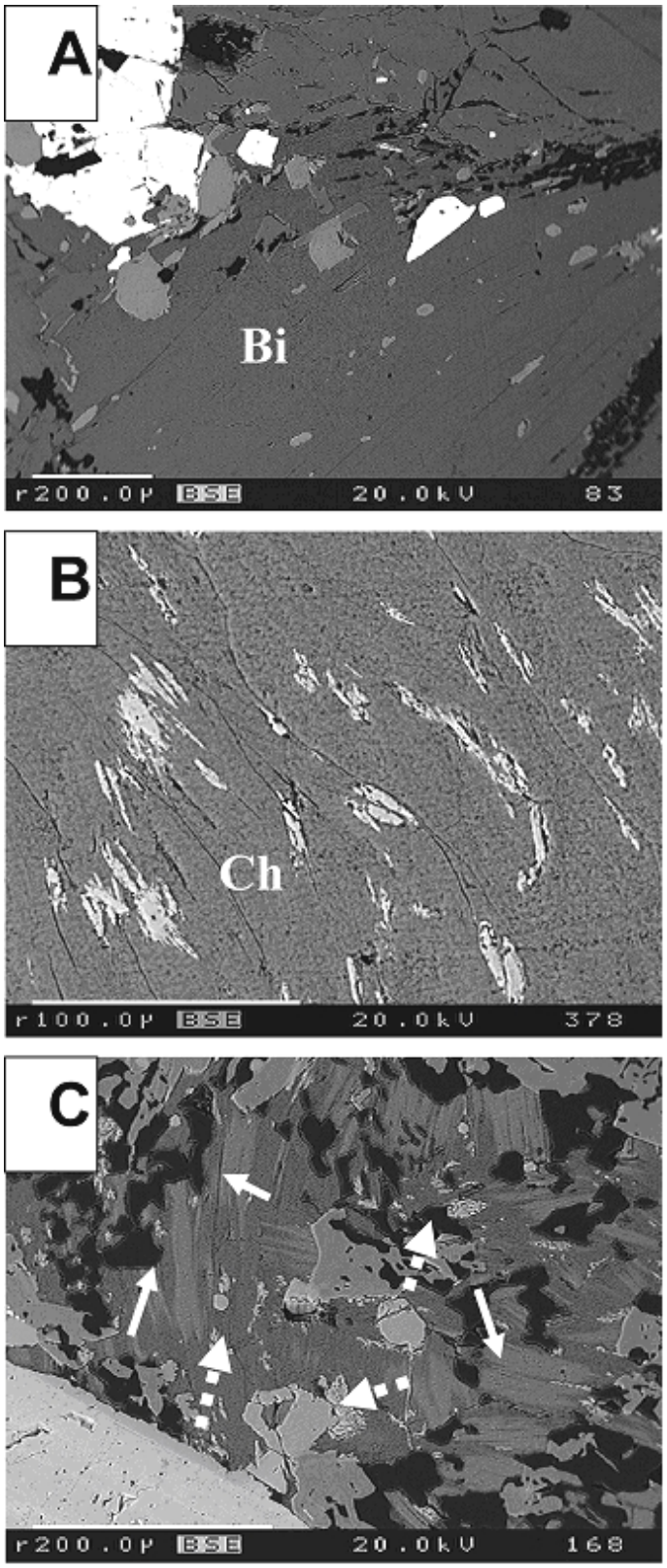

Figure 5-13. *Backscattered electron image showing that the small, lenticular crystals and sheets of secondary, Al-rich titanite are nearly absent in fresh biotite (Figure **A**) compared to severely chloritised biotite (Figure **B** and **C**; solid arrows are biotite remnants and dashed arrows are secondary titanite).*

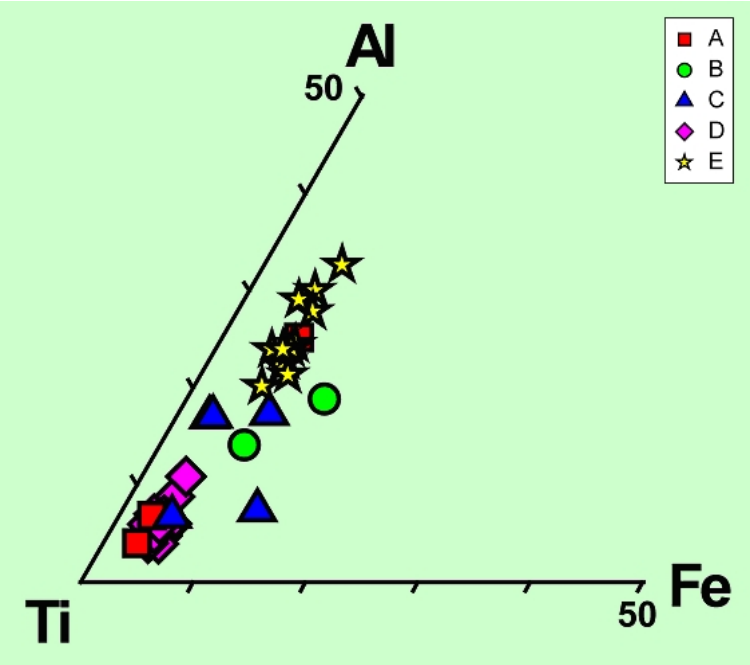

Figure 5-14. *Al-Fe^{3+}-Ti triangular plot showing variations in the composition of the various occurrence habits of titanite in the Äspö granitic basement. (Legend: A = euhedral crystals in chloritized biotite, B = remnants of dissolved magmatic titanite, C = overgrowth on magmatic titanite, D = magmatic titanite, E = lenticular and sheet-like crystals in chlorite) Data are based on this study and from Morad and Aldahan (2002).*

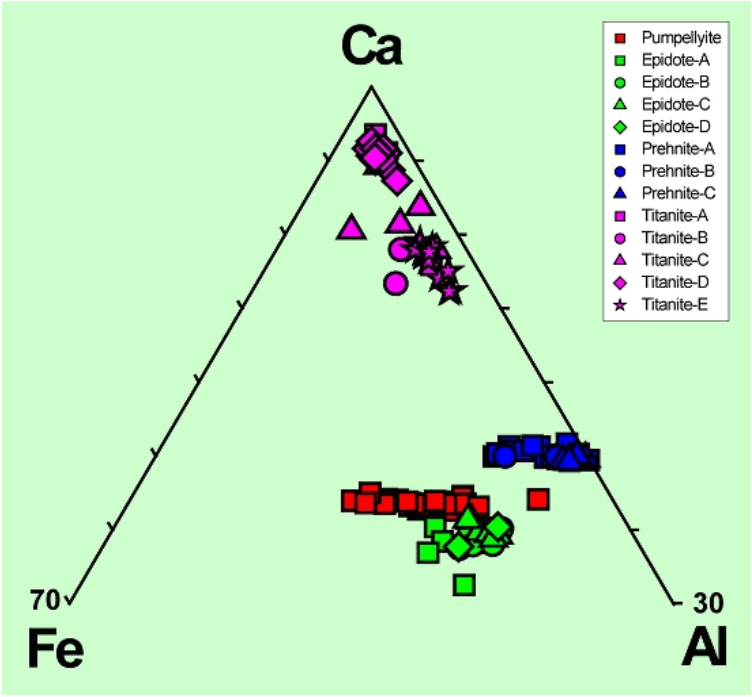

Figure 5-15. *Triangular Ca-Al-Fe^{3+} plot showing that the various occurrence habits of titanite, epidote, pumpellyite, and prehnite display relatively wide variations in chemical composition. Titanite varies mainly in terms of Al and Ca contents, whereas pumpellyite, epidote and prehnite vary mainly in Fe^{3+} and Al contents. (Legend for titanite: A = euhedral crystals in chloritized biotite, B = remnants of dissolved magmatic titanite, C = overgrowth on magmatic titanite, D = magmatic titanite, E = lenticular and sheet-like crystals in chlorite. Legend for epidote: A = in chloritized biotite, B = magmatic, C = in saussuritized plagioclase, D = fracture filling. Legend for prehnite: A = fracture filling, B = in chloritized biotite, C = in K-feldspar) Data are based on this study and from Morad and Aldahan (2002).*

Prehnite: Prehnite occurs mainly in trace amounts to 18% (average 1%) in the studied drill cores, but has been reported by Morad and Aldahan (2002) to be highly abundant in fractured rocks within major deformation zones in other drill cores from the Äspö HRL. Prehnite crystals have a platy, bow-tie and radiating fan habits that mainly fill fractures and voids. Replacement by prehnite is partial to complete and fills fractures in magmatic K-feldspar, biotite and plagioclase (Figure 5-16). Prehnite replacing feldspar occurs along the cleavage planes and as local patches concentrated close to micro-fractures that cut the feldspar, whereas prehnite replacing biotite is closely associated with chlorite (Figure 5-16).

Similar to what has been reported by Morad and Aldahan (2002), the electron microprobe analyses aided by backscattered electron imaging of prehnite revealed the presence of intimate intergrowth of iron-poor and an iron-rich prehnite variety (appendix 5-8). The chemical composition of prehnite reflects the extent of solid solution between two end members, namely: $Ca_2Al_2Si_3O_{10}(OH)_2$ and $Ca_2Fe^{3+}AlSi_3O_{10}(OH)_2$.

The solid solution between these two end members results from the substitution of Fe^{3+} by Al^{3+}. Pure, Fe^{3+} end member has not been reported in nature. The maximum amount of Fe_2O_3 obtained here is 7.7 wt.% (0.81 atoms per formula unit), which is lower than reported by Morad and Aldahan (2002) for prehnite from other drill cores of Äspö HRL, which in turn is lower than the maximum substitution of Fe^{3+} for Al of up to 12.6 wt.% Fe_2O_3 for prehnite reported elsewhere (Freiberger et al., 2001). The various occurrence habits of prehnite display variations in chemical composition, particularly in terms of Al-Fe-Ca ratios (Figures 5-15 and 5-17).

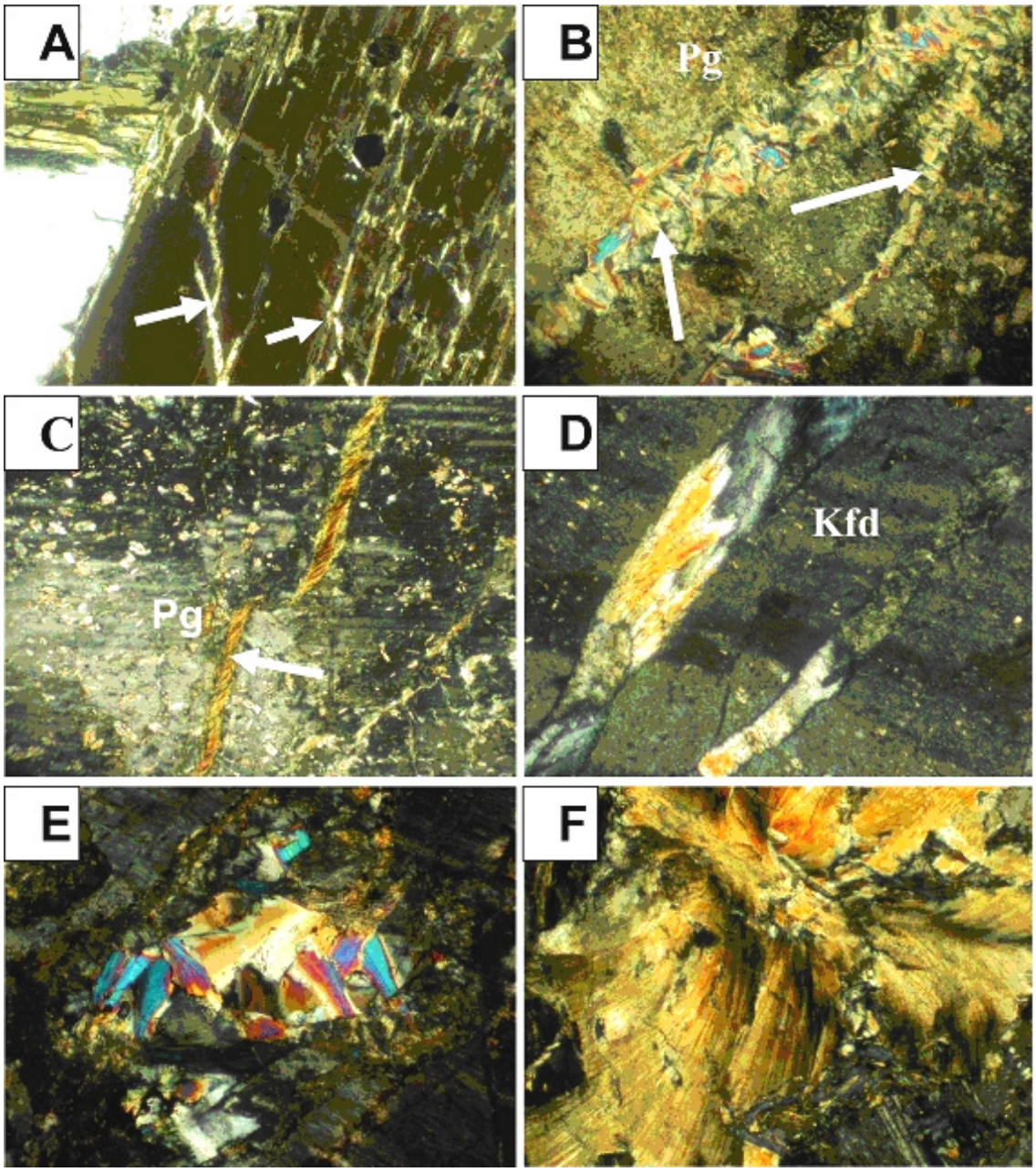

Figure 5-16. *Optical micrograph (X-nicols) showing prehnite that fills fractures (figures **A-D**) and void (figure **E**) in feldspar crystals and pervasively replacing biotite (figure **F**).*

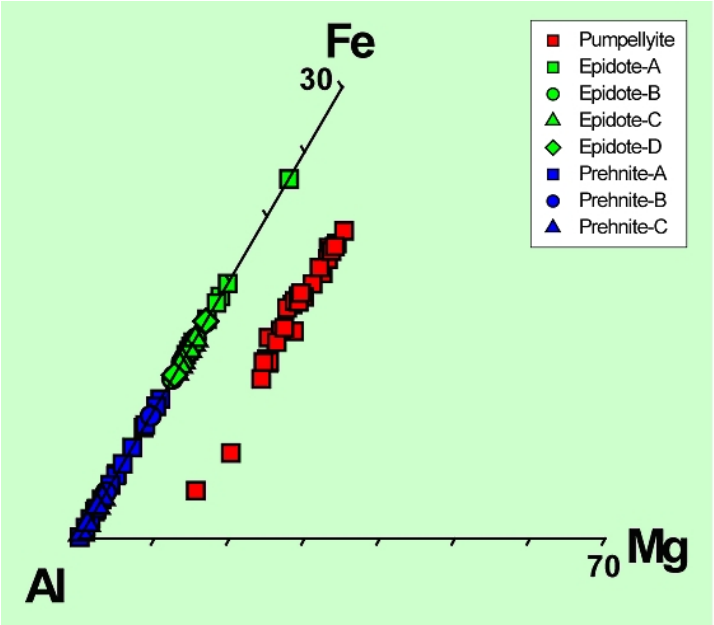

Figure 5-17. *Triangular Al-Fe^{3+}-Mg plot displaying that pumpellyite, epidote and prehnite vary mainly in terms of Al and Fe contents. (Legend – see Figure 5-15) Data are based on this study and from Morad and Aldahan (2002).*

Pumpellyite: Pumpellyite occurs as discrete and coalesced, subhedral to euhedral, leafe- or feather-like crystals. Pumpellyite occurs usually in trace amounts within biotite crystals that are partly to pervasively replaced by pseudomorphic or fine-crystalline chlorite and by mixed-layer illite/vermiculite (Figure 5-18). Less commonly, pumpellyite occurs within altered plagioclase as fracture-filling mineral (Figure 5-18). The backscattered electron imaging and electron microprobe analyses revealed that pumpellyite display considerable variations in Fe and Al contents (Figure 5-19).

Pumpellyite is a mixed group silicate containing isolated [SiO_4] tetrahedra and di-silicate [$Si_2O_6(OH)$] groups. The general formula is commonly indicated as $W_8X_4Y_8Z_{12}O_{56-n}(OH)_n$, where:

- W are sevenfold-coordinated sites commonly occupied by Ca,
- X and Y are two crystallographically independent octahedral sites occupied by divalent and trivalent cations,
- Z indicates tetrahedral sites invariably occupied by Si (Passaglia and Gottardi, 1973).

Thus, the recommended general formula of pumpellyite is $(Ca)CaAl_2(OH)_2(Mg,Mn,Fe^{2+},Al,Fe^{3+})[(OH)O]SiO_4Si_2O_6(OH)$. Iron (mainly as Fe^{3+})-rich pumpellyite is called julgoldite, whereas the Fe-poor member is called pumpellyite (Passaglia and Gottardi, 1973).

Pumpellyite in the Äspö granites displays a relatively wide range of chemical composition (appendix 5-9), particularly in terms of Fe-Al-Ca contents (Figure 5-15 and Figure 5-17). The pumpellyite is moderately enriched in Fe^{3+} (up to 2.0 atoms per

formula unit), which is, in turn, antithetically related to the Al content (up to 3.1 atoms per formula unit), suggesting that the replacement of Al by Fe^{3+} is dominant (cf. Ishizuka,, 1999). The amount of Mg in the pumpellyite analysed is up to 0.8 atoms per formula unit. The relationship between total Fe and Mg is not obvious suggesting that the replacement between Fe^{2+} and Mg is of subordinate importance. The MnO and TiO_2 contents range between 0.01-0.32% and 0.10-0.19%, respectively. Na, K, Sr and Ba occur as trace amounts (< 1 wt.%) or below detection limit.

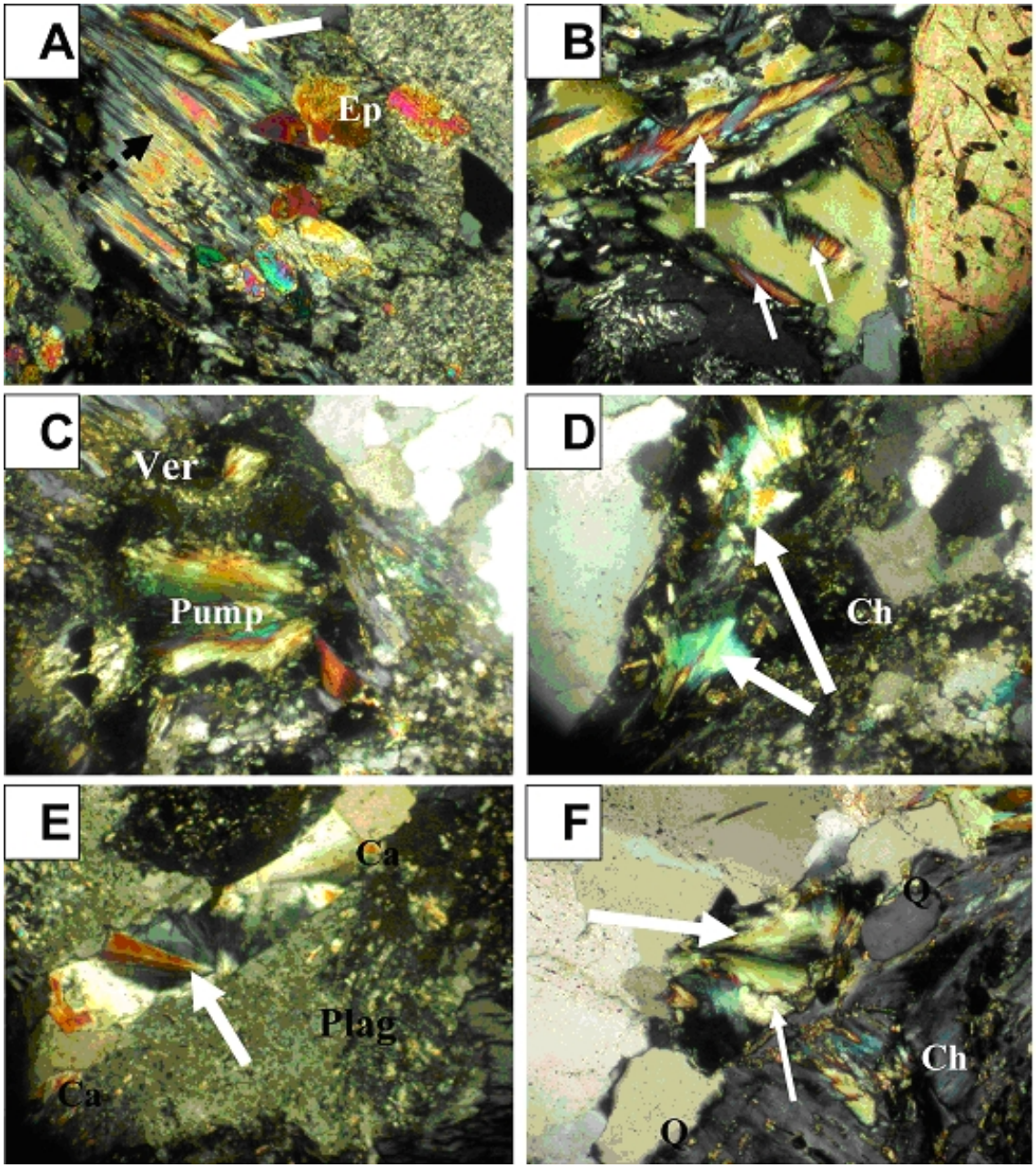

Figure 5-18. *Optical micrographs showing pumpellyite (white arrows and Pump): (**A**) within partly chloritised biotite (black arrow; Ep is epidote), (**B**) within nearly completely chloritised biotite; (**C**) within biotite replaced by chlorite and illite/vermiculite (Ver); (**D**) Within fine-crystalline chlorite (Ch) replacing biotite. Figures **E** and **F** show pumpellyite filling in fractures. Near chloritised biotite the fractures are filled also with calcite (Ca) and quartz (Q), respectively.*

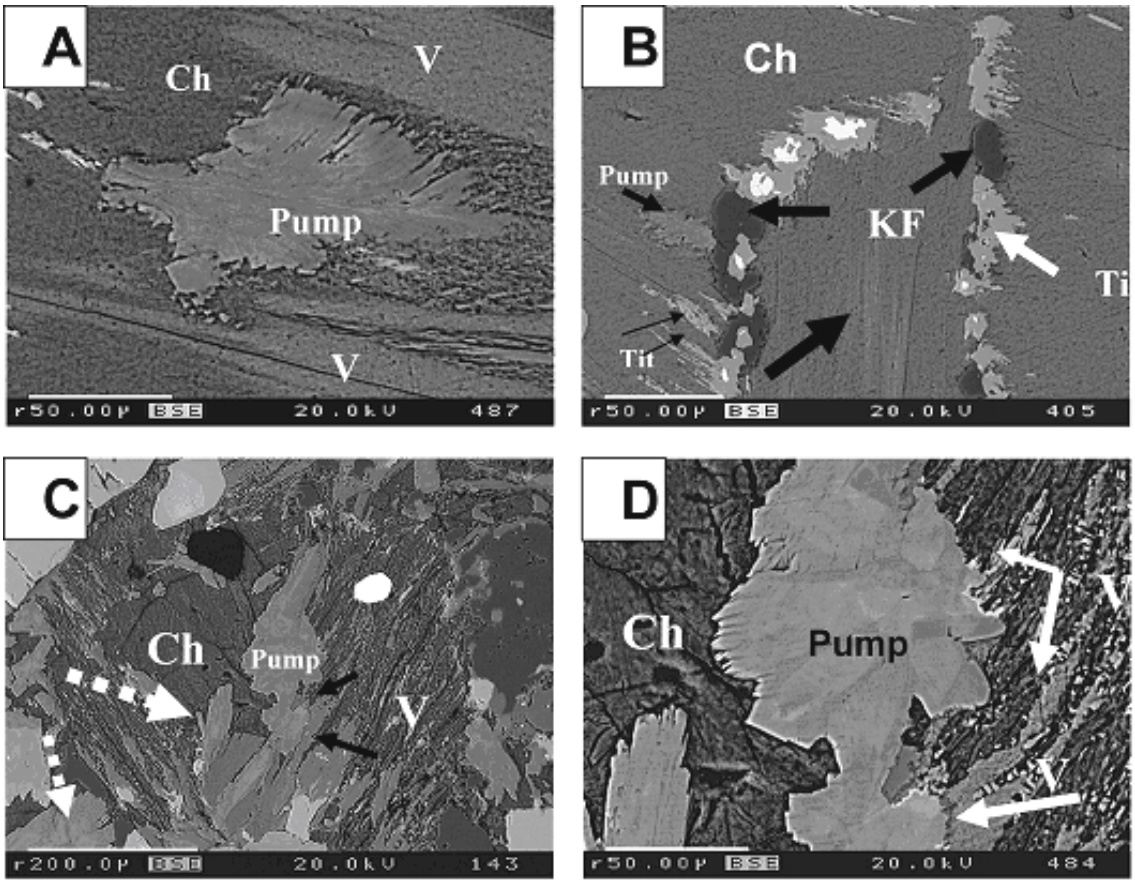

Figure5-19. *Backscattered electron images showing variations in the grey tones of pumpellyite. (**A**) feather-like pumpellyite occurring in biotite replaced by chlorite and tri-octahedral smectite/vermiculite (V); (**B**) pumpellyite occurring within severely chloritised biotite (black thick arrows); note the presence of secondary titanite (Tit) with ilmenite core and of secondary K-feldspar (KF); (**C**) pumpellyite (pump and dashed arrows) occurs within chloritised biotite (Ch) that is largely replaced by illite/vermiculite (V); (**D**)Enlarged part of figure C.*

Laumontite: This mineral is fairly rare in the studied samples, and occurs mainly as micro-fracture (< 60 µm wide) fillings. The associated mineral is usually Fe-oxides. The micro-fractures filled with laumontite cut across, and hence post-date, most other secondary minerals, such as prehnite, epidote, albite and K-feldspar. Laumontite is known to vary widely in chemical composition (Deer et al., 1992), and has an overall mineral formula of $Ca(Al_2Si_4O_{12}).4H_2O$. Laumontite in the Äspö granites displays, however, relatively small variation in chemical composition. The major elements include SiO_2 (av. 53.5%), Al_2O_3 (av. 21.2%), and CaO (av. 9.4%). The minor elements include K (av. 1.1%) and Na (av. 0.43%), which replace Ca according to the substitution Ca ↔2(K, Na) or CaAl↔(K, Na)Si (Deer et al., 1992). Small amounts of Fe (av. 0.14%) and Ba (av. 0.08%) were detected, whereas Mg, Mn, Ti and Sr are, if present, below detection limits.

K-feldspar: Secondary K-feldspar attains various occurrence habits, including fracture filling, replacement of magmatic plagioclase and, less commonly, as discrete crystals within chloritised biotite. K-feldspar that replaces saussuritised plagioclase is poly-synthetically twinned, whereas fracture-filling K-feldspar and K-feldspar replacing albitised plagioclase is un-twinned; the latter K-feldspar has replaced the plagioclase along the cleavage and twinning planes (Figures 5-20 and Figure 5-21). Secondary K-feldspar patches that vary in composition from nearly pure $KAlSi_3O_8$ composition (Or > 99 mole%) to variably barium rich (BaO = trace to 4.1%). Plagioclase that is replaced by secondary K-feldspar displays also extensive albitisation (Figure 5-21).

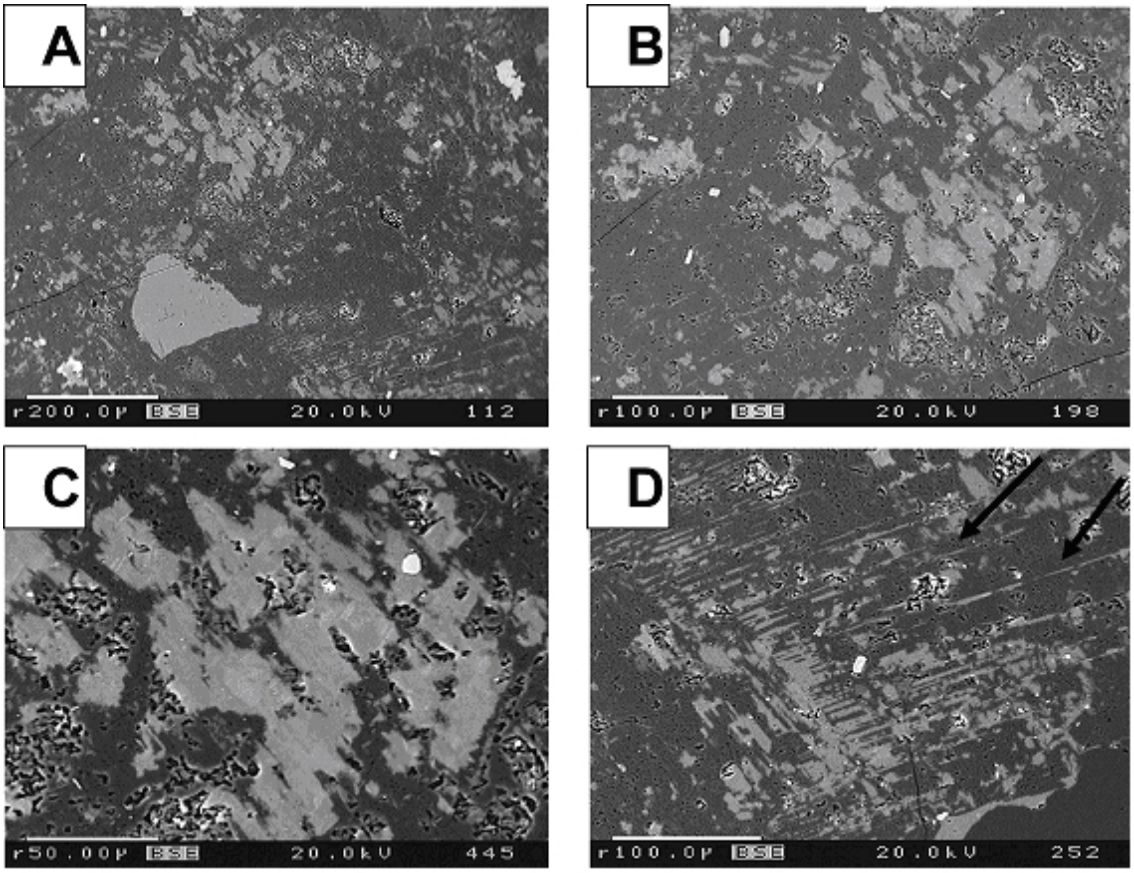

Figure 5-20. *(A) Backscattered electron image showing the replacement of plagioclase (dark grey) by secondary K-feldspar (light grey areas) along twinning (Figure **B**, enlarged part of A. Figure **C**, enlarged part of B) and cleavage planes (Figure **D**; arrows). Note that the secondary K-feldspar in zones in terms of Ba content (lightest areas are most Ba-rich).*

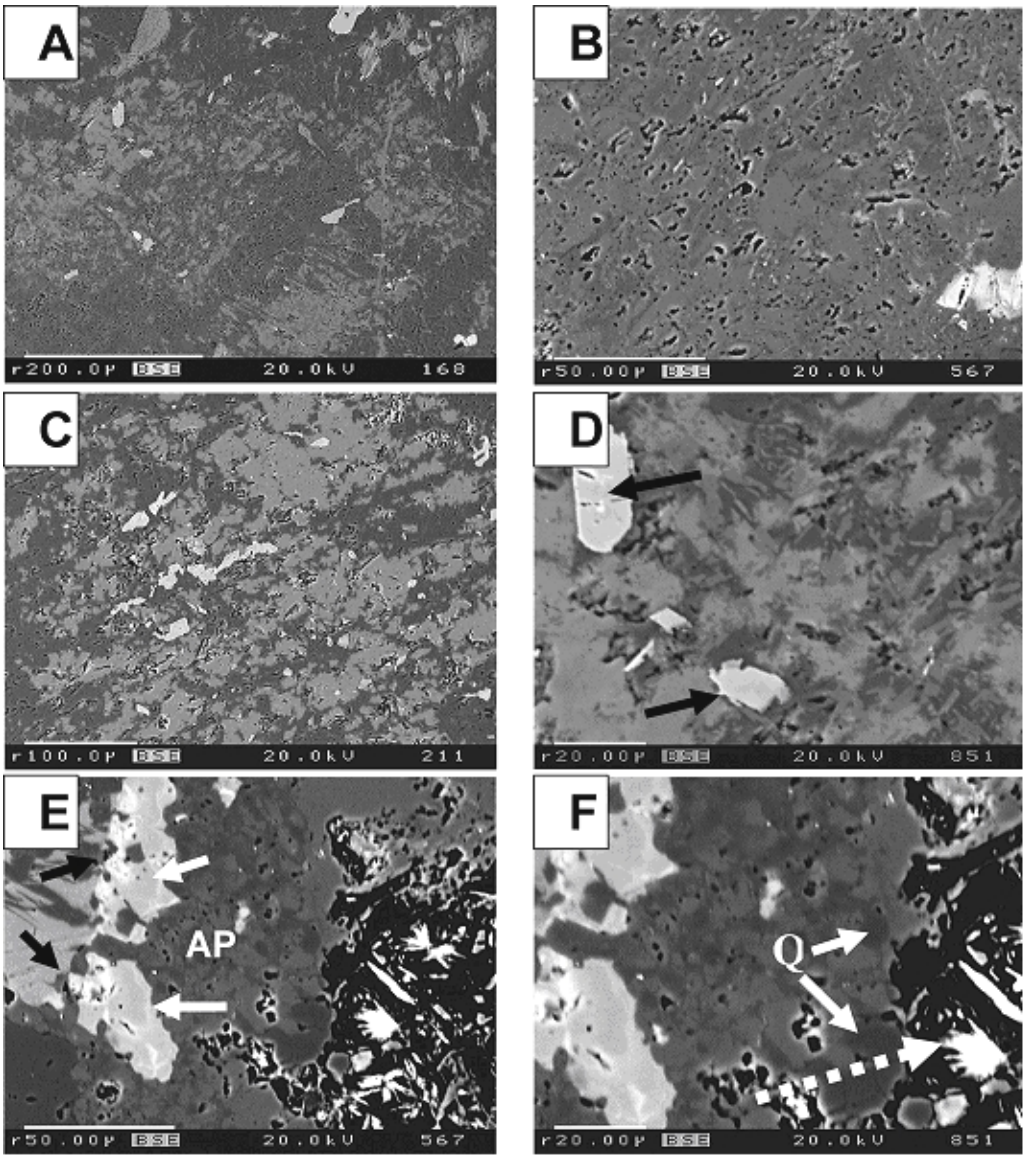

Figure 5-21. *Backscattered electron image showing: (**A**) the replacement of plagioclase (dark grey) by secondary K-feldspar (light grey areas) showing that plagioclase is also severely albitised (Figure **B**; dark patches are albite and lighter patches represent plagioclase remnants). Figure **C** and **D** reveal that the secondary K-feldspar engulfs the secondary albite and remnants of plagioclase; note the presence of epidote (arrows). Figures **E** and **F** show that some of the albitised plagioclase (AP) has been replaced by Ba-rich K-feldspar (light patches); note the presence of secondary quartz replacing plagioclase (Q) and of a void partly filled with flakey chlorite (dotted arrow).*

Saussuritised, magmatic plagioclase crystals that occur within magmatic K-feldspar commonly display overgrowths (ca 50-200 µm wide) that engulf numerous, secondary K-feldspar crystals that show considerable zoning in terms of variations in barium contents (Figure 5-22). Magmatic plagioclase is, in some cases, merely vacuolated and untwinned owing to pervasive albitisation; such albitised plagioclase displays evidence of slight saussuritisation (i.e., contains small amounts of sericite and epidote), and is stained red due to the presence of Fe-oxide pigment. These albitised grains have nearly pure albite end-member composition.

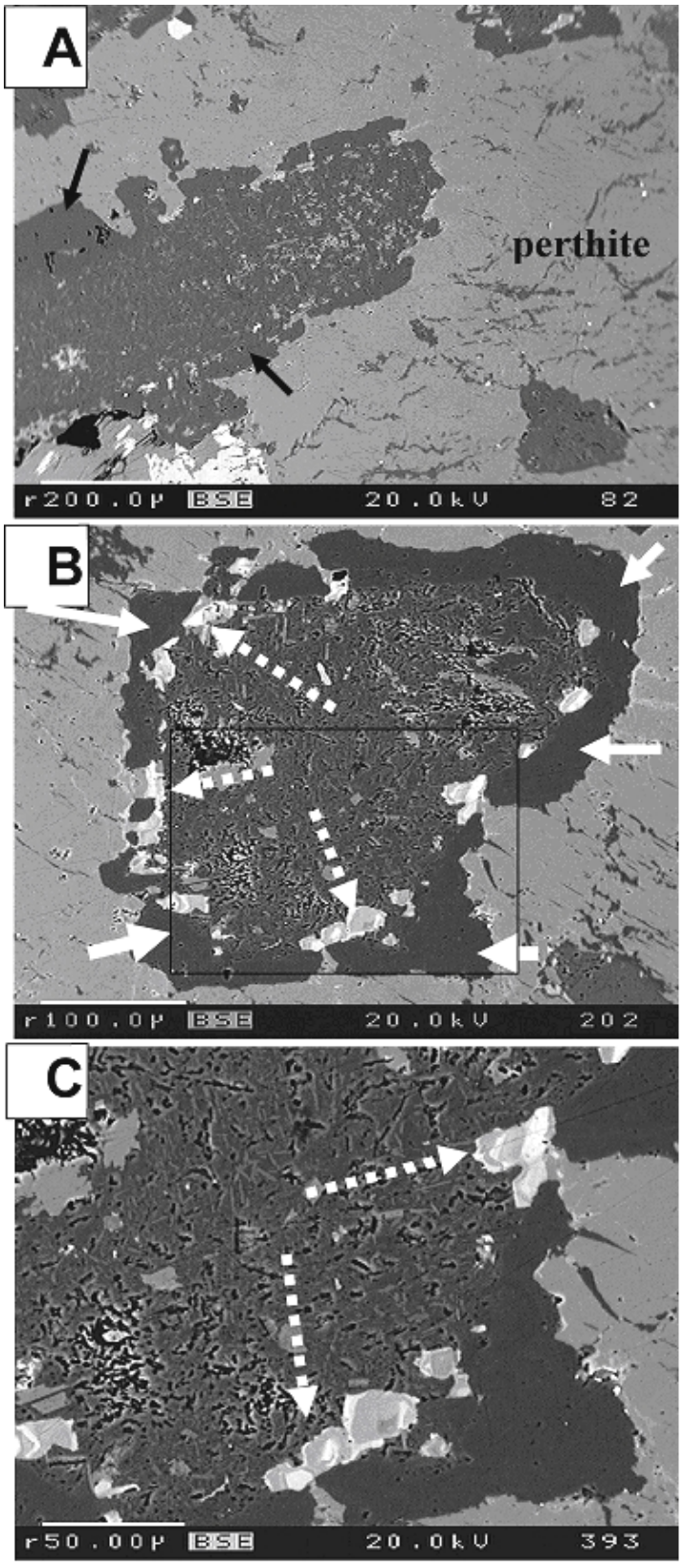

Figure 5-22. *Saussuritised plagioclase (embedded in perthite) with overgrowths of chemically pure, secondary albite (arrows). The albite overgrowths in Figure **B** are engulfing zoned, Ba-rich K-feldspar (light spots; dashed arrows). Figure **C** shows an enlargement of the square in Figure B.*

Calcite: This mineral, which varies in abundance from trace to 10% occurs mainly as fracture filling and as partial replacement of magmatic quartz and feldspar (Figure 5-23). Calcite usually engulfs and replaces partially to pervasively secondary quartz and feldspar crystals. In some cases, the calcite is fractured and filled by a later generation of calcite (Figure 5-23).

Calcite is nearly pure $CaCO_3$ containing only small amounts of Mg (below detection limit to 1 mole% $MgCO_3$), Fe (below detection limit to 1.6 mole% $FeCO_3$) and Mn (below detection limit to 2.5 mole% $MnCO_3$). Mn-bearing calcite has a bright, yellowish-orange luminescence while Mn-poor calcite shows yellowish brown luminescence. Stable isotope analyses of the fracture-filling and silicate-replacing calcite (appendix 8-9A) show a scatter in $\delta^{18}O_{PDB}$ (-18.2 to -7.0‰), $\delta^{13}C_{PDB}$ (-30.1 to +1.4‰), and $^{87}Sr/^{86}Sr$ (0.713821-0.717252).

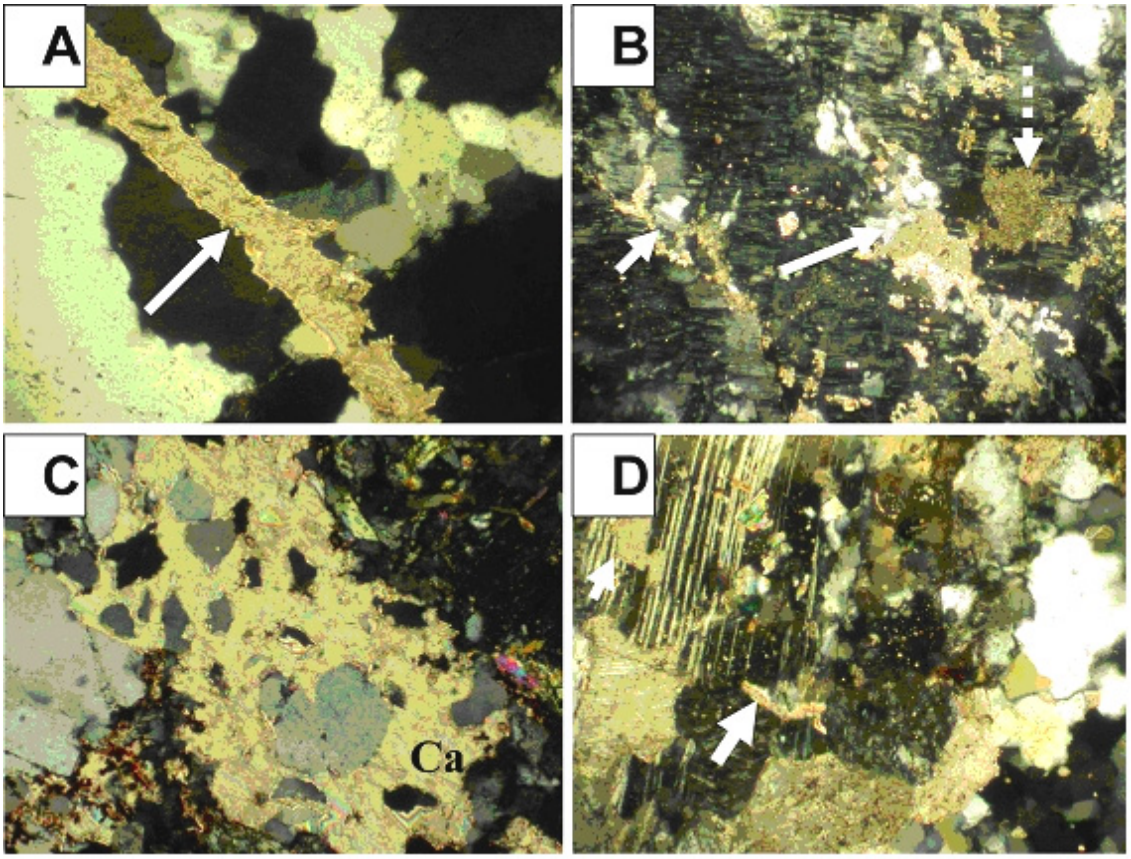

Figure 5-23. *Optical micrographs (X-nicols) showing: (**A**) fracture-filling calcite (arrow); (**B**) calcite partly replacing feldspar (arrows); (**C**) Calcite (Ca) pervasively replacing and engulfing quartz crystals; (**D**) Calcite pervasively replacing plagioclase and quartz.*

Quartz: Secondary quartz occurs as non-luminescent, fracture- and void-filling, crystals that are associated with various other secondary minerals, such as calcite, prehnite, pumpellyite and epidote. Quartz results also from the dissolution and alteration of magmatic titanite. In some cases, abundant euhedral quartz crystals that are finer crystalline than the associated magmatic quartz, have probably been formed during late-magmatic to earliest, post-magmatic in origin at conditions of elevated Si concentration in the magma or exsolved water.

Chlorite: Chlorite varies widely both in origin, occurrence habits (Figure 5-24) and chemical composition, including: (i) chlorite that has pseudomorphically replaced biotite, which is the dominant type, has greenish or greenish brown colour with greenish grey to violet interference colours. (ii) fine-crystalline chlorite that replaces biotite and titanite (usually < 1%) has pale-green colour and yellowish-grey interference colour (Figure 5-25). (iii) fine-crystalline, void- and fracture-filling chlorite.

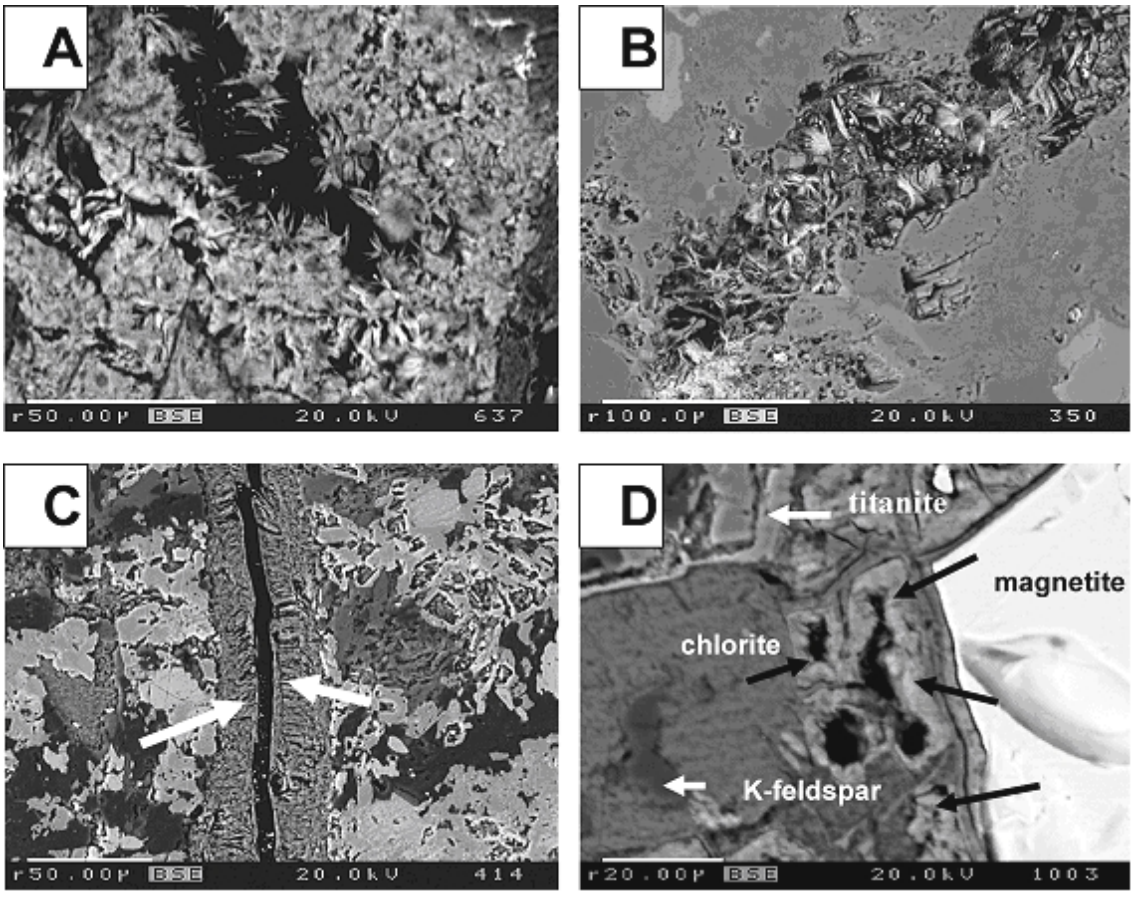

Figure 5-24. *Backscattered electron images of fine-crystalline chlorite partly filling voids (Figures **A** and **B**) and a thin fracture (figure **C**). Figure **D** show chlorite replacing unknown mineral (probably magnetite with titanite rim) and filling partly adjacent void.*

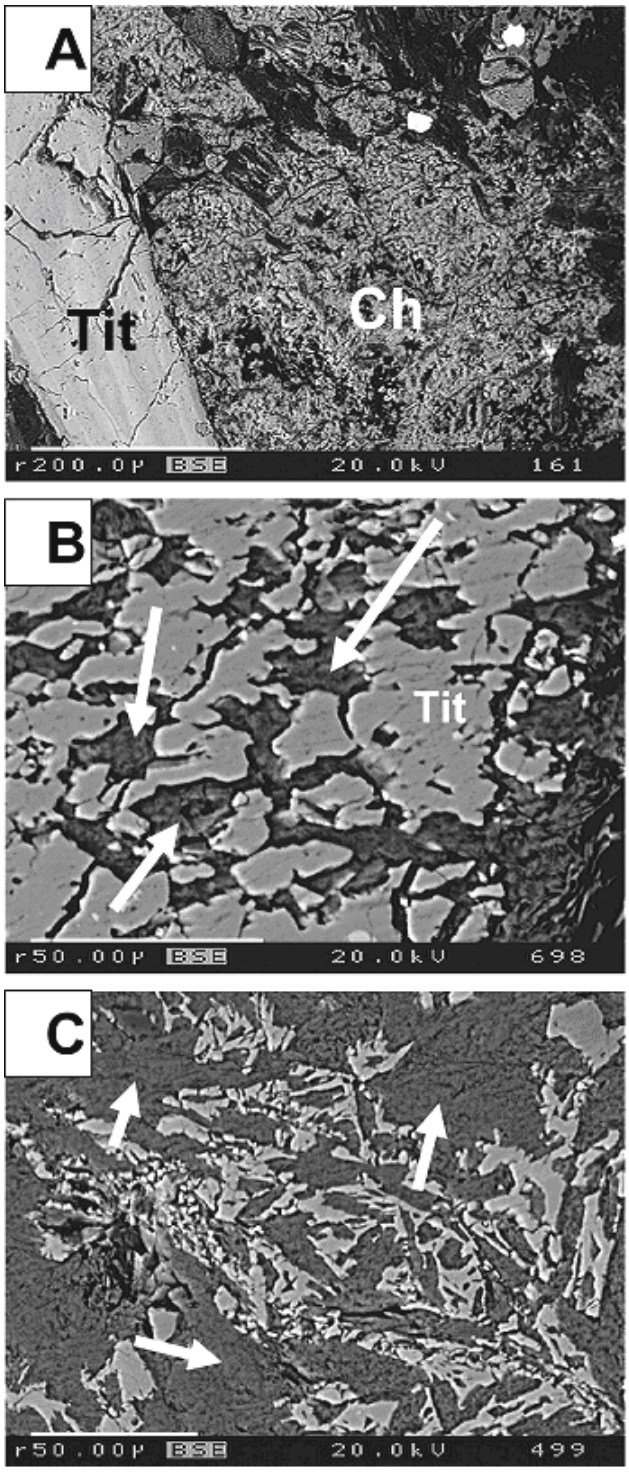

Figure 5-25. *Backscattered electron images of chlorite (Ch and arrows) that is pervasively replacing titanite (Tit and bright patches).*

These two main types of chlorite have different chemical composition, particularly in terms of amounts of Fe, Mg and Al (appendix 5-10; Figure 5-26). The fine-crystalline chlorite has higher Fe (FeO = 30.6 wt.%; Fe = 5.68 atoms per formula unit) but lower Mg ratio (MgO = 11.6 wt.%; 3.87 atoms per formula unit) than chlorite pseudomorphically replacing biotite (FeO = up to 24 wt.%; Fe = 4.29 atoms; MgO = 19.7 wt.%; Mg = 6.03 atoms). The chlorites analysed also contain variable, but low amounts of CaO (up to 1.1 wt%), TiO_2 (up to 0.4 wt.%), Na_2O (up to 0.2 wt.%) and

K_2O (up to 0.2 wt.%). The Fe/(Fe+Mg) ratio indicates that the chlorite that is pseudomorphically replacing biotite is barely dominated by brunsvigite, whereas microcrystalline chlorite that is replacing biotite and occurs as void/fracture fillings are dominantly diabantite (Figure 5-27).

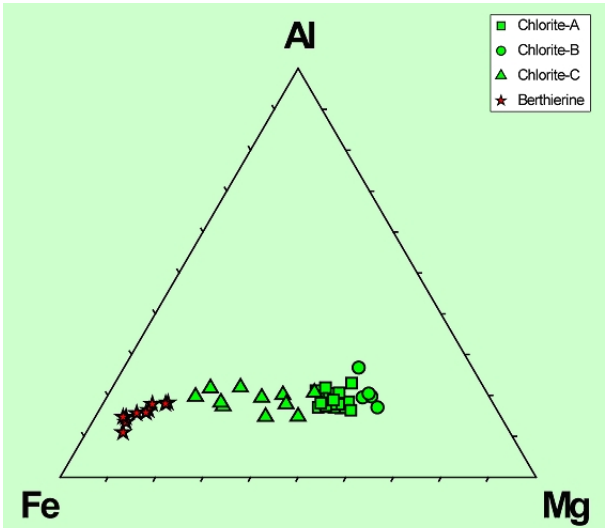

Figure 5-26. *Triangular Fe-Mg-Al plot of chlorite and berthierine showing that the two minerals display a continuous series of chemical variation, perhaps owing to the presence of various extents of mixed-layer chlorite/berthierine. The berthierine has a slightly wider variation in Al content than chlorite. The chlorites vary mainly in terms of Fe and Mg contents; chlorite replacing biotite (A and B) are characterised by higher Fe/(Fe+Mg) ratio than fracture/void filling chlorite (C). Data are based on this study and from Morad and Aldahan (2002).*

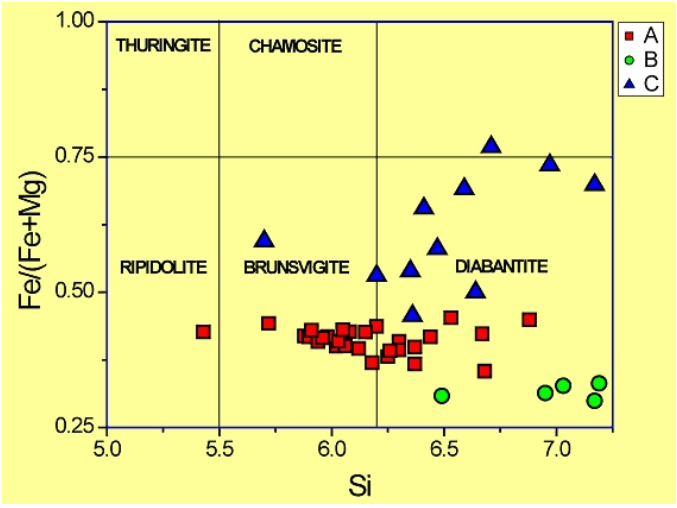

Figure 5-27. *Plot of Fe/(Fe+Mg) versus Si revealing that the chlorites analysed are dominantly brunsvigite and diabantite. A = chlorite pseudomorphically replacing biotite, B = microcrystalline chlorite replacing biotite; C = microcrystalline void/fracture filling chlorite. Data are based on this study and from Morad and Aldahan (2002).*

Berthierine: This mineral occurs as microcrystalline aggregates that have brownish to brownish green colour and brownish grey interference colour, and replaced pervasively to completely magnetite (Figure 5-11 C & D). Biotite replaced by berthierine has also been subjected to dissolution, and filling of the resulting secondary pores by calcite. Berthierine, like the grain-replacing, microcrystalline Fe-chlorite, is common in un-deformed, slightly to moderately altered dioritic rocks. Hence, there is no increase in the abundance of Berthierine/Fe-chlorite towards the zones of pervasive deformation.

Due to its presence in small amounts, the identification of berthierine cannot be verified by means of X-ray diffraction analyses. However, electron microprobe analyses of berthierine crystals (Figure 5-26**)** show as much as 46 wt.% FeO (Fe up to 9.3 atoms per 28 O, OH anions) and lower Al_2O_3 (ca 10 wt.%; Al < 3.0 atoms per formula unit) and, particularly, MgO (< 3.0 wt.%; Mg < 1 atom per formula unit) content, compared to chlorite (appendix 5-10). These chemical characteristics were arbitrary considered as representing composition of berthierine. In fact, transmission electron microscopy of similar crystals revealed intimate, interlamination of chlorite and berthierine (Coombs et al., 2001).

Epidote: Secondary epidote is colourless to yellowish green with moderate pleochroism under plane polarized light, and varies in abundance from trace to about 3%. Epidote has various occurrence habits, including: (i) tiny (< 10 μm) crystals in deformed rocks, being closely associated with recrystallised quartz, chlorite, and, in a few cases, prehnite and calcite. (ii) euhedral crystals (< 100 μm) that line and/or extensively fill fractures and voids, either solely or, most commonly, together with prehnite, chlorite and/or calcite. Calcite may replace epidote slightly to pervasively (iii) within chloritised biotite and saussuritised plagioclase. Electron microprobe analyses (appendix 5-7) of secondary epidote reveal variations mainly in the Al^{3+} and Fe^{3+} contents **(**Figures 5-15 and Figure 5-17**).**

The yellowish-green coloured epidote which engulfs, and hence post dates, the colourless epidote core has the highest iron content, i.e. the highest pistacite content (40 mole%). Secondary epidote displays much lower REE concentrations (La = 236 ppm; Ce = 371 ppm; Pr = 117 ppm; Nd = 486 ppm; Sm = 91 ppm; Gd = 145 ppm; Th = 211 ppm) compared to magmatic epidote (Morad and Aldahan, 2002).

Mixed-layer illite/vermiculite: A clay mineral that is replacing biotite and, in many cases, closely associated by pumpellyite indicates a chemical composition that we interpret here as illite/vermiculite. The host biotite crystals commonly display evidence of pervasive chloritisation and presence of relatively abundant micro-porosity (Figure 5-28). The illite/vermiculite mineral is colourless to pale green in colour, has a yellowish green interference colours, and has higher relief than chlorite. In some cases, illite/vermiculite occurs as tiny crystals (< 5 μm). Electron microprobe analyses (appendix 5-11) revealed that this mineral has a composition that is intermediate between sericite and chlorite.

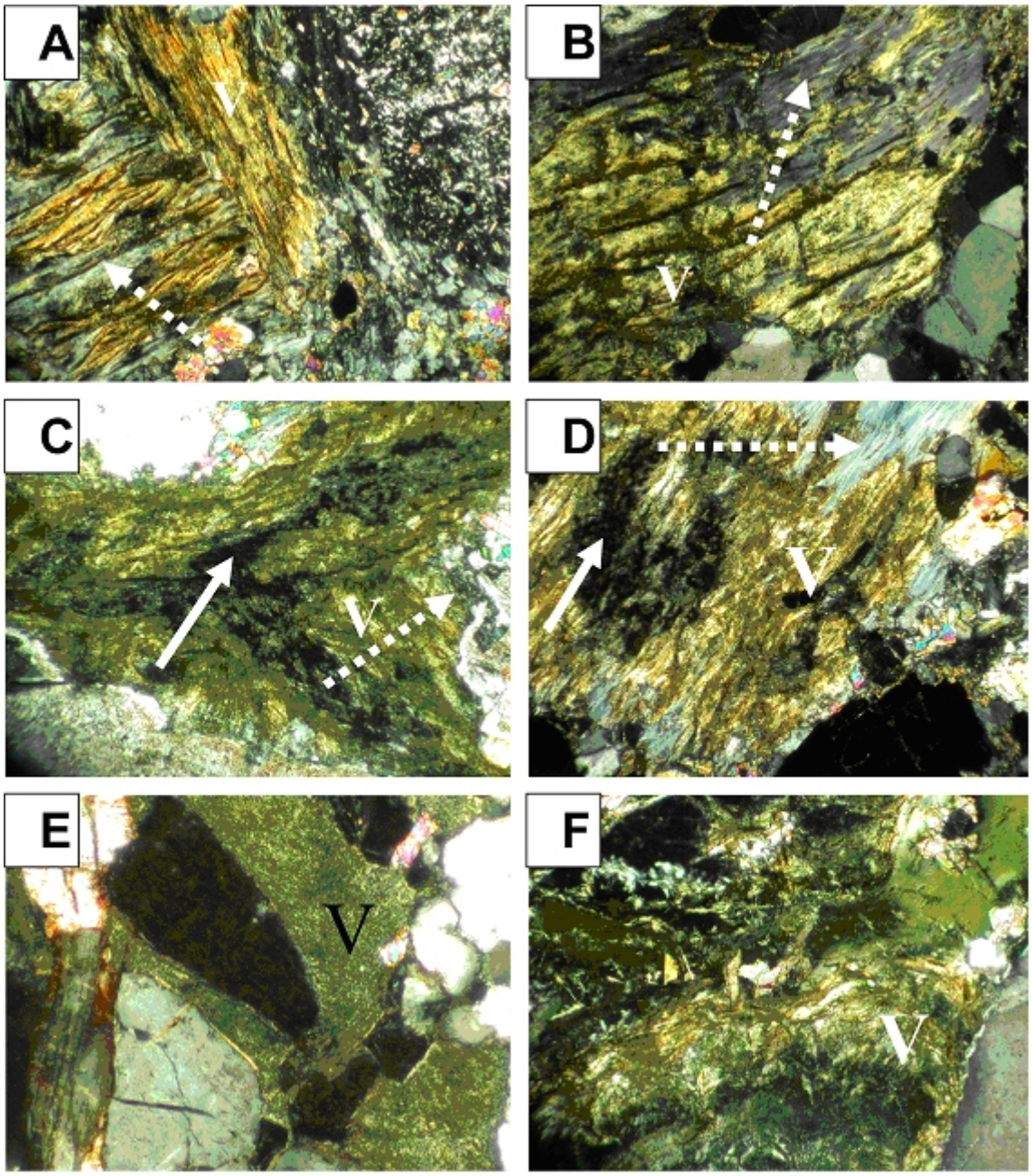

Figure 5-28. *Optical micrographs (X-nicols) showing the replacement of chloritised biotite (dotted arrows) by illite/vermiculite (V), which has a coarse, flakey habit (Figures **A-D**) or microcrystalline habit (Figures **E** and **F**).*

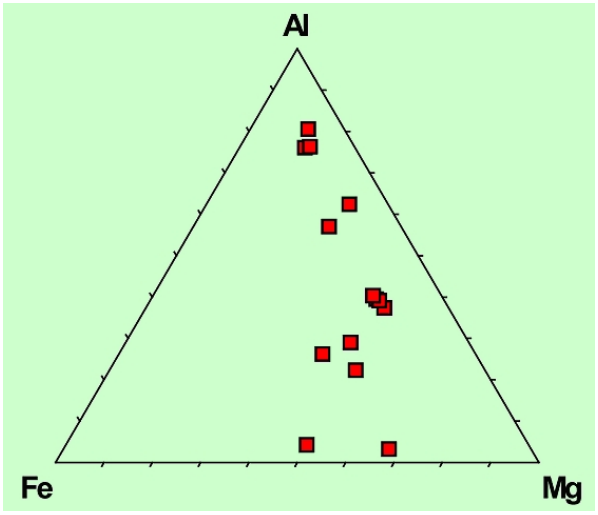

Figure 5-29. *Triangular Fe-Mg-Al plot of illite/vermiculitic clays displaying wide chemical variations i composition.*

Fe-oxides: These minerals occur primarily as fine pigment along micro-fractures, twinning and cleavage planes of altered feldspars, and within biotite altered into illite/vermiculite (Figure 5-30) and pseudo-hexagonal crystals (about 15-30 µm in size) within chloritised biotite, and as oxidation products of pyrite and magnetite (Figures 5-31).

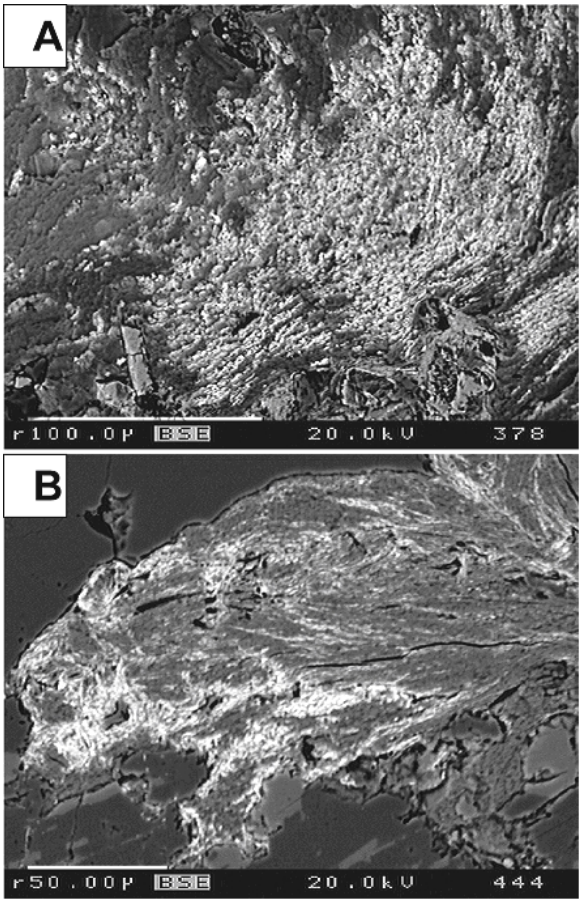

Figure 5-30. *Backscattered electron image showing the presence of Fe-oxide pigment within biotite that has been altered into illite/vermiculite. Fe-oxide pigments are the bright patches.*

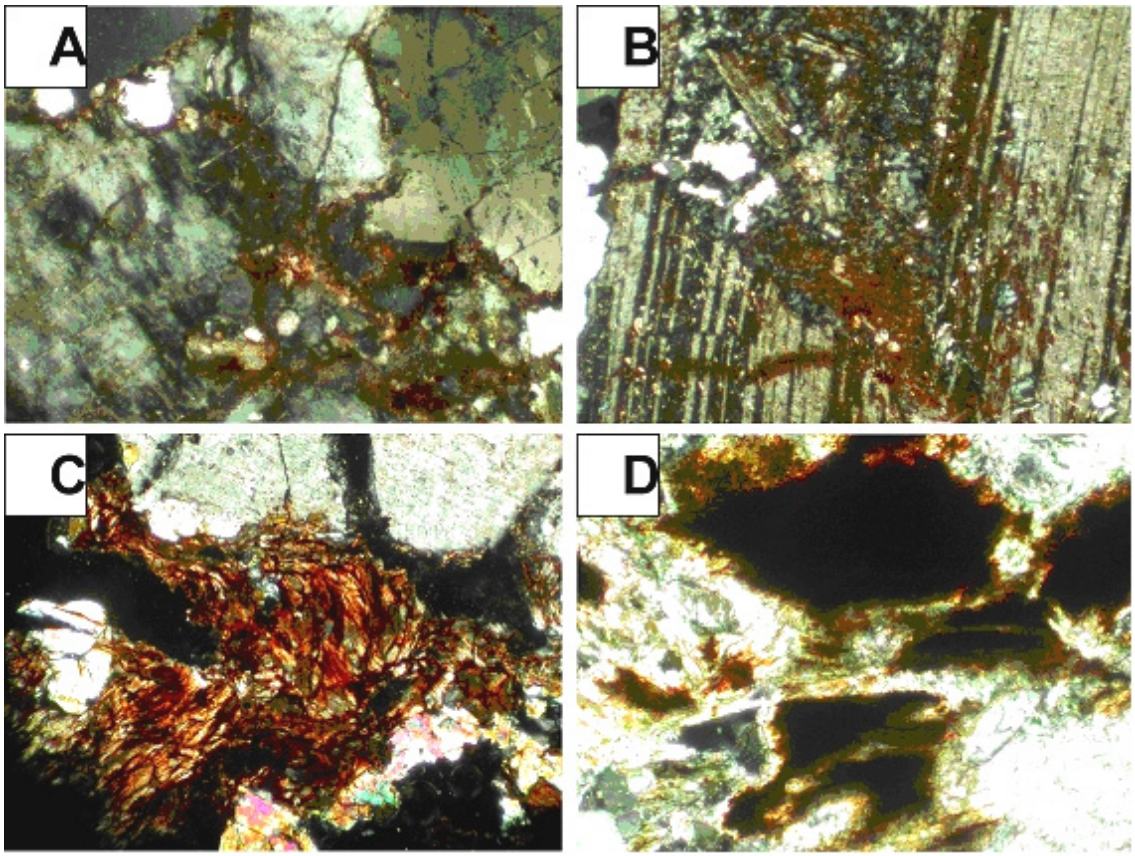

Figure 5-31. *Optical micrographs showing the presence of Fe-oxides within fractures in feldspars (Fgures **A** and **B**), whereas Figures **C** and **D** show biotite and pyrite replaced by Fe-oxides.*

Pyrite: This mineral occurs in trace amounts as small cubic crystals (< 50 µm across) in fractures and voids, being engulfed by calcite, and is hence among the latest low-temperature minerals to be formed in the studied rocks.

6 Spatial distribution of mineral alterations

6.1 KAS09

The lithology, well-log porosity, distribution patterns of primary and secondary minerals are displayed in Figures 6-1A, B, C, D, and E. Based on core description, the drill cores of this borehole are dominated by Äspö diorite (≈ 80%), fine-grained granite (≈15%) and a minor portion of greenstone (undifferentiated mafic rocks). Generally, all the rock types show little evidence of alteration. However, the modal analyses of the studied samples show that they are dominated by syeno-granite, monzo-granite and granodiorite. The fine-grained granite is randomly distributed in the cored section, but the greenstone (basic volcanic and/or sedimentary in origin) appears at the interval below 280 m. The latter two rock types are not fully represented in this study.

Various types of fractures are encountered in the borehole, including open (i.e., without mineral fillings), sealed (closed) and filled (with minerals). Fracture-filling materials were identified during core description. The width of these fractures can vary from microscopic to a few cm. In the later case, generally several fractures may occur together where, in some cases, the primary rock texture is totally obliterated by fracturing and deformation and thus forming a brittle deformation zone. Although fractures are common in most of the cored section of KAS09, parts of the section at about 100-110, 128-147, 249-255 and 391-420 show strongly deformed zones (Table 4-1). Deformation zone NE-1, which has shown a high transmissibility (10^{-4} m^2/s), occurs at the interval 128-147 m.

The distribution pattern of primary and secondary minerals in the sampled section of KAS09 is strongly dominated by the rock type and/or magnitude of fracturing and alteration. In this report, we will use the term “fractured or altered” for rock in which fractures and/or alteration can be recognised with the naked eye, and the term “seemingly unaltered” for rock in which fracturing and alteration are visible only under the microscope.

Fracturing and alteration are fairly common in most of the cored section in which several portions show relatively high porosity (up to 5%). These features (fracture types and estimation of relative porosity based on sonic, and single point resistance, SPR logging) are displayed together with major deformation zones and mineral variability in Figures 6-1A, B, C, D, and E.

Variation ranges (maximum and minimum) and averages of magmatic (primary quartz, K-feldspar-perthite, plagioclase, biotite and amphibole, muscovite, titanite, magnetite, fluorite and apatite) and secondary mineral alteration (chloritised biotite, argillised grains, chlorite, saussuritised/albitised plagioclase, epidote, calcite, altered titanite, secondary quartz, secondary K-feldspar, prehnite, pumpellyite, hematite and pyrite) are shown in Table 6-1. Quartz, K-feldspar and plagioclase show the highest average values (22, 17 and 14% respectively) along the whole cored section of KAS09. These minerals together with biotite, amphibole, muscovite, magnetite, and titanite comprise about 65% of average composition of the cored section. The remaining 35% includes the secondary minerals of which the average of saussuritised/albitised plagioclase stands for about 50% (about 18 out of 35%).

Table 6-1. The ranges of mineral alterations in the studied rocks.

	KAS09			KAS14		
	Minimum	**Maximum**	**Mean**	**Minimum**	**Maximum**	**Mean**
Chloritised biotite	0.0	18.4	2.7	0.0	6.4	1.7
Argillised grains	0.0	23.6	1.6	0.0	9.9	2.4
Secondary chlorite	0.0	20.2	2.9	0.0	22.3	6.4
Total epidote	0.0	42.1	5.1	0.0	20.5	7.1
Sauss./alb. Plagioclase	0.0	49.1	18.5	6.5	50.0	24.8
Calcite	0.0	10.9	0.8	0.0	7.4	1.0
Altered titanite	0.0	2.9	0.3	0.0	2.8	0.5
Secondary quartz	0.0	16.2	1.6	0.0	5.8	1.4
K-feldspar	0.0	8.8	0.9	0.0	6.6	1.3
Prehnite	0.0	17.7	0.5	0.0	11.3	1.2
Pumpellyite	0.0	1.9	0.0	0.0	0.0	0.0
Hematite	0.0	9.5	0.5	0.0	3.9	0.5
Pyrite	0.0	1.3	0.0	0.0	0.4	0.0
Primary quartz	0.5	49.3	22.4	4.8	54.1	15.8
K-feldspar/perthite	1.4	51.4	16.8	2.3	33.5	13.3
Plagioclase	0.5	44.1	14.3	1.3	37.6	13.4
Biotite	0.0	33.6	6.8	0.0	20.9	5.8
Amphibole	0.0	22.5	1.7	0.0	11.9	0.7
Muscovite	0.0	13.7	0.4	0.0	2.4	0.1
Magnetite	0.0	13.5	0.7	0.0	6.2	0.9
Titanite	0.0	3.8	1.0	0.0	3.3	1.4
Fluorite/apatite	0.0	5.0	0.3	0.0	1.4	0.2
Voids/fractures	0.0	5.2	0.1	0.0	2.4	0.1
Alteration index	0.0	3.5	0.8	0.1	5.1	1.3

Correlation coefficient matrix between the different minerals, using a linear least square function, is presented in appendix 6-1. There is no significant correlation between the minerals, but rather weak negative correlation coefficient values between primary and secondary minerals. The negative trend is expected, but the absence of strong correlation suggests lack of direct link between the primary minerals and the alteration products, which can be related to the complex alteration episodes and condition which the rock section has experienced.

The distribution pattern of the primary minerals indicates a high amount (average of 35%) of quartz in the fine-grained granite and the mylonite portions and a lesser amount (average of 20%) in the Äspö diorite. The distribution of K-feldspars resembles that of quartz, whereas the amount of plagioclases generally decreases in the fine-grained granite and in the deformed/fractured portions of the section. Biotite and amphibole are abundant within the Äspö diorite, but their amounts decrease sharply in the deformation zones. Muscovite appears sporadically in the section of KAS09 and the mineral is more common in the fine-grained granite. Titanite, magnetite, apatite and fluorite are more abundant in the Äspö diorite than in the fine-grained granite or deformation zones.

Saussuritised/albitised plagioclase is the most common alteration feature in the cored section that may include up to about 50% of a rock composition. In some portions of the rock section primary plagioclases are almost free from this alteration. A relatively significant correlation (correlation coefficient ≈ 0.5) occurred between primary plagioclase and saussuritised/albitised plagioclase which may partly explain the higher amounts of saussuritised/albitised plagioclase in the Äspö diorite compared to the fine-grained granite. Although the abundance of saussuritised/albitised plagioclase is somewhat higher in the deformation zones, some sections outside these zones contain high amounts of saussuritised/albitised plagioclase too.

The variability trends of partly chloritised biotite and completely replaced biotite (named chlorite) show overall distribution patterns that resemble those of the saussuritised/albitised plagioclase, but have narrower ranges and averages (Table 6-1). The distribution pattern of the argillised minerals (Figure 6-2) reveals smaller correlation with rock types and/or deformation zones and the amount of these minerals is both small and rather sporadic in the cored section.

The other category of secondary minerals is that occurring in overall fairly small amounts (< 5%) and with few localised abundances. These minerals include calcite, prehnite, and hematite. Relatively high amount (up to 17%) of prehnite is found in samples near (about 4-5 m) to the upper boundary of deformation zone around 100-110 m. The variability in the amounts of calcite (up to 10%) occurs within and outside deformation zones. Hematite is common in the upper 100 m the borehole section and deformation zones, but generally less frequent in the seemingly unaltered rocks. Even small amounts (< 1%) of hematite pigments are enough to give a reddish colour to the rocks. The occurrence habit of pumpellyite can also be described in this category of alteration minerals, but the amounts of pumpellyite are very small.

The third category of secondary mineral includes those that show low but yet detectable amounts (1-2 %), with a range of variability narrower than that of the other types. This category includes secondary quartz and K-feldspar and altered titanite. Relatively large amounts of these secondary minerals (up to 8%) appear at the top 40 m of the borehole section and there after the content decrease to the detectable level of 1-2%. At the deformation zone (249-255 m), one sample (253.5 m) shows amount of secondary quartz that reaches about 16%.

Relatively few portions of the “seemingly unaltered” rock did not show considerable amounts of secondary minerals. The seemingly unaltered rock occurs within or outside major deformation zones and show low values of alteration index; the alteration index = total sum of secondary minerals/ total sum of primary minerals. The overall variability in the alteration index along the cored section of KAS09 is from about 0.1 to 3.5 and an average of 0.8 (Table 6-1). This means that in some part of the rock section about 75% of the rock composition is secondary (alteration) minerals. The magnitude of scatter in the values seems to be larger in the top 200 m of the section compared to the lower one.

The alteration index is strongly controlled by the amounts of category 1 secondary minerals (i.e., saussuritised/albitised plagioclase, epidote, chloritised biotite, chlorite, and argillised minerals). This control is also demonstrated by the relatively low alteration index value at the few places that show considerable amounts of category 2 and 3 secondary minerals. In general, deformation zones show high values of alteration, but this feature occurs also in the rock section outside the deformation zones. However, the relatively high porosity values at the deformation zones correlate partly with the elevated alteration index values.

Although most of the red-coloured rocks show relatively high alteration index value and occurrence of hematite, some portions of seemingly unaltered rocks were red-coloured (for example the interval between about 50 and 65 m). Overall, plagioclase in the oxidised, reddish-coloured rocks is always albitised and replaced by K-feldspar. However, in some of these rocks, secondary K-feldspars occur in fractures that are lined with hematite is common. Fractured or deformed greyish-greenish coloured rocks have dominantly chlorite, epidote, quartz and occasionally calcite and prehnite as mineral fillings.

6.1.1 Mineral distribution about the NE-1 deformation zone

The passage of the main deformation zone NE-1, which is a water-bearing, high porosity and permeability zone, in KAS09 occurs around 128-147 m. The deformation pattern in NE-1 is rather complex in term of spatial and temporal distribution of fractures as indicated by Munier (1992) and Landström and Tullborg (1993). The rocks in the NE-1 zone include the Äspö diorite, fine-grained granite and about 1 m wide mylonite/cataclasite layer. Variability in primary mineralogy of the rocks indicates similar variation trends for quartz (up to 45%) and K-feldspars (up to 35%).
The amounts of primary plagioclase, biotite, amphiboles and muscovite are always below 10% in the NE-1 zone. The reduction in the amounts of primary mineral is accompanied by increase in amounts of secondary minerals and the associated high porosity.

Saussuritisation/ albitisation of magmatic plagioclase is the most common alteration feature within the deformation zone. This alteration process has affected most of the cored section of KAS09, and its extent is not different in rocks within (the interval at about 128-147 m) or outside the deformation zone as illustrated by similar fluctuations. However, the distribution pattern of saussuritised/albitised plagioclase shows a gradual decrease (from about 40% to about 20%) in the amounts from the central part towards the boundaries of the NE-1 zone. Similar trend is also displayed regarding variation in the amounts of chloritised biotite which reach up to about 15% in the central part compared to the <5% at the boundaries. No considerable differences were detected in the amounts of argillised minerals and microcrystalline chlorite along the section of NE-1 deformation zone. The abundance of epidote remains at a fairly constant value of <5% within the deformation zone.

The distribution patterns of other mineral alterations including the formation of titanite, calcite, prehnite, pumpellyite, hematite, pyrite, secondary quartz and K-feldspar do not show specific link to the deformation zone compared to other parts of the cored section. The lack of links between mineral alteration patterns and the NE-1 deformation zone is further traced in the variability of the alteration index. The alteration index displays fluctuations, which have comparable intensities and ranges in rocks within and outside the NE-1 deformation zone. However, there is a portion of the section, which shows relatively low alteration index values that extends from the deformation zone into seemingly unaltered rocks at the interval between133 m and 123 m. Limited by the number of samples examined, complex fracture types and patterns and occurrence of more than one lithologic type, it was difficult to link with a reasonable confidence a specific alteration feature as a characteristic indication of the NE-1 deformation zone.

6.1.2 Mineral distribution about the other, smaller deformation zones

In addition to the main deformation zone NE-1, there are three other major deformation zones (100-110 m, 249-255 m and 391-420 m) in KAS09. Inspection of fracture type and porosity logs, however, indicates occurrence of elevated porosity values and extensive fracturing close to the zone demarcations adopted here. The Äspö diorite and mylonite/cataclasite are the common features in these deformation zones with relatively higher amounts of quartz in the mylonite layers.

The most common alteration feature in these deformation zones is saussuritisation/albitisation of plagioclase (up to about 40%), which is neither more extensive nor has characteristic distribution than in the rock outside the zones. Greater amounts of microcrystalline chlorite and chloritised biotite occur in the deformation zones at 100-110 m and 249-255 m compared to the rocks close (few meters above and below) to these zones. This enhancement of chloritisation is not observed in the deformation zone at 391-420 m. Enrichment in secondary quartz (up to about 16%) is also observed in the deformation zone at 249-255 m and a peak of calcite (up to 10%) at the lower part of deformation zone 391-420 m. Variability in the other mineral alteration (K-feldspar, prehnite, and altered titanite) does not differ between rocks within and outside the deformation zones.

The values of the alteration index at the deformation zones (0.3 to 3.5) are similar to rocks outside these zones. As observed also for the whole cored section of KAS09, there is no relationship between the alteration index and colour of the rocks in the deformation zones. However, except the zone at 100-110 m, which contains only reddish-coloured rocks, both reddish and greyish coloured rocks occur in the other two (249-255 m and 391-420 m) deformation zones.

In summary the examined cores from KAS09 revealed that:

(i) There are no systematic trends in the extent of secondary mineral alteration with respect to the main deformation zones and in particular the NE-1.

(ii) Most core intervals that are “seemingly unaltered” show various degrees of alteration, but contain less saussuritised/albitised plagioclase and epidote than altered rock.

(iii) Rock that show least value of alteration index (<0.25) occurs outside the main deformation zones.

(iv) Apparently, each of the deformation zones behaves differently with respect to alteration mineral assemblages, which makes demarcation of the deformation zones or the sections outside, by a specific alteration domain unfeasible and corroborates earlier observations achieved by Morad and Aldahan (2002) for other drilled sections in the HRL area.

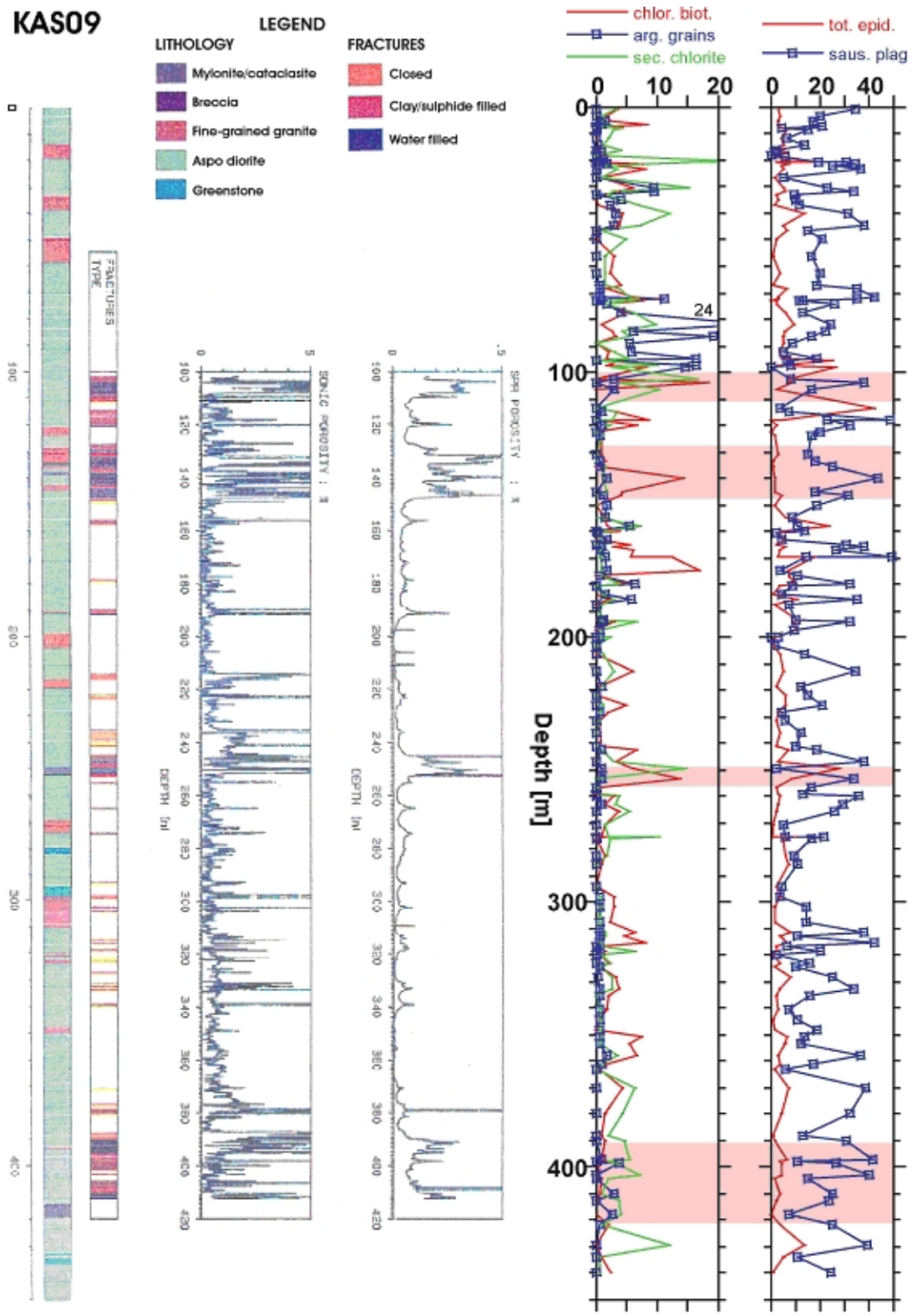

Figure 6-1A.

Figure 6-1A-E. *Borehole KAS09: Lithology, well-log porosity, and distribution pattern of magmatic and secondary minerals. Light brown -pinkish bands in the two rightmost columns denote major deformation zones. Rock colour (only in Figure 6-1E): G = grey, GR = greyish red, RG = reddish grey, R = red.*

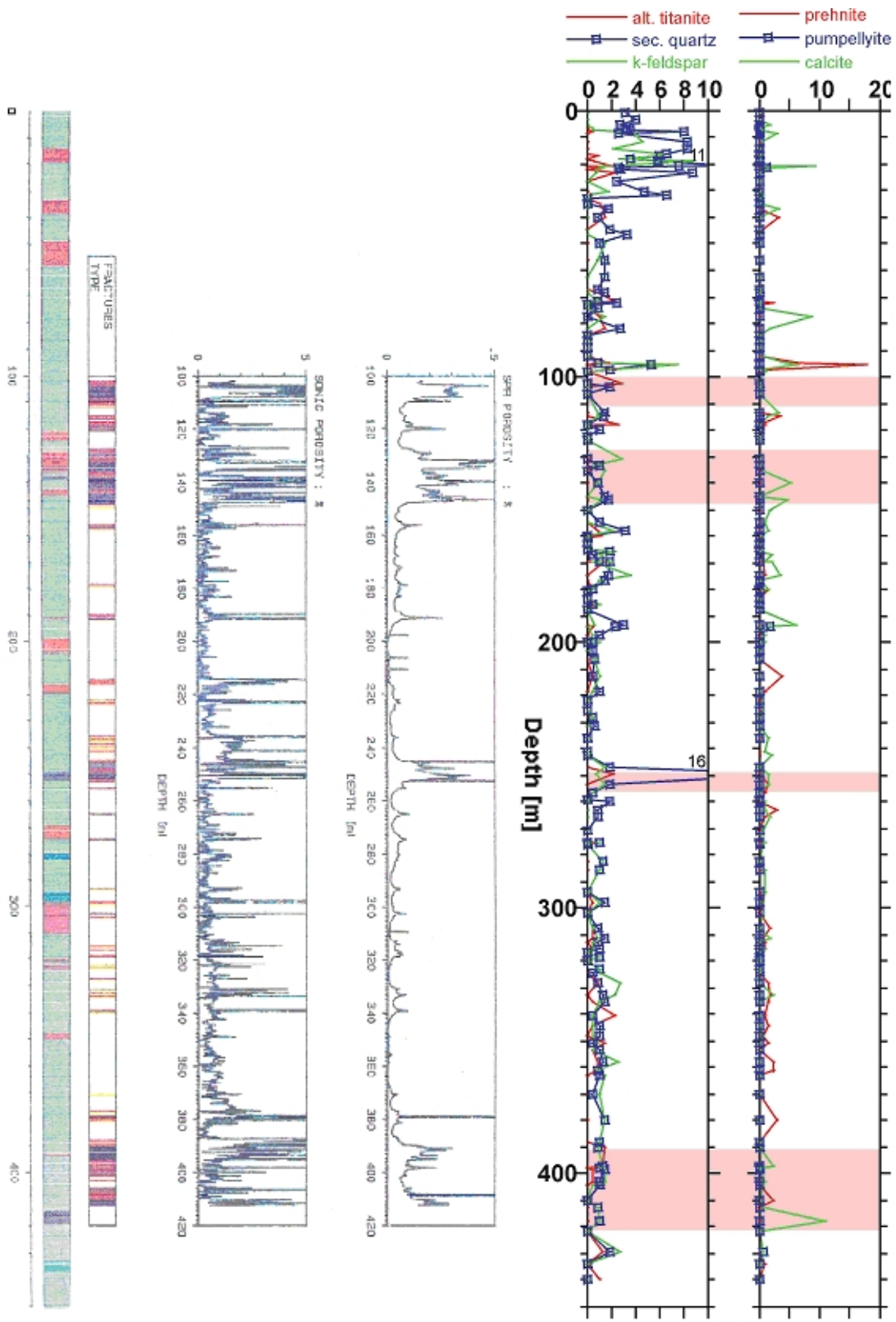
alt. titanite
sec. quartz
k-feldspar
prehnite
pumpellyite
calcite
Depth [m]
11
16

Figure 6-1B.

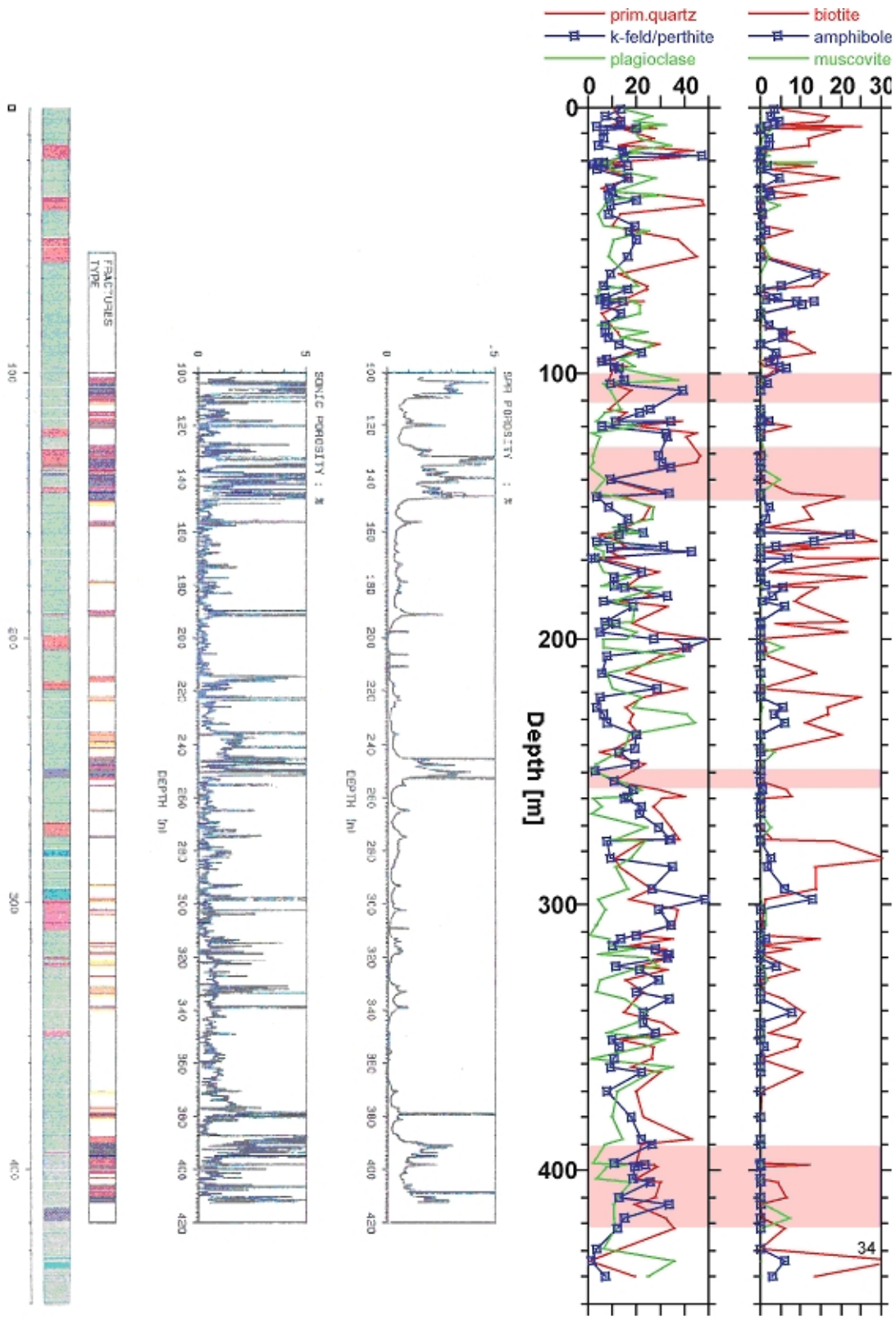
prim.quartz
k-feld/perthite
plagioclase
biotite
amphibole
muscovite
Depth [m]
34

Figure 6-1C.

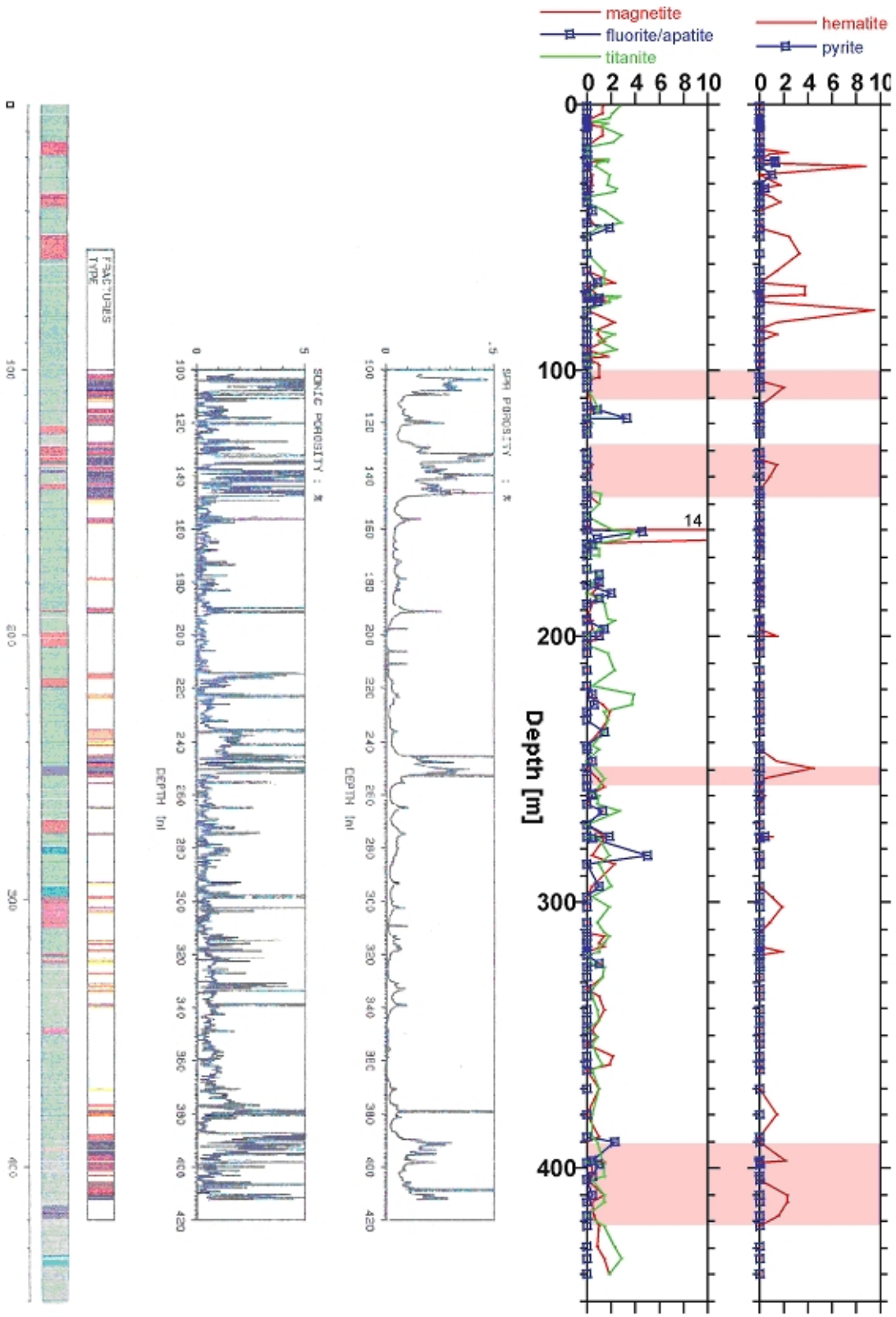
magnetite
fluorite/apatite
titanite
hematite
pyrite
0 2 4 6 8 10
0 2 4 6 8 10
0
100
200
300
400
Depth [m]
14
FEATURES
TYPE
SONIC POROSITY : %
DEPTH [m]
SPR POROSITY : %
DEPTH [m]

Figure 6-1D.

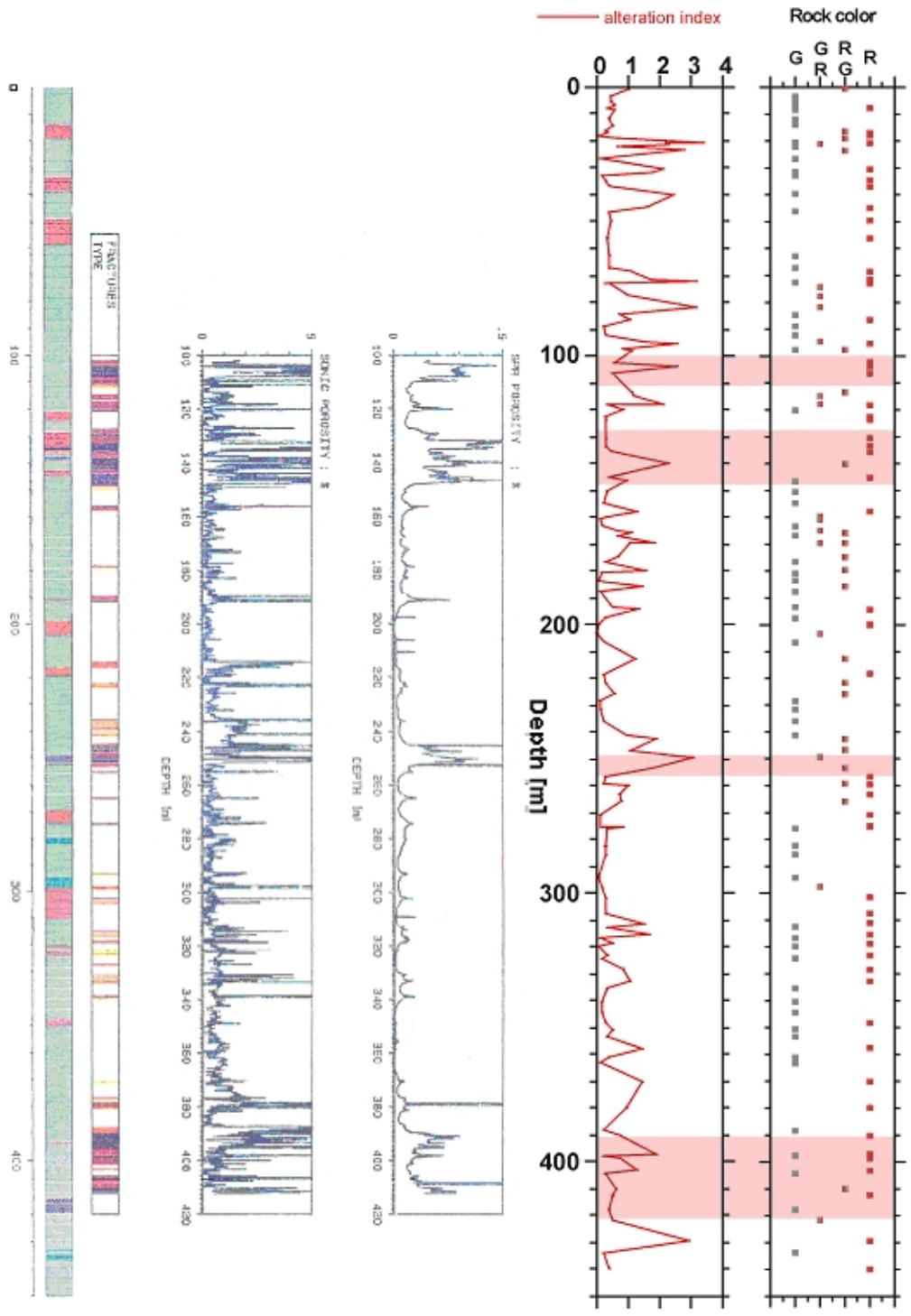
alteration index
Rock color
0 1 2 3 4
G
G R
R G
R
0
100
200
300
400
Depth [m]

Figure 6-1E.

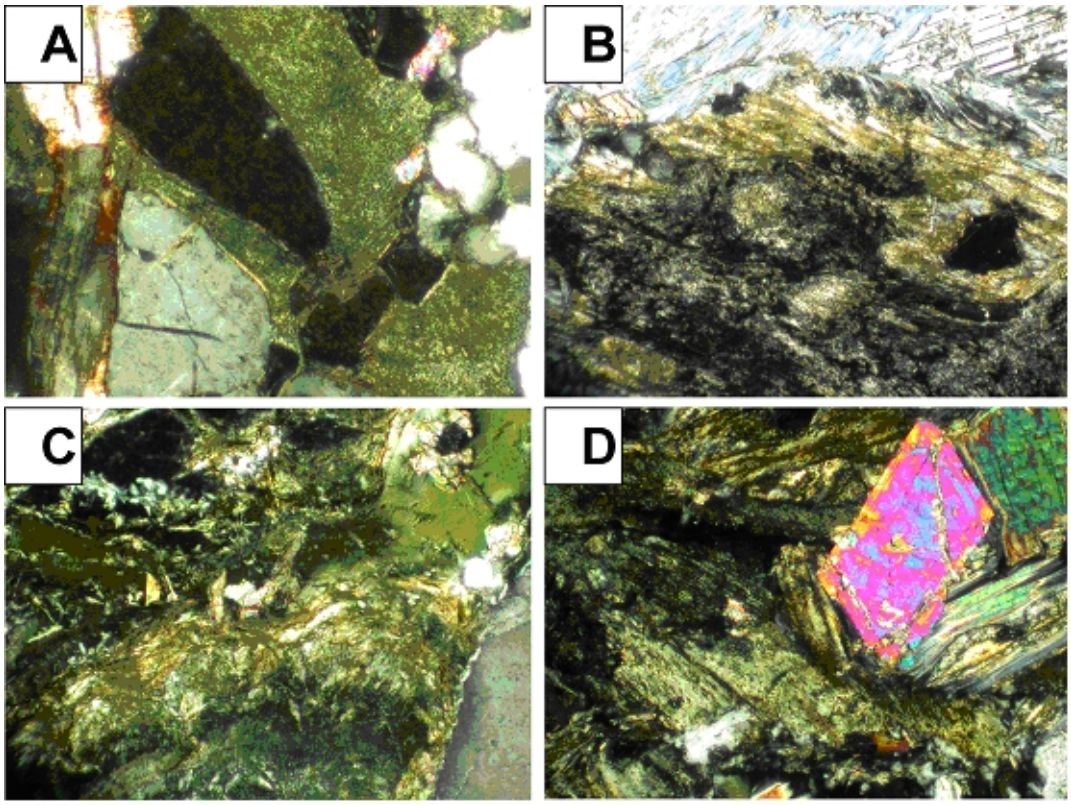

Figure 6-2. *Optical micrographs (X-nicols) showing various textural types of argillised magmatic minerals.*

6.2 KAS14

The lithology, well-log porosity, distribution patterns of primary and secondary minerals encountered in borehole KAS14 are displayed in Figures 6-3A, B, C, D, and E.

Although KAS14 was drilled at about only 100 m east of KAS09 and covers a depth interval of about 212 m, its lithologic section shows some differences with respect to abundance and type of rocks (Table 4-1). The Äspö diorite dominates (75%) the cored interval, followed by the fine-grained granite (18%), Småland granite (16%) and the greenstone (1%). The types of fractures encountered in KAS14 are rather similar to those observed in KAS09, but the frequency of fractures per meter is relatively higher in KAS14. The location of the main deformation zone NE-1 in KAS14 is located at about section 98-129 m. In addition to the NE-1, there are four other major deformation zones at 51-57 m, 81-89 m, 154-166 m and 183-202 m.

The abundant fracturing and deformation in the cored section of KAS14 is reflected by the relatively frequent occurrence of high porosity zones, and a few cm wide mylonite/cataclasite bands. The range of variability in the amounts of primary magmatic minerals (quartz, K-feldspar-perthite, plagioclase, biotite, amphibole, muscovite, titanite, magnetite, fluorite and apatite) of KAS14 is shown in Table 6-1. The data reveal relatively lower average values for the amounts of quartz, K-feldspar, biotite and amphibole, but a higher average value for titanite in KAS14 compared to KAS09. No significant difference in the average amounts of plagioclase, muscovite, magnetite, fluorite and apatite is observed between the two borehole sections.

The depth-related trends of change in the distribution pattern of primary minerals in the cored section of KAS14 indicate a generally decreasing amount of quartz with depth. The variability in the amount of K-feldspar shows also a similar tendency to that of quartz. The amount of plagioclase in the rock is fairly low (< 10%) at the top (the upper 30 m), but it does not exceed 40% at deeper parts of the borehole. There is no clear difference between the amounts of quartz, K-feldspars and plagioclase within and outside the deformation zones. The biotite distribution trend is not depth-related in the rock section and its amounts vary from near zero to about 20%. A narrower variability range is observed for amphibole. The amounts of both minerals do not depend on occurrence within or outside the deformation zones. Muscovite occurs in rather small amounts (≤ 2%) at sporadic places in the rock section and there is no correlation to the deformation zones. Similarly, low abundance and scares occurrence mode is found for fluorite and apatite. The amounts of titanite and magnetite show, however, observable fluctuations in the cored section that are obviously not related to location within or outside the deformation zones.

As is the case in the rock section of KAS09, saussuritised/albitised plagioclase is usually the most abundant mineral alteration in the rock section of KAS14. The average abundance of saussuritised/albitised plagioclase is higher (about 25%) in the section of KAS14 compared to the average value of about 18% in the section of KAS09. Furthermore, all the rocks examined in KAS14 have amounts of saussuritised/albitised plagioclase above 6%, whereas the abundance of this alteration becomes nearly nill (<0.1%) in some rocks of KAS09.

The overall variability in the amounts of saussuritised/albitised plagioclase along the rock section of KAS14 is from about 6 to 50% with an average of 25%. The magnitude of scatter in the values does not depend on occurrence within or outside the deformation zones, although the lowest amount (about 10%) of saussuritised/albitised plagioclase in KAS14 is found in rocks outside the deformation zones.

The amounts of chloritised biotite indicates maximum and average values of 6% and 1.7% respectively, which are lower than those found in KAS09 (18% and 2.6%, respectively). There are no differences in distribution pattern of chloritised biotite in KAS14 with regard to occurrence in or proximity to deformation zones. Similar variation trends are shown by the amounts of chlorite and argillised minerals with the latter being absent from the top 70 m of the borehole. The maximum (22%) and average (6%) values of chlorite in the section of KAS14 are higher than in the section of KAS09. The average amount (2.3%) of argillised minerals in the section of KAS14 is higher than in KAS09, but a higher maximum value is found in the section of KAS09.

Large differences are also found in the amounts of epidote between the two boreholes, where maximum and average values of 20% and 7%, respectively, occur in KAS14 compared to the 42% and 5%, respectively, in KAS09. The distribution pattern of epidote along the cored section of KAS14 shows some variations. The highest amount (20%) occurs in a sample within a deformation zone at 183-202 m, but this value dose not alter the general picture of absence of correlation between variation in abundance of epidote near or in deformation zones compared to other parts of the section.

Secondary quartz shows lower average (1.4%) and maximum (6%) values in KAS14 than in KAS09 (1.7% and 16% respectively), whereas the average amount of secondary K-feldspar is higher in KAS14 (1.3%) compared to the value in KAS09 (0.9%). No difference is found in the maximum amount (about 3%) of altered titanite between the two boreholes, but the average amount is higher in KAS14 (0.5%) compared to that in

KAS09 (0.2%). The occurrence of secondary quartz, K-feldspar and altered titanite in the rocks of KAS14 is in amounts < 6% as well as with distribution patterns that is not accentuated by the deformation zones.

Although prehnite and calcite are commonly found in fairly small amounts (<1%), these minerals reach up to 11% and 7% in a few localised places in the rock section. However, relatively higher average amount (1.2%) of prehnite is found in KAS14 than in KAS09 (0.5%), but higher maximum amount is found in KAS09. The occurrence habit of calcite in the two boreholes is also similar to prehnite, where higher average and lower maximum amounts are found in KAS14 compared to that in KAS09. Distribution patterns of prehnite and calcite display no specific variations with respect to proximity to boundary of, or with regard to occurrence within or outside, the deformation zones.

Pumpellyite is a rare mineral in the rocks of KAS14 and when it occurs, it is in amounts <1%. Similar trend of occurrence is also shown by pyrite, and both minerals do not show any correlation between their abundance and the deformation zones. Hematite is generally a more frequent mineral in KAS14 than pyrite. The amount reaches up to 4%. Similar to what is observed in KAS09, small amounts (< 1%) of hematite are enough to make the colour the rock reddish. This feature is not related to location of rock within or outside the deformation zones.

Correlation between the overall degree of rock alteration and proximity to deformation zone is not indicated by the distribution of alteration index values in section of KAS14. Except for one sample (with a value of 5), the scatter in the alteration index values falls between about 0.1 and 3; a range comparable to values found in KAS09. As is also the case in KAS09, there is no correlation between the colour of the rocks and alteration index.

The correlation coefficient matrix between the different minerals of KAS14 is shown appendix 6-2. The data indicate lack of significantly correlated parameters, and the values of the correlation coefficient are similar to those observed in the correlation matrix of KAS09. Indications of rather weak negative correlation coefficient values between primary and secondary minerals persist also in KAS14. As mentioned above, the passage of the main deformation zone NE-1occurs at about 98-129 m. Distribution patterns of alteration minerals in the NE-1 zone and other deformation zones do not show specific trends compared to the rocks outside the zones.

Overall, the intensity of fracturing and deformation in KAS14 is higher than in KAS09. This feature, however, did not largely alter the distribution patterns of mineral alteration with regard to occurrence within or at proximity to deformations zones. The general patterns of alteration in KAS14 can be summarised as:

(i) Saussuritisation/albitisation of plagioclase and chloritisation are the most common alteration phenomena in the rock section which do not show correlation with deformation zones.

(ii) Epidote, secondary quartz and K-feldspar, and altered titanite show distribution pattern that is not accentuated by the deformation zones and the same trend is shown for prehnite and calcite.

(iii) The spatial and temporal complexity of fracture patterns conforms to the lack of correlation between intensity and/or type of mineral alteration and the deformation zones.

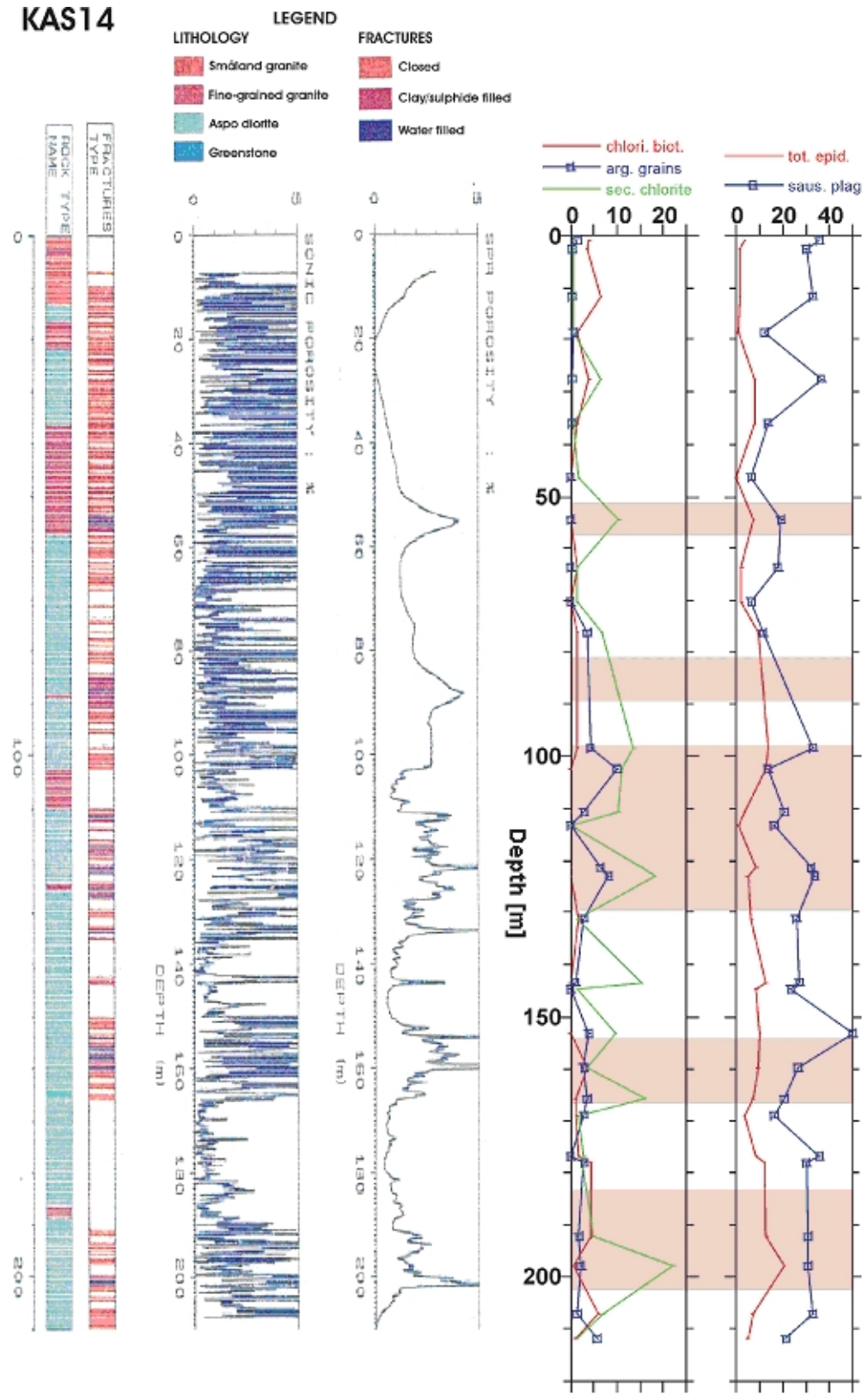

Figure 6-3A.

Figure 6-3A-E. *Borehole KAS14: Lithology, well-log porosity, and distribution pattern of magmatic and secondary minerals. Light brown-pinkish colour bands in the rightmost columns denote major deformation zones. Rock colour (only in Figure 6-3E): G = grey, GR = greyish red, RG = reddish grey, R = red.*

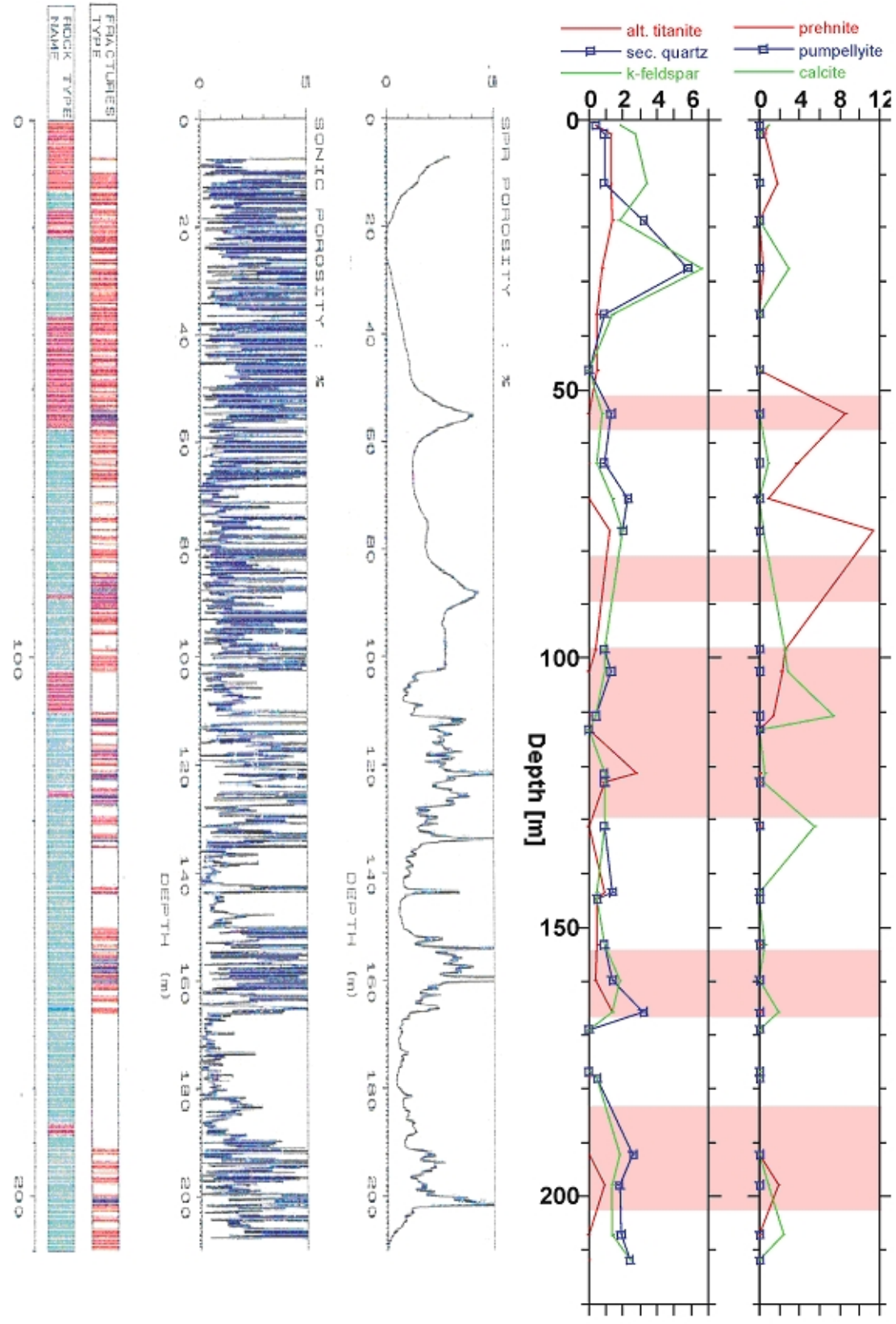
alt. titanite
sec. quartz
k-feldspar
prehnite
pumpellyite
calcite
Depth [m]
ROCK NAME
ROCK TYPE
FRACTURES
TYPE
SONIC POROSITY : %
SPR POROSITY : %
DEPTH (m)

Figure 6-3B.

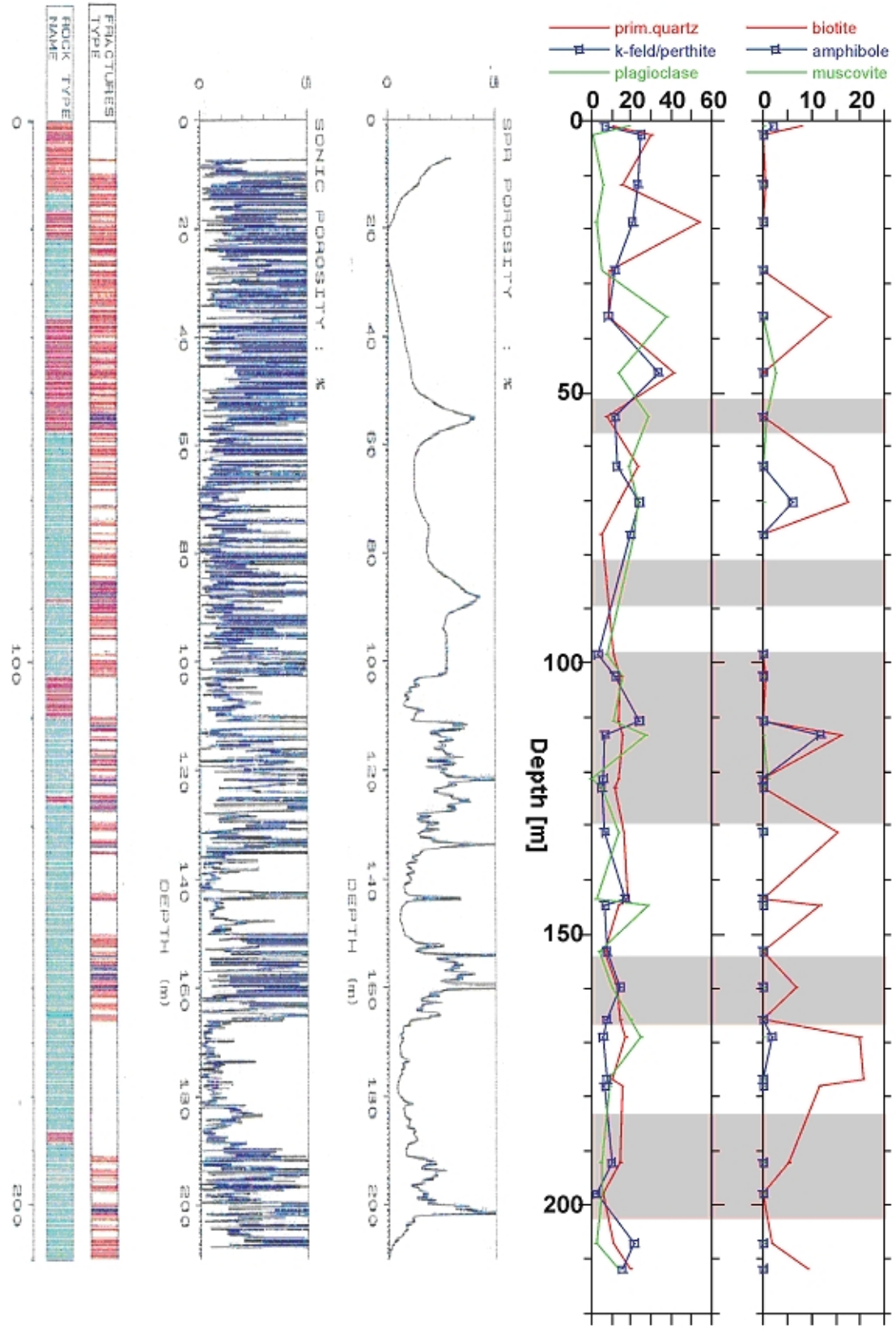
ROCK NAME
TYPE
FRACTURES
TYPE
SONIC POROSITY : %
DEPTH (m)
SPR POROSITY : %
DEPTH (m)
prim.quartz
k-feld/perthite
plagioclase
biotite
amphibole
muscovite
Depth [m]

Figure 6-3C.

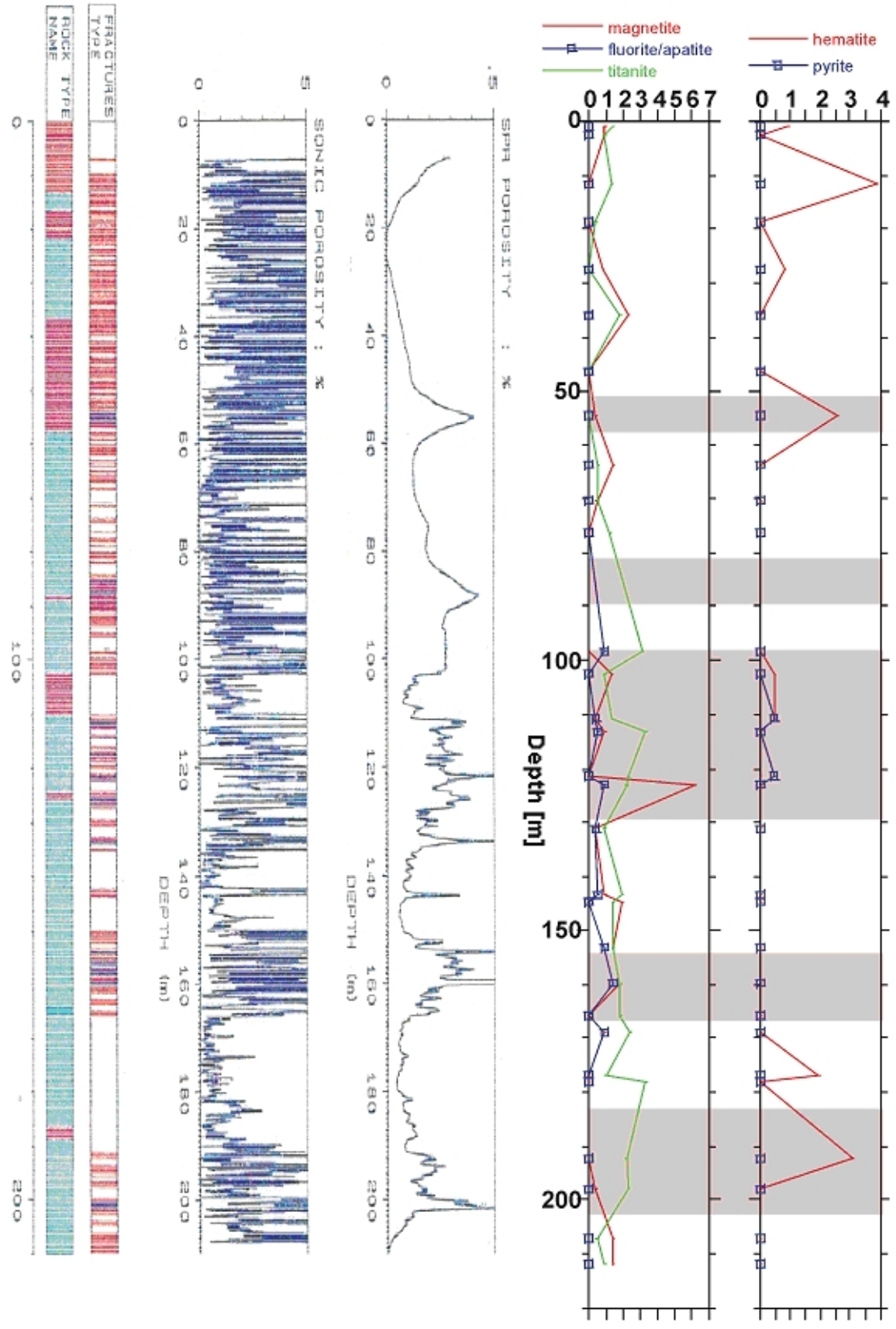
magnetite
fluorite/apatite
titanite
hematite
pyrite
Depth [m]
SONIC POROSITY : %
SPH POROSITY : %
DEPTH (m)
ROCK NAME
ROCK TYPE
FRACTURES TYPE

Figure 6-3D.

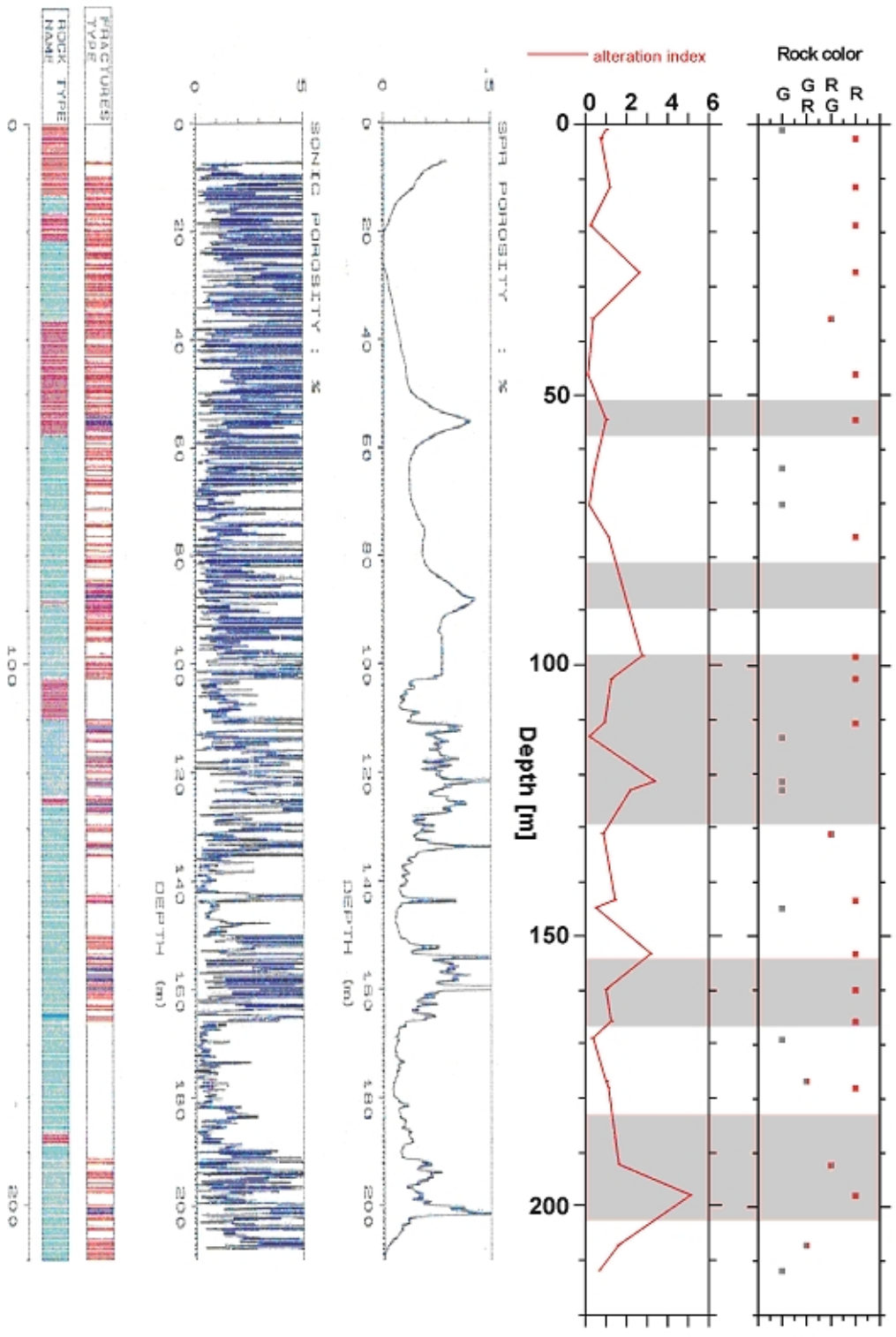
alteration index
Rock color
G
G R
R G
R
0 2 4 6
Depth [m]
0
50
100
150
200
ROCK TYPE
FRACTURES TYPE
SONIC POROSITY : %
SPR POROSITY : %
DEPTH (m)

Figure 6-3E.

7 Secondary porosity

Porosity in unaltered, non-fractured rocks of the Äspö granitic rocks has been shown by Eliasson (1993) to fall mainly in the narrow range of 0.13-0.20%, whereas the altered rocks have porosity values ranging between 0.15 and 0.83%. The relatively wide range of porosity values in the altered rocks was attributed by Eliasson (1993) to heterogeneous distribution of open fractures. Porosity in granites may also develop owing to episynitization (Petersson and Eliasson, 1997; Recio et al, 1997). Well-log porosity reveals higher values (up to ca 5%) in the fractured zones.

Results of our work indicate that porosity in the studied rocks occurs as secondary micro pores (< 10 μm), which occurs mainly within albitised and saussuritised plagioclase, and to smaller extent within K-feldspar and argillised grains, primarily chloritised biotite, feldspar and titanite. The amounts of micro-pores are difficult to quantify by means of petrographic studies.

Although the formation of micro-pores does not modify considerably fluid flow in the bedrock, it can enhance mineral reactions in the system through promoting the diffusive, ionic flux. Ionic diffusion and the resulting mineral alterations are most significant on the scales of 10 metres or less. Moreover, rocks containing micro-porosity and have extremely low permeability values enhance increase in fluid pressure (Lockner and Byerlee, 1995) and indicate that fluid flow occurred along the fractures, whereas reactions in the host rocks were mediated by ionic diffusion.

8 Discussion

8.1 Spatial distribution of secondary minerals about the deformation zones

The complex array of secondary mineral alterations in Äspö granitic rocks and their spatial distribution about deformation zones are influenced by the tectonic fracturing as well as by local variation in the composition of hydrothermal fluids and to variations in the primary mineralogical composition of the rocks (Tullborg et al., 1995, 1996; Morad and Aldahan, 2002). The spatial distribution of secondary alterations in the two drill cores is complicated by the presence of major deformation zones at certain intervals as well as of a number of local fractured zones that vary in intensity and extent throughout the cored intervals. Thus, the types, extent and distribution patterns of secondary mineral alterations vary among the two studied drill cores and display little or no consistent and systematic spatial relationships in terms of distance from the main deformation zones.

Several types of mineral alterations occur throughout the cored sections, both within and outside the main deformation zones; in the latter cases, alterations are bounded to local fractures. Thus, peaks of relatively high alteration index values occur in the close vicinity of the main deformation zone as well as in the vicinity of moderate-sized and local, minor fractures. The amounts of albitised/saussuritised plagioclase display a weak, general increment tendency towards the main deformation zone.

Although the alteration index values are generally higher in fractured rocks, considerable alteration degrees are also encountered in the seemingly unaltered rocks located at distances of several tens of metres or more from the main deformation zones. Some of the alteration features (e.g., amounts of argillised grains as microcrystalline quartz and feldspar) are abundant within a few metres thick zone around the anomalously porous zone. Although there is no systematic pattern of mineral association throughout the cored sections, some of the mineral alterations show a general trend of co-variation. Examples of such alterations include: (i) saussuritisation/albitisation of plagioclase and pseudomorphic chloritisation of biotite, and (ii) presence of fracture- and void-filling chlorite and epidote.

8.2 Secondary-mineral assemblages: clues to conditions of granite-fluid interaction and mineral paragenesis

The types and extents of mineral formation and alteration in crystalline bedrock of Äspö vary widely at different scales ranging from one grain to another or one fracture to another even on thin-section scale. This complex pattern is attributed to variations in: (i) the spatial and temporal chemical composition of hydrothermal fluids, (ii) pressure-temperature conditions, (iii) kinetic control on the hydrothermal reactions related to parameters such as the composition of magmatic minerals, and duration of fluid-rock interaction, and (iv) rates of fracture sealing and consequent rates of decrease in permeability, due to tectonic stresses and mineral precipitation. However, the overall mineral paragenesis is interpreted to have been accomplished during several episodes

that were presumably associated with successively falling temperatures and recursive formation of numerous secondary minerals. Recursive formation of secondary minerals during cooling of granitic bodies is probably aided by hydrothermal fluid convections, as revealed by D/H and $^{18}O/^{16}O$ isotope studies by, e.g., Jenkin et al. (1992). Convection cells are induced by temperature differences between a deep, hot zone and a shallower, colder regime.

The resulting complex paragenetic history, together with the lack of detailed fluid inclusion analyses, makes it difficult to determine the precise formation timing of each secondary mineral. However, a paragenetic sequence was reconstructed by Morad and Aldahan (2002) based on textural relationships among secondary minerals in individual void/fractures and on their cross cutting relationships. Alteration of the granitic rocks and the formation of secondary minerals are believed to have occurred during at least five main episodes that are related to major tectonic events that have influenced the region (Morad and Aldahan, 2002). The conditions prevailed during formation of various mineral assemblages will be constrained based on equilibrium diagrams and the chemical composition of individual secondary mineral phases.

8.3 Chloritised biotite and saussuritised plagioclase

Initial hydrothermal alterations, which have occurred concomitantly with and/or immediately after crystallisation of the magma and related release of magmatic fluids, include:

(i) Pseudomorphic chloritisation of biotite, which can tentatively be envisaged as follows (assuming that the immobile aluminum is conserved among the solid phases):

Eq. 1

$$1.4K_{1.96}(Fe_{2.3}Mg_{3.1}Al_{0.3}Ti_{0.2})(Al_{2.4}Si_{5.6})O_{20}(OH)_4 + 0.5Fe^{2+} + 1.5Mg^{2+} + 0.3Ca^{2+} + 4H_2O \rightarrow$$

Biotite

$$(Fe_{3.9}Mg_{5.8}Al_{2.1})(Al_{1.8}Si_{6.2})O_{20}(OH)_{16} + 2.7K^{+} + 0.3CaTiSiO_4 + 0.5H_4SiO_4 + 2H^{+}$$

chlorite titanite

This chloritisation reaction has thus consumed iron, magnesium, calcium and water, but resulted in the liberation of potassium (incorporated in sericite within saussuritised plagioclase), silica and protons. The incorporation of potassium ions in sericite is an important prerequisite for the chloritisation of biotite that requires low a_{K^+}/a_{H^+} ratio in the hydrothermal fluids (Figure 8-1).

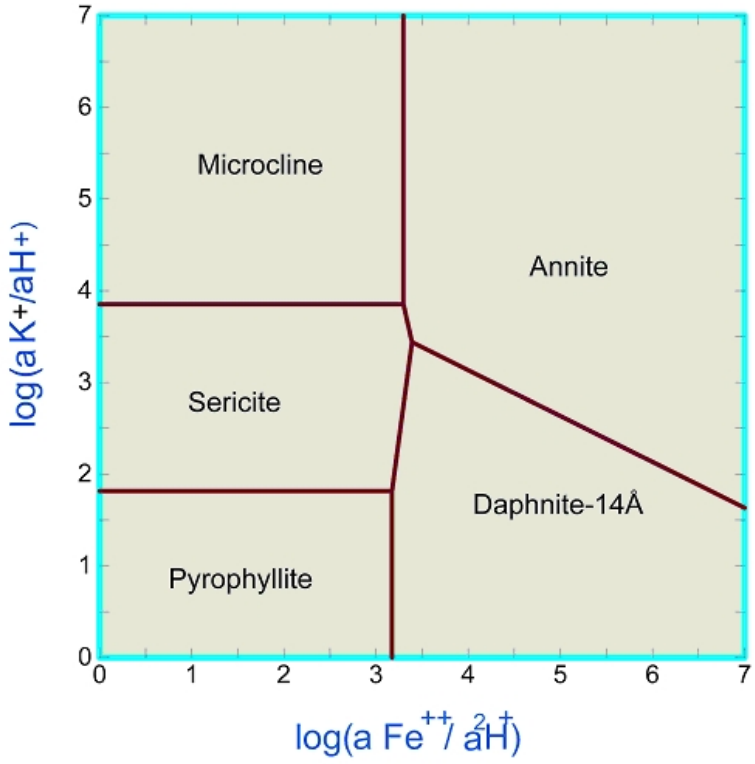

Figure 8-1. *Stability relations among K_2O-FeO-Al_2O_3-SiO_2-H_2O minerals as a function of activity ratios of $a_{Fe}^{2+}/a^2_{H}^{+}$ and a_K^+/a_H^+ at 300ºC and 2000 bars showing that alteration of Fe-biotite (annite) into Fe-chlorite (daphnite) requires mainly a decrease in a_K^+/a_H^+.*

(ii) Saussuritisation of magmatic plagioclase (i.e., formation of albite, epidote and sericite) can be presented tentatively as follows:

Eq. 2

$$6.0Na_{0.7}Ca_{0.3}Al_{1.3}Si_{2.7}O_8 + 0.8Fe^{2+} + 0.8K^+ + 1.9Ca^{2+} + 0.7H^+ + 14H_2O \rightarrow$$

Plagioclase

$$NaAlSi_3O_8 + Ca_{1.9}Fe_{0.8}Al_{2.2}Si_{3.0}O_{12.5} + K_{0.8}(Fe_{0.5}Mg_{0.2}Al_{3.3})(Al_{1.7}Si_{6.3})O_{10}(OH)_2 +$$

Albite epidote sericite

$$+ 7.4H_4SiO_4 + Na^+ + 5.2H^+$$

Thus, this reaction consumes potassium, iron, calcium, water and protons; potassium and iron are anticipated to be derived from the concomitant chloritisation of biotite (Eq. 1).

These alteration processes, which display no obvious relationship to main deformation zones, are believed to have occurred due to advective and diffusive mass flux in fluid-filled fracture systems and along thin water films that occurred along crystal boundaries and along dislocation, cleavage and twinning planes. The overall hydrothermal alteration reactions of biotite chloritisation and plagioclase saussuritisation that occurred at this stage can thus be summarised as follows:

Biotite+plagioclase→chlorite+albite+sericite+epidote+Al-rich titanite (± prehnite).

These alteration reactions were probably mediated by hot, aqueous solutions exsolved from the granitic magma at a temperature of 400ºC (± 50ºC; Turpault et al., 1992; Eliasson, 1993). The Fe-rich composition of secondary epidote suggests formation temperatures of ≤ 350ºC, but f_{O2} and P_{fluid} influence epidote composition too (Liou et al., 1983). The Al^{iv} content and the equation of Cathelineua (1988) indicate that the chlorites in the studied rocks have been formed at wide range of temperatures; the chlorites that have replaced the biotite crystals pseudomorphically display higher formation temperatures, up to ca 350ºC (Figure 8-2).

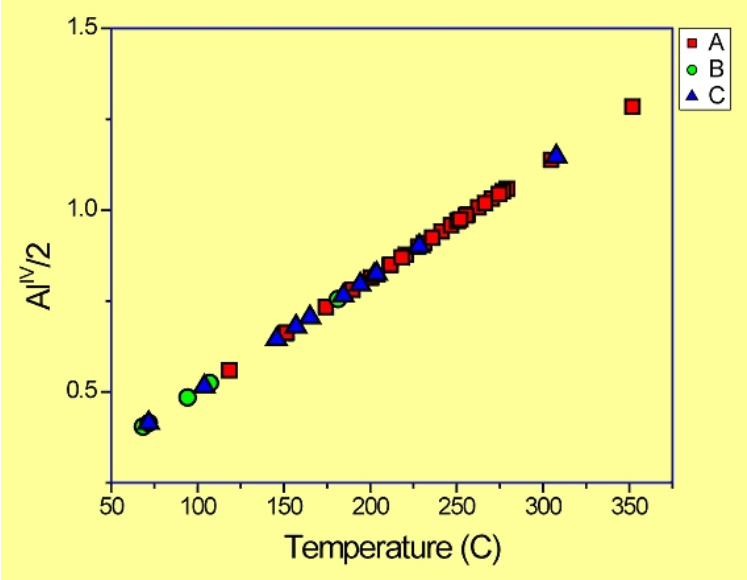

Figure 8-2. *Plot of Al^{iv} content in chlorites with various occurrence habits as a function of temperature. Temperatures are constructed based on the equation of Cathelineua (1988). Although this is not an accurate method, the formation temperatures of chlorite vary widely between 350ºC, which is obtained for chlorite pseudomorphically replacing biotite. A = chlorite pseudomorphically replacing biotite, B = microcrystalline chlorite replacing biotite; C = microcrystalline void/fracture filling chlorite.*

Although the phengitic composition of sericite indicates elevated formation temperatures, it is difficult to determine the precise formation temperature. The reaction above was most likely enhanced by Fe- leaching from the biotite (Cerney and Povandra, 1972; Coombs et al., 1977). The presence of pseudo-hexagonal hematite within chloritised biotite suggests that these fluids had elevated oxygen fugacity.

8.3.1 Chlorite, albite, epidote, titanite and prehnite

Hydrothermal alteration resulted in the formation of a chlorite, epidote, titanite, and prehnite assemblage and in further chloritisation of biotite. Morad and Aldahan (2002) suggested that the hydrothermal alterations occurred at temperatures of about 300-400ºC (± 50ºC; Tulloch, 1979; Freiberger et al., 2001) induced by the Gothian

orogeny (1500-1400 Ma). The alterations were aided by tectonic deformation and/or by emplacement of the Götemar granite. Granite emplacement supplies fluids by exsolution and induce convectional fluid flow. The formation of hydrogarnet (Morad and Aldahan, 2002), together with the presence of unaltered amphibole and the formation of this suite of secondary minerals, is suggested to have occurred at temperatures up to 300-400ºC and pressures up to a few kilobars (Coombs et al., 1977; Liou et al., 1983; Ishizuka, 1999). The Fe-rich epidote and prehnite are common in active geothermal fields and form often together at temperatures of about 300ºC (Bird et al., 1984).

8.3.2 K-feldspar, albite, chlorite/berthierine, prehnite, smectite/vermiculite, pumpellyite, and laumontite

The stability fields and chemical composition of the secondary mineral assemblage formed at this stage of hydrothermal alteration suggest formation at temperatures of about 200-300ºC (± 50ºC; e.g., Liou et al., 1983; Frey et al., 1991; Affaton et al., 1 997; Gianelli et al., 1998), and resulted in the precipitation of K-feldspar, albite, Fe-chlorite/berthierine, fluorite, trioctahedral smectite or vermiculite, pumpellyite, and laumontite (± prehnite; ± Al-titanite). These minerals occur as fracture/void fillings and as replacement of magmatic minerals, primarily biotite and plagioclase.

Although pumpellyite is usually believed to be part of the prehnite-epidote assemblage of low grade metamorphic conditions (Coombs et al., 1977; Aldahan, 1989), we have no textural evidence to support such a postulation. Instead, the presence of pumpellyite exclusively within biotite that is partly chloritised and partly altered into illite/vermiculite suggests lower precipitation temperature than needed for the prehnite-pumpellyite-epidote assemblage (Liou et al., 1983). This pattern of pumpellyite formation further suggests that biotite provided suitable geochemical conditions and/or ions needed for pumpellyite formation. All ions except Ca^{+2} could be provided by the host biotite, whereas K was diffused outside the biotite crystals to precipitate as sericite and secondary K-feldspar. The latter has in some cases crystallized within biotite crystals that are replaced by chloritic and smectitic minerals.

Ca-plagioclase is believed to be a sufficient source for the formation of Ca-Al silicates in granitic and dioritic rocks (Tulloch, 1979). Ca^{+2} ions needed for the formation of Ca-Al silicates in the studied rocks have likely been derived from the replacement of plagioclase by albite and K-feldspar. Biotite may also have had a catalytic effect on pumpellyite formation related to leaching of K from biotite and incorporation of H^+, which would in turn enhance a local increase in pH that promotes the precipitation of pumpellyite (Freiberger et al., 2001). Fluids within chloritised biotite were thus characterized by high $a_{Ca}^{2+}/a^2_{H}{}^{+}$. According to the constructed stability diagram of log $(a_K{}^{+}/a_H{}^{+})$ vs log $a_{Fe}{}^{2+}/a^2_H{}^{+}$), the replacement of biotite (annite) by Fe-chlorite occurs when the fluids become characterised by decreasing $a_K{}^{+}/a_H{}^{+}$; considerably lower log $(a_K{}^{+}/a_H{}^{+})$ ratios are needed to stabilise Fe-chlorite at the expense of biotite with increase in the $a_{Fe}{}^{2+}/a^2_H{}^{+}$ ratio (Figure 8-3).

Alterations in the host rock occurred mainly by the replacement of plagioclase and biotite by these secondary minerals. Thus, this mineral assemblage was formed according to the following overall reaction:

Eq. 3

Anorthite + biotite + magnetite + H_2O + H_2CO_3 → K-feldspar (± albite) + prehnite +

Fe-chlorite/berthierine + Al-rich titanite

The merle albitisation of plagioclase was not accompanied by considerable precipitation of sericite and epidote, and instead resulted in vacuolated albitised plagioclase grains. Subsequent to partial albitisation, the plagioclase crystals were subjected to increasingly more replacement by hydrothermal K-feldspar that engulfs, and hence post-dates, the albite. This paragenetic sequence is also manifested by the fracture-filling feldspars, where the early fracture-lining albite was immediately followed by the much more abundant secondary K-feldspar. This trend of secondary feldspar evolution is in agreement with calculations of polythermal reaction path, in which a 1 molal NaCl fluid revealed that a decrease in temperature of the fluids is accompanied by progressive increase in secondary K-feldspar relative to albite when temperatures decreases to < 250ºC (Morad and Aldahan, 2002).

The replacement of magnetite by microcrystalline Fe-chlorite/berthierine indicates that while Fe^{2+} was derived from the dissolved magnetite, whereas other elements (Si^{4+} and Mg^{2+}) were provided by the hydrothermal fluids, as follows:

Eq. 4

$Fe_3O_4 + 6H_4SiO_4 + 3.6Al^{3+} + 3.0Mg^{2+} + 4H_2O$ → chlorite/berthierine + $17H^+$

This reaction occurs even in non-fractured, relatively unaltered rocks, suggesting that ionic supply has occurred mainly by diffusion rather than by advection along fractures. The replacement of titanite (source of Si^{4+}) by similar Fe-chlorite/berthierine further suggests that even iron could be supplied from external sources. Thus, destabilisation of magnetite and titanite has apparently provided suitable local conditions for the precipitation of hydrothermal chlorite/berthierine.

The cross-cutting relationship of laumontite with other secondary minerals suggests that it is the final hydrothermal Ca-Al silicate to form in the studied rocks. The upper stability limit of laumontite was determined experimentally to be 220-230ºC at 1-2 kbar (Liou, 1971), which was confirmed by observations on rhyolitic, andesitic and basaltic rocks from geothermal fields (Cathelineau et al., 1985; Reyes, 1990; Goff et al., 1992; Gianelli et al., 1998). At a temperature of 300ºC, the formed Ca-Al minerals are dominated by prehnite and epidote (Figure 8-3).

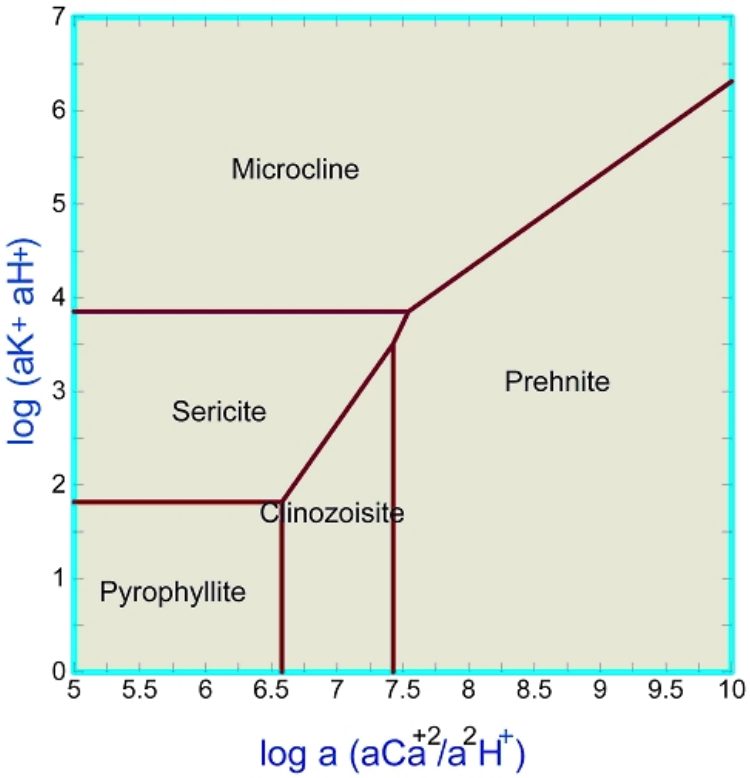

Figure 8-3. *Stability relations among K_2O-CaO-Al_2O_3-SiO_2-H_2O minerals as a function of activity ratios of $a_{Ca}^{2+}/a^2_{H}^{+}$ and a_K^+/a_H^+ at 300ºC and 2000 bars.*

The formation of laumontite at lower temperatures than these Ca-Al silicates is further supported by its appearance instead of epidote as the temperature on the stability diagram of log($a_{Ca}^{2+}/a^2_{H}^{+}$) vs log(a_K^+/a_H^+) decreases to 200ºC (Figure 8-4). Additionally, even at low temperatures (< 200ºC), the stability field of laumontite is narrow compared to sericite and K-feldspar. Overall, the stability of laumontite occurs at narrow range of log ($a_{Ca}^{2+}/a^2_{H}^{+}$) compared to prehnite and illite. The stability field of laumontite is widened slightly as temperature decreases to < about 140ºC (Figure 8-5). A further decrease in temperature coupled with a fairly small decrease in log ($a_{Ca}^{2+}/a^2_{H}^{+}$) results in the formation of smectite rather than laumontite (Figure 8-6). Additionally, the stability of laumontite is encountered at a narrow range of a_{SiO2} and temperature (ca 130-145ºC) compared to sericite (illite), K-feldspar and prehnite **(**Figure 8-7**).** The overall narrow stability field of laumontite within the accompanied mineral assemblage is believed to account for its rare occurrence in the studied rocks.

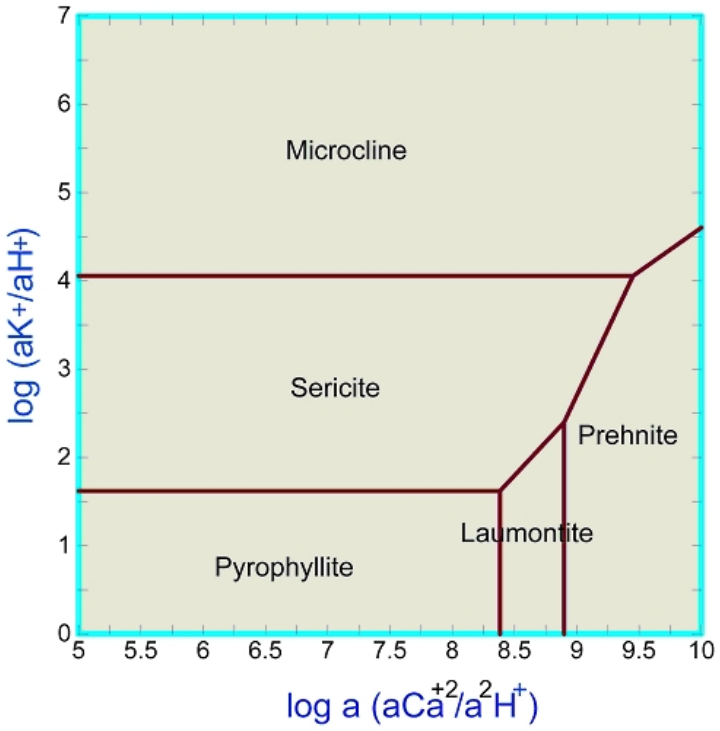

Figure 8-4. *Stability relations among K_2O-CaO-Al_2O_3-SiO_2-H_2O minerals as a function of activity ratios of $a_{Ca}^{2+}/a^2_{H}{}^{+}$ and $a_{K}{}^{+}/a_{H}{}^{+}$ at 200ºC and 1500 bars.*

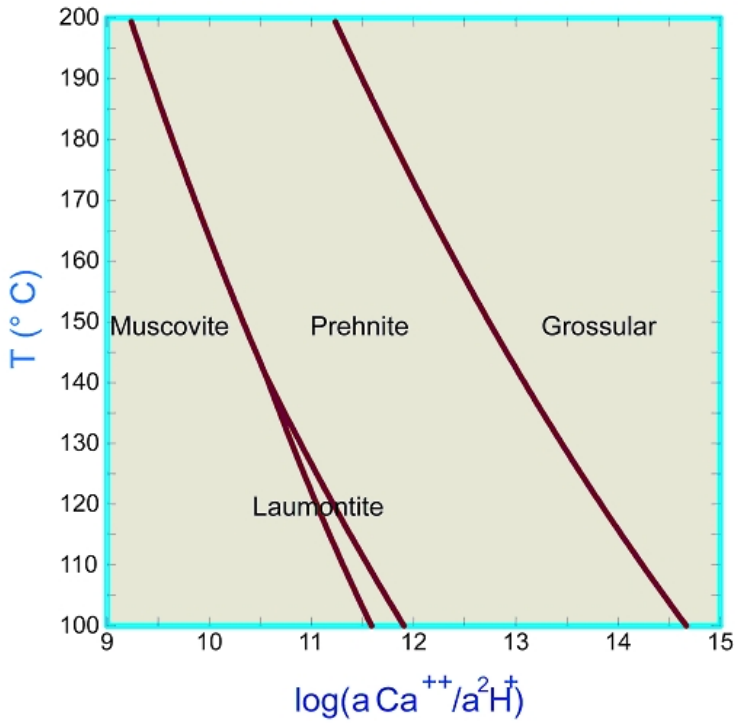

Figure 8-5. *Equilibrium diagram of log ($a_{Ca}^{2+}/a^2_{H}{}^{+}$) versus temperature demonstrating that the stability field of laumontite is narrow compared to prehnite particularly as temperature increases.*

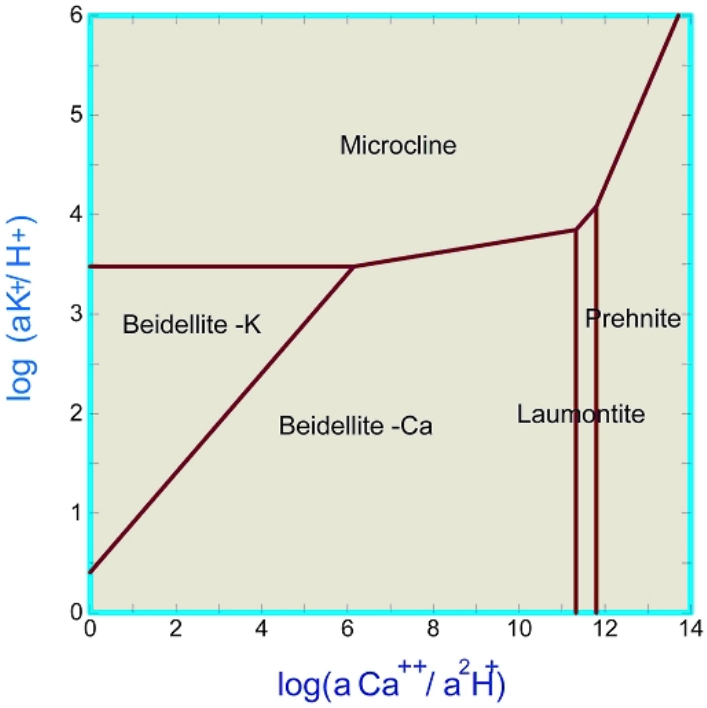

Figure 8-6. *Stability relations among K_2O-CaO-Al_2O_3-SiO_2-H_2O minerals as a function of activity ratios of log ($a_{Ca}^{2+}/a^2_{H}{}^{+}$) and log ($a_K^+/a_H^+$) at 100°C and 1000 bars showing that the stability of smectite increases, whereas the stability field of laumontite is narrow and prehnite is not formed at most of these ionic activity ratios in natural waters.*

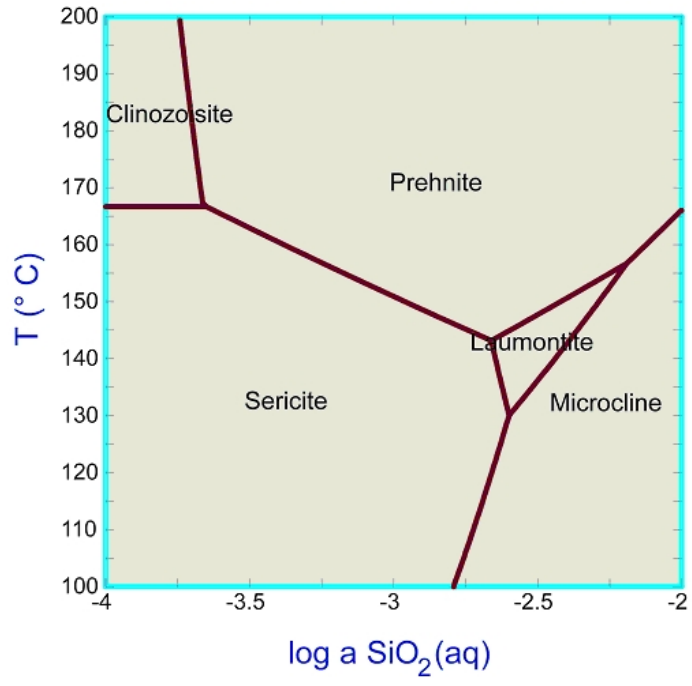

Figure 8-7. *Plot of log $a_{SiO2}(aq)$ versus temperature showing that the stability field of laumontite is overall very narrow compared to common secondary silicates. As temperature increases, prehnite rather than laumontite forms. If the increase in temperature is accompanied by considerable decrease in $a_{SiO2}(aq)$ in the fluid, epidote rather than prehnite forms.*

The assemblage illite/vermiculite, which is closely associated with chloritised biotite, is stable at temperatures as high as 270ºC (Gianelli et al., 1998). The replacement of biotite by dominantly trioctahedral smectite/vermiculite rather than chlorite in some of the samples may have occurred at temperatures as high as 200-300ºC (Seyfried and Bischoff, 1981; Berger et al., 1987; Patrier et al., 1996; Gianelli et al., 1998). Vermiculite has been reported from active geothermal fields at various temperature ranges: 326-361ºC at the Salton Sea (McDowell and Elders, 1980), 190-230ºC in Iceland (Krismannsdótter, 1975), 150-275ºC at Langano, Ethiopia (Teklemariam et al., 1996) and 150ºC to more than 300ºC at DSDP hole 504B (Alt et al., 1986).

The stability relationship between the set of secondary minerals epidote-prehnite-pumpellyite-K-feldspar-sericite is controlled by temperature, P_{CO2} as well as by the $a_{SiO2(aq)}$, $a_{Ca}^{2+}/a^2_{H}^{+}$ and a_{K}^{+}/a_{H}^{+} ratios, which is commonly encountered at 200-300ºC (e.g. Tulloch, 1979; Morad and Aldahan, 2002). The stability fields of epidote and prehnite become narrower with decrease in temperature from 300ºC to 200ºC. The formation of Ca-Al silicates requires low P_{CO2} in the pore fluids (Robinson and Bevins, 1999). An upper limit of X_{CO2} of ca 0.002 is required in order to form stable pumpellyite-prehnite assemblage at 250ºC (Digel and Ghent, 1994). At higher X_{CO2}, the assemblage epidote + chlorite forms instead.

Subsequently, a decrease in a_{K}^{+}/a_{H}^{+} ratio and/or an increase in $a_{Ca}^{2+}/a^2_{H}^{+}$ ratio has resulted in the precipitation of prehnite. The increase in $a_{Ca}^{2+}/a^2_{H}^{+}$ (and alkalinity) can result from a decrease in a_{CO2} due to fluid decompression and effervescence during fault rupture (Morad and Aldahan, 2002). Indeed, the formation of prehnite requires a low X_{CO2} (< 0.002; or a_{CO2} < 0.01 mole) in the fluids, even at temperatures as high as 300ºC in some of the fractures/voids (Liou et al., 1983; Digel and Ghent, 1994; Robinson and Bevins, 1999). Lower crystallization temperatures enhance substitution of Fe^{3+} in octahedral sites in prehnite and epidot (Bird and Helgeson, 1981; Liou et al., 1983), which explains the later paragenetic origin of Fe-rich prehnite and epidote (Morad and Aldahan, 2002). Fe-chlorite and berthierine are most common in diagenetic environments where temperatures are usually below 200ºC, but can be persistent to temperature of about 250ºC (Coombs et al., 1996).

Modelling of the pathways of mineralogical evolution during the interaction of granite with hydrothermal water at temperatures between 200 and 300ºC agrees well with the reconstructed paragenetic sequence (Morad and Aldahan, 2002). Successive decrease in temperature is associated with changes in chlorite chemistry towards more Fe-rich composition as well as a decrease in amounts of epidote and increase in amounts of prehnite. The increase in abundance of secondary albite occurs at somewhat higher temperatures than increase in K-feldspar.

Calcite has a complex paragenetic relationship with, but mostly post-dating, other hydrothermal mineral assemblages. The obtained oxygen isotopic values of calcite (-18.2 to -7.0‰) suggest wide formation temperatures (45-143ºC) assuming that precipitation occurred from hydrothermal waters with $\delta^{18}O_{SMOW}$ value of -6‰ and using the fractionation equations of Friedman and O'Neil (1977) (Appendix 8-9A; Figure 8-8). Much lower precipitation temperatures are obtained (19-90ºC) if it is assumed that precipitation occurred from hydrothermal fluids with $\delta^{18}O_{SMOW}$ value of -6‰.

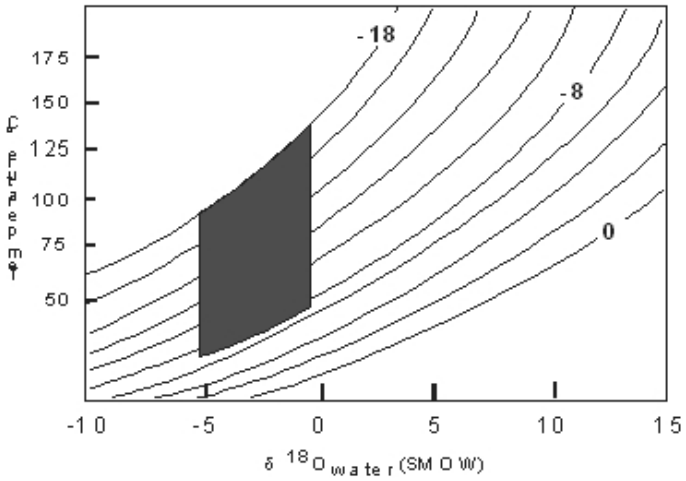

Figure 8-8. *The oxygen isotope fractionation curve between calcite and water showing that the precipitation temperatures of Äspö calcites were 45-143ºC and 19-90ºC assuming $\delta^{18}O_{SMOW}$ of water value of -1‰ and -6‰, respectively.*

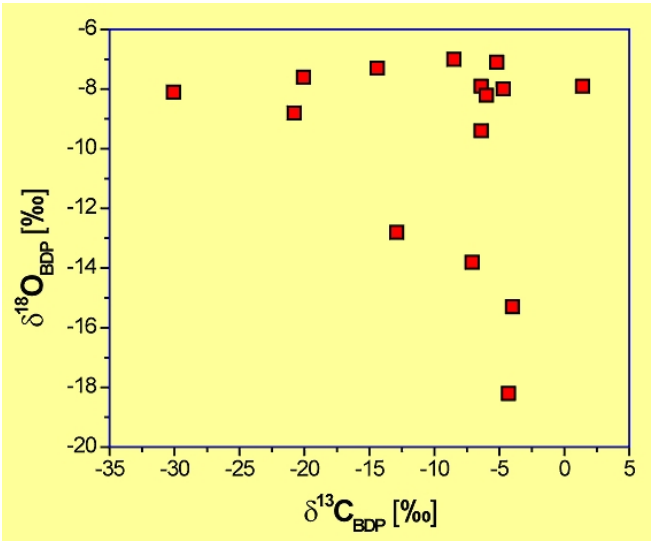

Figure 8-9 *Correlation between $\delta^{13}C$ and $\delta^{18}O$ values in calcite is very weak (R = -0.25) suggesting that calcite precipitation occurred from fluids with variable compositions and under various geological conditions.*

Although dissolved carbon needed for formation of calcite presumably could have been derived from CO_2 exsolution and degassing from the magma (Amorsson and Barnes, 1983; Barnes et al., 1988), the relatively low range of temperatures obtained based on $\delta^{18}O$ of the calcite suggests derivation of carbon from surficial waters, such as meteoric and marine waters. Furthermore, the low $\delta^{13}C$ values of calcite indicate derivation of dissolved carbon from the oxidation of organic matter (Tullborg et al., 1998). $\delta^{13}C$ values of -30 to -20‰ suggest derivation of carbon from the oxidation of methane (Morad, 1998). Enrichment of calcite analysed in ^{87}Sr suggests that strontium was derived, at least partly, from the host granite. There is no systematic trend of changes in the strontium isotopic composition in relation to the main deformation zones, suggesting that there is no regular, spatial variation in the composition of fluid in relation to the deformation zones. The correlation between $\delta^{18}O$ and $\delta^{13}C$ is weakly negative (R = -0.25; Figure 8-9), Neither the oxygen nor the carbon isotopes are correlated with strontium isotopic composition of calcite. The lack of correlation among these isotopes suggests that calcite precipitation occurred from fluids with variable compositions and under various geological conditions.

However, the decrease in $\delta^{18}O$ and, to lesser extent, $\delta^{13}C$ values of calcite that is occurring within the main deformation zones in KAS09 (Figure 8-10A) suggests precipitation from water with elevated temperatures and derivation of carbon from the oxidation of methane. In KAS14 the pattern is less obvious (Figure 8-10B). A larger number of calcite isotope analyses are required before a certain link between the isotopic composition and proximity to the deformation zones can be made.

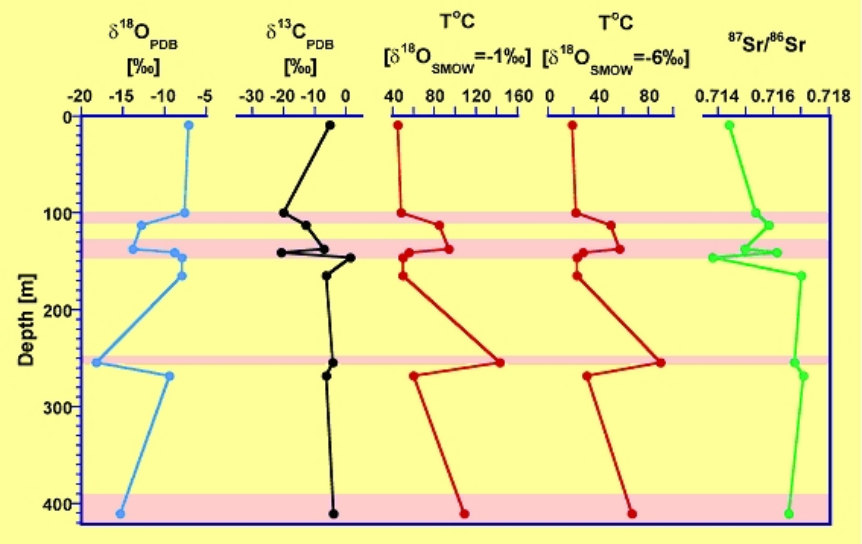

Figure 8-10A

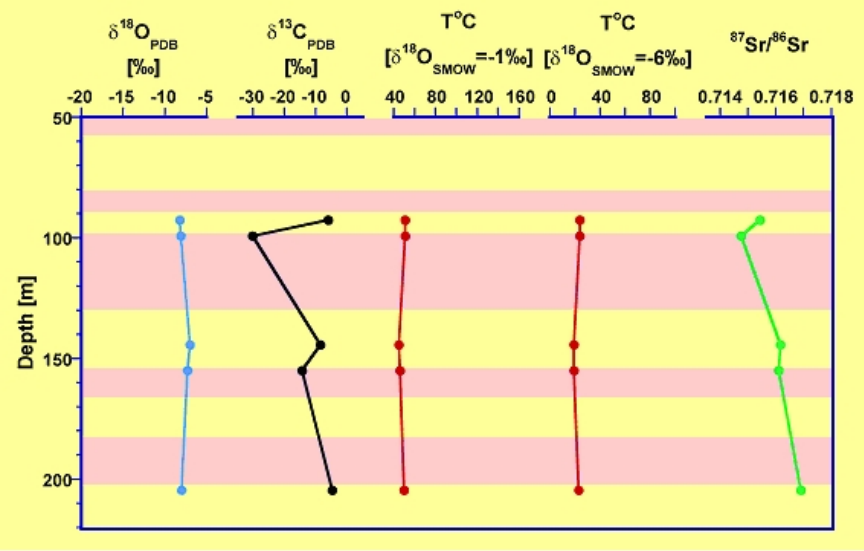

Figure 8-10B

Figure 8-10A-B. *Plot of the $\delta^{13}C$ and $\delta^{18}O$ values of calcite with depth in the sampled drill cores KAS09 (**A**) and KAS14 (**B**). There is an indication of a decrease in these isotopes in calcite from the major deformation zones in KAS09. The Sr isotopes display no systematic variation. The light brownish – pinkish bands in the diagrams indicate deformation zones.*

9 Conclusion

Petrographic and mineral chemical investigations of granitic basement rock from the Äspö Hard Rock Laboratory (boreholes KAS09 and KAS14) revealed a number of interesting findings regarding the types, extent and distribution patterns of mineral alterations. Distinguished, secondary mineral assemblages (including epidote, chlorite, prehnite, pumpellyite, titanite, laumontite, mixed-layer illite/vermiculite, albite, and K-feldspar) suggest formation by rock-fluid interactions at temperatures less than about 350ºC during various tectonic episodes that have influenced the region. Episodic alteration events coupled with the presence of numerous fracture zones that vary in intensity and geometry throughout the drill cores account for the non-systematic, spatial distribution of the secondary alterations.

These data should strongly enhance the development of accurate models of the chemical and mechanical properties, and hence suitability of the bedrock for the disposal of spent nuclear fuel. The findings of this work include:

(1) The mineral alterations are most common in fractured rocks, which were characterised by more active fluid flow compared to the host rocks. Thus, the seemingly unaltered rocks contain smaller amounts of secondary mineral alteration, the distribution patterns of which are non-systematic in relation to the main deformation zones, but are, instead, rather fairly strongly controlled by the presence of local fracture zones of various dimensions.

(2) The volumetrically most important mineral alteration (up to 50%) is the saussuritisation/ albitisation of primary plagioclase ($An_{25}Ab_{74}Or_1$). This alteration has depleted the rocks in plagioclase relative to primary quartz and K-feldspar (i.e., more present-day felsic composition) but enriched the rocks in secondary albite, sericite and epidote.

(3) The intensity of the saussuritisation of plagioclase and concomitant chloritisation of biotite are greater in the dioritic than in the granitic rocks.

(4) Granitic and dioritic rocks characterised by the presence of thin fracture planes are reddened and contain albitised plagioclase (± illite) crystals that are also replaced by barium-rich K-feldspar (BaO up to ca 4.1 wt.%).

(5) Pumpellyite is closely associated with prehnite, and occurs strictly within biotite crystals that have been strongly replaced by chlorite and mixed-layer illite/vermiculite. The prehnite-pumpellyite assemblage suggests a formation temperature of ca 200-300ºC and pressure of 2-3 kilo bars. The Fe-richer varieties of pumpellyite and prehnite texturally post-dates, and hence formed at lower temperatures than the Fe-poorer varieties.

(6) The rare occurrence of laumontite in the studied rocks compared to secondary epidote, prehnite, pumpellyite, and K-feldspars is attributed to its narrow field of thermodynamic stability compared to these minerals.

(7) Chlorite that is pseudomorphically replacing biotite has been formed at higher temperatures (ca 300-350ºC) than the more Fe-rich, fine-crystalline chlorite/berthierine that was formed by biotite, titanite and magnetite replacement and as void fillings.

(8) Most of the calcite has been precipitated at fairly low temperatures (45-143ºC) assuming that the fluids were hydrothermal in origin with the typical $\delta^{18}O_{SMOW}$ value of -6‰. Calcite that occurs in the main deformation zones is characterized by lower $\delta^{18}O$ values, and hence higher precipitation temperatures. The carbon isotopic values of calcite in these zones presumably show an enrichment in ^{12}C, which is attributed to methane oxidation. However, more detailed sampling and isotopic analyses are required before concrete conclusions about the links between the deformation zones and isotopic composition of calcite can be reached.

10 Acknowledgments

We would like to thank Björn Magnor for his interest in the present work and for helping us sharpen the focus of the report and for support he provided us during the planning and performance of sampling and for guiding us through the Äspö area. We thank the referees for the constructive criticism of the manuscript.

References

Affaton P, Aguirre L, Menot R P, 1997. Thermal and geodynamic setting of the Buem volcanic rocks near Tiele, Northwest Benin, West Africa. Precambrian Research, 82, 191-209.

Aldahan, A., 1989. The paragenesis of pumpellyite in granitic rocks from the Siljan area, central Sweden. N. Jb. Miner. Mh., H.8, 367-383.

Alt J C, Honnorez J, Laverne C, Emmermann R, 1986. Hydrothermal alteration of a 1 km section through the upper oceanic crust, Deep Sea Drilling Project Hole 504B: mineralogy, chemistry, and evolution of seawater-basalt interactions. Journal of Geophysical research, 91, 10390-10335.

Amorsson S, Barnes Y, 1983. The nature of carbon dioxide in Snaellsnes Western Iceland. Geothermics, 12, 171-176.

Banwart S, Gustafsson E, Laaksoharju M, Nilsson A-C, Tullborg E-L, Wallin B, 1994. Large scale intrusion of shallow water into a vertical fracture zone in crystalline bedrock: Initial hydrochemical perturbation during the tunnel construction at the Äspö Hard rock Laboratory, southeastern Sweden. Water Resources Research, 30, 1747-1763.

Barnes Y, Evans W C, White L D, 1988. The role of mantle CO_2 in volcanism. Applied Geochemistry, 3, 281-285.

Berger G, Schott J, Loubet M, 1987. Fundamental processes controlling the first stage of alteration of basalt glass by seawater: an experimental study between 200ºC and 320ºC. Earth and Planetary Science Letters, 84, 431-445.

Bird D K, Helgeson H C, 1981. Chemical interaction of aqueous solutions with epidote-feldspar mineral assemblages in geological systems. II. Equilibrium constraints in metamorphic/geothermal processes. American Journal of Science, 281, 576-614.

Bird D K, Schiffman P, Elders W A, Williams A E, McDowell S D, 1984. Calc-silicate mineralization in active geothermal systems. Economic Geology and the Bulletin of the Society of Economic Geologists, 79, 671-695.

Carlsten S, 1990. Borehole radar measurements at Äspö; Boreholes KAS09, KAS10, KAS11, KAS12, KAS13 and KAS14. SKB Progress Report 25-90-05, 46pp.

Cathelineau M, 1988. Cation site occupancy in chlorite and illites as a function of temperature. Clay Minerals, 23, 471-485.

Cathelineau M, Lespinasse M, Boirion M C, 1994. Fluid inclusion planes: a geochemical and structural tool for the reconstruction of paleofluid migration. In: De Vivo and Frezzotti (editors), Short Course, Fluid Inclusions in Minerals: Methods and Applications. Virginia tech., 271-282.

Cerney, P., Povondra, P, 1972. An Al-rich metamict titanite from Czechoslovakia. Nueus Jahrbuch Mineralogie, H9, 400-406.

Coombs D S, Kawachi Y, Houghton B F, Hyden G, Pringle I J, Williams J G, 1977, Andradite and andradite-grossular solid solution in very low-grade regionally metamorphosed rocks in southern New Zealand. Contributions to Mineralogy and Petrology, 63, 229-246.

Coombs D S, Kawachi Y, Ford P B, 1996. Porphyroblastic manganaxinite metapelagites with incipient garnet in prehnite-pumpellyite facies, near Meyer Pass, Torlesse Terrane, New Zealand. Journal of Metamorphic Geology, 14, 125-142.

Coombs D S, Zhao G., Peacor D R, 2001. Manganoan berthierine, Meyers Pass, New Zealand: occurrence in the prehnite-pumpellyite facies. Mineralogical Magazine, 64, 1037-1046.

Deer W A, Howie R A, Zussman J, 1992. An introduction to rock forming minerals. Second Edition, Longman Group, UK Limited, Essex, 696pp.

Digel S, Ghent E D, 1994. Fluid-mineral equilibrium in prehnite-pumpellyite to greenschist facies metabasites near Flin Flon, Manitoba, Canada: implications for petrogenetic grids. Journal of Metamorphic Geology, 12, 467-477.

Eliasson T, 1993. Mineralogy, geochemistry and petrophysics of red coloured granite adjacent to fractures. SKB TR 93-06, Swedish Nuclear Fuel and Waste Management Co.

Freiberger R, Hecht L, Cuney M, Morteani G., 2001. Secondary Ca-Al silicates in plutonic rocks: implications for their cooling history. Contributions to Mineralogy and Petrology, 141, 415-429.

Friedman I, O'Neil J R, 1977. Compilation of stable isotopic fractionation factors of geochemical interest. United States Geological Survey, USGS, Professional paper 440-KK, 12p.

Frey M, De Capitani C, Liou G J, 1991. A new petrogenetic grid for low grade metabasite. Journal of Metamorphic Geology, 9, 497-509.

Gianelli G, Mekuria N, Battaglia, Chersicla A, Garofalo P, Ruggieri G., Manganelli M, Gebregziabher Z, 1998. Water-rock interaction and hydrothermal mineral equilibria in the Tendaho geothermal system. Journal of Volcanology and Geothermal Research, 86, 253-276.

Goff S J, Goff F, Janik C J, 1992. Tecuamborro Volcanao, Guatemala: exploration geothermal gradient drilling and results. Geothermics, 21, 483-502.

Hogarth D D, 1989. Pyrochlore, apatite, amphibole: distinctive minerals in carbonatite. In Bell K (editor), Carbonatites: Genesis and Evolution. Unwinn Hyman, London, UK, 105-148.

Holl A, Althaus E, Lempp C, Natau O, 1997. The petrophysical behaviour of crustal rocks under the influence of fluids. Tectonophysics, 275, 253-260.

Ishizuka H, 1999. Pumpellyite from the ocean crust, DSDP/ODP Hole 504B. Mineralogical Magazine, 63, 891-900.

IUGS, 1973. Classification and nomenclature of plutonic rocks. Reccomendations. N. JB. Miner. Mh., H4, 149-164.

Janecke S U, Evans J P, 1988. Feldspar-influenced rock rheologies. Geology, 16, 1064-1067.

Jenkin G R T, Fallick A E, Leake B E, 1992. A stable isotope study of retrograde alteration in SW Connemara, Ireland. Contributions to Mineralogy and Petrology, 110, 269-288.

Johansson H, Siitari-Kauppi, M, Skålberg M, Tullborg E L, 1998. Diffusion pathways in crystalline rock – examples from Äspö-diorite and fine-grained granite. Journal of Contaminant Hydrology, 35, 41-53.

Kirby S H, Kronenberg A K, 1987. Rheology of the lithosphere: Selected topics. Reviews in Geophysics, 25, 1219-1244.

Kornfält K-A, Wikman H, 1988, The rocks of the Äspö Island: Description to the detailed maps of solid rocks including maps of 3 uncovered trenches. SKB P R 25-88-12. Swedish Nuclear Fuel and Waste Management Co. 35p.

Krismannsdótter H, 1975,. Hydrothermal alteration of basaltic rocks in Icelandic geothermal areas. Proceeding 2nd UN Symposium on Development and Use of Geothermal Resources, pp. 441-445, San Francisco, CA.

Landström O, Tullborg E-L, 1993. Results from a geochemical study of zone NE-1, based on samples from the Äspö tunnel and drillcore KAS 16 (395-451 m). Progress Report SKB 25-93-01, Swedish Nuclear Fuel and Waste management Co.

Landström O, Tullborg E-L, Eriksson G, 2001. Effects of glacial/post-glacial weathering compared with hydrothermal alteration – implications for matrix diffusion. SKB R-01-37, Swedish Nuclear Fuel and Waste management Co.

Liou J G, 1971, Synthesis and stability relations of prehnite, $Ca_2Al_2FeSi_3O_{12}(OH)$. Journal of Petrology, 14, 381-413.

Liou J G, Kim H S, Maruyama S, 1983. Prehnite-epidote equilibria and their petrologic applications. Journal of Petrology, 24, 321-342.

Lockner D A, Byerlee J D, 1995. An earthquake instability model based on faults containing high fluid-pressure compartments. In Wang R, Aki K (editors), Mechanics Problems in Geodynmaics, part I, Pure and Applied Geophysics, 145, 717-745.

Markström I, Erlström M, 1996. Äspö Hard Rock Laboratory: Overview of documentation of tunnel, niches and core boreholes. SKB P R HRL-96-19, Swedish Nuclear Fuel and Waste Management Co.

McDowell S.D., Elders W.A., 1980. Authigenic layer silicate minerals in borehole Elmore 1, Salton Sea geothermal field, California, USA. Contributions to Mineralogy and Petrology, 74, 293-310.

Milnes A G, Gee D G, Lund K-E, 1998, Crustal structure and regional tectonics of SE Sweden and the Baltic Sea. SKB T R 98-01, Swedish Nuclear Fuel and Waste Management Co. 58p.

Morad S, 1998. Carbonate cementation in sandstones in sandstones: distribution pattern and geochemical evolution. In Morad S (editor), Carbonate Cementation of Sandstones, International Association of Sedimentologists, IAS, Special Publication 26, 1-26.Blackwell

Morad s, Aldahan A, 2002. Spatial and temporal distribution of mineral alterations in granitic bedrock around main deformation zones in the Äspö HRL, SE Sweden. Technical Report TD-02-12, Swedish Nuclear Fuel and Waste Management Co. 91p.

Munier R, 1992.

Munier, R, 1993, Four-dimensional analysis of fracture arrays at the Äspö hard rock laboratory, SE Sweden. Engineering Geology, 33, 159-175.

O'Reilly C O, Jenkin GRT, Feely M, Alderton D H M, Fallick A E, 1997. A fluid inclusion and stable isotope study of 200 Ma of fluid evolution in the Galway Granite, Connemara, Ireland. Contributions to Mineralogy and Petrology, 129, 120-142.

Passaglia E, Gottardi G, 1973. Crystal chemistry and nomenclature of pumpellyite and julgoldite. Canadian Mineralogists, 12, 219-223.

Patrier P., Papapanagiotou P, Beufort D, Traineau H, Bril H, Rojas J, 1996. Role of permeability versus temperature distribution of the fine (0.2 μm) clay fraction in the Chipilapa geothermal system (El Salvador, Central America). Journal of Volcanaology and Geothermal Research, 72, 101-120.

Petersson J, Eliasson T, 1997. Mineral evolution and element mobilit episyenitization (dequartzification) and albitization in the postkinematic Bohus granite, southwest Sweden. Lithos, 42, 123-146.

Recio, C, Fallick A E, Ugidos J M, Stephens W E, 1997. Characterization of multiple fluid-granite interaction processes in the episyenites of Avila-Bejar, central Iberian Massif, Spain. Chemical Geology, 143, 127-144.

Reyes A, 1990. Petrology of Philippines geothermal systems and applications of alteration mineralogy to their assessment. Journal of Volcanology and Geothermal research, 43, 279-309.

Rhén, I., Gustafson, G., Stanfors, R., and Wikberg, P., 1997. Äspö HRL - Geoscientific evaluation 1997/5. Models based on site characterization 1986-1995. TR 97-06 Swedish Nuclear Fuel and Waste Management Company (SKB).

Robinson D, Bevins R E, 1999, Patterns of regional low-grade metamorphism in metabasites. In Frey M, Roninson D (editors), Metamorphism in Metabasites,. Blackwell, oxford, pp. 143-168.

Sahama T G, 1946. On the crystal chemistry of the mineral titanite. Bull. Comm. Geol. Finland, 138, 88-120.

Sehlstedt S, Stråhle A, Triumf C-A, 1990, Geological core mapping and geophysical borehole logging in the boreholes KBH02, KAS09, KAS11-KAS14 and HAS18-HAS20 at Äspö. SKB P R 25-90-06, Swedish Nuclear Fuel and Waste Management Co

Seyfried W E, Bischoff J L, 1981.Experimental seawater-basalt interaction at 300ºC, 500 bars, chemical exchange, secondary mineral formation and implications for the transport of heavy metals. Geochimica et Cosmochimica Acta, 45, 135-147.

Stanfors R, 1996, Geological investigations in M. Hammarström and O. Olsson eds., Äspö Hard Rock Laboratory, 10 years of research. Swedish Nuclear Fuel and Waste Management Co. 18-31.

Stanfors R, Olsson P, Stille H, 1997, Äspö HRL- Geoscientific evaluation 1997/3: Results from pre-investigation and detailed site characterization, Comparison of predictions and observations, Geology and mechanical stability. SKB T R 97-04. Swedish Nuclear Fuel and Waste Management Co.

Stanfors R, Rhén I, Tullborg E-L, Wikberg P, 1999, Overview of geological conditions of the Äspö hard rock laboratory site. Applied Geochemistry, 14, 819-834.

Teklemariam M, Battagalia S., Gianelli G, Ruggieri G, 1996. Hydrothermal alteration in the Aluto-Langano geothermal field, Ethiopia. Geothermics, 25, 679-702.

Tullborg E-L, Larson S Å, Björklund L, Samuelsson L, Stigh J, 1995. Thermal evidence of Caledonide foreland, molasses sedimentation in Fennoscandia. SKB TR 95-18, Swedish Nuclear Fuel and Waste management Co.

Tullborg E-L, Larson S Å, Stiberg J-P, 1996. Subsidence and uplift of the present land surface in the southern part of the Fennoscandian Shield, GFF, 112, 215-225.

Tullborg E-L, Landström O, Wallin B, 1998. Low-temperature trace element mobility influenced by microbial activity – indications from fracture calcite and pyrite in crystalline basement. Chemical Geology, 157, 199-218.

Tulloch A J, 1979. Secondary Ca-Al silicates as low-grade alteration products of granitoid biotite. Contributions to Mineralogy and Petrology, 69, 105-117.

Turpault M P, Berger G, Meunier, A, 1992. Dissolution-precipitation processes induced by hot water in a fractured granite. Part 1: wall-rock alteration and vein deposition processes. European Journal of Mineralogy, 4, 1457-1475.

Wikman H, Kornfält K-A, 1995, Updating of a lithological model of the bedrock of the Äspö area. SKB P R 25-95-04, Swedish Nuclear Fuel and Waste Management Co.

Wintsch R P, Christoffersen R, Kronenberg A K, 1995. Fluid-rock reaction weakening of fault zones. Journal of Geophysical Research, 100, 13021-13032.

Zulauf G, Palm S, Petschick R, Spies O, 1999. Element mobility and volumetric strain in brittle and brittle-viscous shear zones of the super deep well KTB (Germany). Chemical Geology, 156, 135-149.

Appendix 5-1. Modal analyses of the sampled rocks from KAS09 based on counting of 400 points in each thin section.
(KAS09 core depth 0.40-106.60).

Core depth [m]	Chloritised biotite	Argillised grains	Secondary chlorite	Total epidote	Sauss./alb. plagioclase	Calcite	Altered titanite	Secondary quartz	K-feldspar
0.40	3.6	0.0	3.1	3.1	34.2	0.0	0.0	3.1	0.0
3.45	1.8	0.0	0.9	3.5	19.8	0.0	0.0	4.0	0.0
5.33	2.3	1.4	0.9	3.2	17.5	1.8	0.0	2.8	0.0
6.46	8.4	0.9	2.3	2.8	17.3	0.0	0.0	3.3	0.5
7.42	2.7	0.0	0.9	2.7	21.0	0.5	0.0	3.6	0.5
7.78	0.4	0.0	4.2	4.2	4.2	1.3	0.4	8.0	2.5
8.43	0.0	0.0	3.0	6.8	15.3	3.0	0.0	2.6	3.8
11.87	0.0	0.0	2.1	4.1	6.6	0.4	0.0	8.2	4.5
13.95	0.4	0.4	1.3	4.8	13.9	0.0	0.0	8.2	2.2
16.43	0.0	0.0	4.1	2.1	2.1	0.0	0.0	6.6	6.2
17.00	1.3	0.9	3.0	6.4	1.3	0.0	0.9	6.0	6.0
17.90	0.0	0.0	0.0	0.0	0.0	0.0	0.0	3.6	2.7
19.01	1.7	0.0	6.3	1.3	5.5	0.0	0.4	5.9	8.8
20.67	0.0	1.2	20.2	21.0	19.3	0.8	2.1	10.7	2.5
20.77	0.0	0.3	15.4	2.1	30.8	9.3	0.0	7.5	1.0
21.01	7.4	1.7	8.2	7.4	34.2	2.2	0.9	2.6	1.3
22.10	3.6	0.0	1.4	4.5	25.1	0.9	0.0	2.7	0.9
23.55	8.0	0.0	3.4	4.9	36.4	0.0	2.3	8.7	0.8
26.70	1.0	0.0	1.0	1.4	4.8	0.0	0.0	2.4	0.0
30.54	6.1	9.6	15.2	4.8	23.0	0.0	0.0	4.8	1.7
31.50	3.8	9.5	2.8	5.7	33.7	0.5	0.0	6.6	0.0
32.81	1.4	0.0	1.9	1.9	9.4	0.0	0.0	0.0	0.0
34.60	0.0	3.9	4.4	2.9	10.2	0.0	1.0	0.0	0.0
36.95	0.4	2.2	7.0	1.8	11.8	3.1	1.3	1.8	0.0
39.70	4.2	3.2	12.0	13.4	31.5	0.0	1.4	0.9	0.0
44.85	3.8	2.8	7.0	5.2	38.0	0.0	0.0	1.9	0.0
46.15	0.5	0.0	0.9	6.5	14.9	0.0	0.0	3.3	0.0
49.60	0.0	0.0	4.8	1.9	21.0	0.0	0.0	1.0	1.4
56.20	2.8	0.0	1.4	0.5	16.6	0.0	0.0	1.4	0.9
62.87	2.4	0.0	1.4	3.4	20.1	0.0	0.0	1.4	0.0
67.20	4.1	0.5	1.4	0.9	18.4	0.0	0.0	0.9	0.0
68.60	1.9	0.5	3.7	6.5	34.9	0.0	0.9	1.4	0.0
71.45	6.1	0.5	5.6	2.8	41.9	0.0	2.3	0.9	0.9
72.27	9.6	11.2	6.9	3.1	35.2	0.0	0.0	2.5	0.0
72.70	4.8	1.0	1.9	0.0	12.9	0.0	0.0	0.0	0.0
72.95	7.7	0.0	5.9	2.3	11.4	0.0	0.0	0.0	0.0
74.40	1.4	1.9	1.4	1.9	26.1	0.0	0.0	0.9	0.0
77.70	5.0	4.0	6.0	5.5	13.0	8.5	1.0	0.0	1.5
81.75	0.9	23.6	9.7	9.3	24.1	1.9	1.4	2.8	0.0
84.75	2.5	5.9	4.4	5.9	22.2	0.0	0.0	0.0	0.0
86.56	3.3	19.1	5.6	5.1	16.3	0.0	0.0	0.0	0.0
88.90	0.0	5.4	0.0	4.9	8.8	0.0	0.0	0.0	0.0
92.30	1.9	5.8	2.9	3.9	5.3	0.5	0.0	0.0	0.0
94.60	1.7	16.4	5.0	4.6	18.9	4.2	1.7	0.8	0.8
95.40	3.9	0.0	0.0	24.8	6.2	6.2	0.0	5.3	7.5
97.71	1.8	16.4	10.0	3.2	7.7	0.0	2.3	1.8	1.8
97.75	8.0	14.6	2.5	26.1	0.0	1.0	0.0	0.0	0.0
102.25	0.0	2.9	16.7	7.1	8.1	0.0	2.9	0.0	0.0
103.85	18.4	0.0	3.8	8.5	38.1	0.0	0.0	1.9	0.0
106.60	0.0	2.9	10.2	2.0	16.6	0.0	0.0	0.0	0.0

Appendix 5-1. Cont.
(KAS09 core depth 0.40-106.60).

Core depth [m]	Prehnite	Pumpellyite	Hematite	Pyrite	Primary quartz	K-feldspar/ perthite	Plagioclase	Biotite	Amphibole
0.40	0.4	0.0	0.0	0.0	11.1	13.3	15.1	5.3	3.6
3.45	0.4	0.0	0.0	0.0	13.2	7.1	26.4	16.7	2.6
5.33	0.0	0.0	0.0	0.0	14.3	13.8	19.4	15.7	4.6
6.46	0.5	0.0	0.0	0.0	10.3	13.6	32.2	4.2	3.3
7.42	0.0	0.0	0.0	0.0	14.7	3.6	21.0	25.0	1.8
7.78	0.0	0.0	0.0	0.0	27.9	20.3	24.5	0.8	0.0
8.43	0.0	0.0	0.0	0.0	15.7	6.8	18.3	19.6	0.0
11.87	0.0	0.0	0.0	0.0	27.2	6.6	21.8	11.9	2.1
13.95	0.4	0.0	0.0	0.0	13.0	4.3	34.2	12.1	2.2
16.43	0.0	0.0	0.0	0.0	43.8	14.5	17.4	1.2	0.0
17.00	0.0	0.0	0.0	0.0	36.3	14.5	21.8	1.3	0.0
17.90	0.0	0.0	2.2	0.0	30.0	47.1	12.1	0.0	0.0
19.01	0.0	0.0	0.8	0.0	37.8	15.1	15.6	0.8	0.0
20.67	0.0	0.0	0.0	0.0	9.9	4.5	6.2	0.0	0.0
20.77	0.0	0.0	0.0	0.0	6.2	6.5	3.8	0.0	0.0
21.01	0.0	1.3	0.0	1.3	13.0	2.2	9.1	3.5	0.0
22.10	0.5	0.0	0.0	1.4	16.6	16.6	10.3	13.0	1.8
23.55	0.0	0.0	8.7	0.0	7.6	3.8	8.7	2.3	0.0
26.70	0.0	0.0	0.0	1.0	17.6	16.7	27.6	19.5	4.8
30.54	0.0	0.0	1.7	0.0	5.7	9.6	14.8	0.9	0.0
31.50	0.0	0.0	0.0	0.5	9.0	10.0	10.0	3.3	2.4
32.81	0.0	0.0	0.0	0.0	29.0	8.4	31.3	11.2	2.8
34.60	0.0	0.0	1.0	0.0	47.1	20.4	8.3	0.0	0.0
36.95	0.0	0.0	1.8	0.0	48.0	9.2	7.0	0.0	0.0
39.70	3.2	0.0	0.0	0.0	13.9	8.8	4.2	0.9	0.5
44.85	0.5	0.0	0.0	0.0	10.3	19.3	6.6	0.9	0.0
46.15	0.0	0.0	0.0	0.0	18.6	17.2	25.1	7.9	1.4
49.60	0.0	0.0	2.4	0.0	37.1	20.0	10.5	0.0	0.0
56.20	0.0	0.0	3.2	0.0	45.2	16.1	8.3	1.4	0.0
62.87	0.0	0.0	1.4	0.0	12.9	9.1	15.8	16.8	13.9
67.20	0.0	0.0	0.0	0.0	24.3	6.4	20.6	12.8	5.1
68.60	0.0	0.0	3.7	0.0	24.2	16.3	4.7	0.5	0.0
71.45	0.0	0.0	3.7	0.0	16.7	7.4	4.2	1.9	4.2
72.27	2.4	0.0	0.0	0.0	5.6	5.2	9.6	0.6	1.4
72.70	0.0	0.0	0.0	0.0	22.9	7.6	19.5	11.4	13.3
72.95	0.0	0.0	0.0	0.0	18.1	14.0	18.1	10.0	9.2
74.40	0.0	0.0	0.0	0.0	14.4	7.0	21.4	8.8	10.2
77.70	0.0	0.0	9.5	0.0	6.0	13.5	21.5	1.0	0.0
81.75	0.0	0.0	1.4	0.0	9.3	6.9	4.2	0.0	2.3
84.75	0.0	0.0	0.0	0.0	12.3	7.4	24.1	8.4	5.4
86.56	0.0	0.0	1.4	0.0	14.0	8.4	13.5	4.7	5.6
88.90	0.0	0.0	0.0	0.0	29.3	12.7	27.3	9.3	0.0
92.30	0.0	0.0	0.0	0.0	17.5	22.3	20.4	13.1	3.9
94.60	6.7	0.0	0.0	0.0	10.9	7.6	13.9	1.7	3.4
95.40	17.7	0.0	0.0	0.0	4.4	6.1	15.5	0.0	2.2
97.71	1.8	0.0	0.0	0.0	15.9	10.9	19.6	0.9	4.6
97.75	0.0	0.0	0.0	0.0	10.6	12.6	12.6	4.5	6.5
102.25	0.0	0.0	0.0	0.0	8.6	14.8	37.1	0.0	0.0
103.85	0.0	0.0	0.0	0.0	9.5	9.0	6.6	0.8	1.9
106.60	0.0	0.0	2.0	0.0	18.1	39.0	9.3	0.0	0.0

Appendix 5-1. Cont.
(KAS09 core depth 0.40-106.60).

Core depth [m]	Muscovite	Magnetite	Titanite	Fluorite/ apatite	Voids/ fractures	Total %	Rock color	Alteration index
0.40	0.0	1.3	2.7	0.0	0.0	100	RG	0.9
3.45	0.0	1.3	2.2	0.0	0.0	100	G	0.4
5.33	0.0	0.5	1.8	0.0	0.0	100	G	0.4
6.46	0.0	0.0	0.5	0.0	0.0	100	G	0.6
7.42	0.0	0.5	1.8	0.0	0.0	100	G	0.5
7.78	0.0	0.0	1.3	0.0	0.0	100	R	0.3
8.43	2.6	1.3	1.3	0.0	0.0	100	G	0.5
11.87	0.4	1.2	2.9	0.0	0.0	100	G	0.4
13.95	0.0	0.4	2.2	0.0	0.0	100	G	0.5
16.43	2.1	0.0	0.0	0.0	0.0	100	RG	0.3
17.00	0.4	0.0	0.0	0.0	0.0	100	R	0.3
17.90	2.2	0.0	0.0	0.0	0.0	100	R	0.1
19.01	0.0	0.0	0.0	0.0	0.0	100	RG	0.4
20.67	1.7	0.0	0.0	0.0	0.0	100	G	3.5
20.77	13.7	1.7	1.7	0.0	0.0	100	R	2.0
21.01	1.3	0.9	1.7	0.0	0.0	100	GR	2.2
22.10	0.0	0.0	0.9	0.0	0.0	100	G	0.7
23.55	0.0	0.0	0.8	0.0	3.8	100	RG	3.2
26.70	0.0	0.5	1.9	0.0	0.0	100	G	0.1
30.54	0.0	0.4	1.7	0.0	0.0	100	R	2.0
31.50	0.0	0.0	2.4	0.0	0.0	100	G	1.7
32.81	0.0	0.5	2.3	0.0	0.0	100	G	0.2
34.60	1.0	0.0	0.0	0.0	0.0	100	R	0.3
36.95	4.8	0.0	0.0	0.0	0.0	100	R	0.5
39.70	0.0	0.0	1.4	0.5	0.0	100	G	2.3
44.85	0.0	0.5	2.8	0.0	0.5	100	R	1.5
46.15	0.0	0.9	0.9	1.9	0.0	100	G	0.4
49.60	0.0	0.0	0.0	0.0	0.0	100	R	0.5
56.20	2.3	0.0	0.0	0.0	0.0	100	R	0.4
62.87	0.0	0.0	1.4	0.0	0.0	100	G	0.4
67.20	0.0	2.3	1.4	0.9	0.0	100	G	0.4
68.60	0.0	0.0	0.9	0.0	0.0	100	R	1.2
71.45	0.0	0.9	0.0	0.0	0.0	100	R	1.8
72.27	0.0	0.0	2.7	0.0	3.2	100	R	2.8
72.70	0.0	1.4	2.4	1.0	0.0	100	G	0.3
72.95	0.0	0.0	1.8	0.0	0.0	100	R	0.4
74.40	0.0	1.9	1.9	0.9	0.0	100	GR	0.5
77.70	1.0	0.0	0.0	0.0	3.0	100	GR	1.3
81.75	0.0	2.3	0.0	0.0	0.0	100	GR	3.0
84.75	0.0	1.0	0.5	0.0	0.0	100	G	0.7
86.56	0.0	0.9	2.3	0.0	0.0	100	R	1.0
88.90	0.0	1.5	1.0	0.0	0.0	100	G	0.2
92.30	0.0	0.0	2.4	0.0	0.0	100	G	0.3
94.60	0.0	1.7	0.0	0.0	0.0	100	GR	1.6
95.40	0.0	0.0	0.0	0.0	0.0	100	R	2.5
97.71	0.0	0.9	0.5	0.0	0.0	100	G	0.9
97.75	0.0	1.0	0.0	0.0	0.0	100	RG	1.1
102.25	0.5	1.0	0.5	0.0	0.0	100	R	0.6
103.85	0.0	0.0	0.0	0.0	0.0	100	R	2.5
106.60	0.0	0.0	0.0	0.0	0.0	100	R	0.5

Appendix 5-1. Cont.
(KAS09 core depth 113.50-253.50).

Core depth [m]	Chloritised biotite	Argillised grains	Secondary chlorite	Total epidote	Sauss./alb. plagioclase	Calcite	Altered titanite	Secondary quartz	K-feldspar
113.50	0.0	0.0	0.0	42.1	3.7	3.2	0.0	1.4	0.9
114.86	3.1	0.9	3.5	30.8	7.5	1.3	0.0	1.3	0.9
117.85	8.6	0.0	2.6	4.0	48.3	0.0	2.6	0.0	0.0
118.25	0.0	0.0	0.0	0.0	22.8	0.0	0.0	0.0	0.0
120.09	6.6	0.9	2.4	1.9	32.4	0.0	0.0	0.9	0.0
122.65	0.0	0.0	0.0	0.0	20.4	0.0	0.0	0.0	0.0
123.80	1.0	0.5	1.0	1.5	16.8	0.0	0.0	0.0	0.0
130.60	1.0	0.0	0.0	2.9	14.8	0.0	0.0	0.0	2.9
133.30	1.5	0.5	0.0	1.0	17.6	0.0	0.0	1.0	0.5
135.75	0.0	0.5	1.4	0.9	25.0	0.5	0.0	0.0	1.4
140.20	14.2	1.7	1.3	1.3	43.5	5.2	0.0	0.9	0.9
145.26	4.4	0.0	1.6	1.8	17.8	0.0	0.0	1.4	0.0
146.70	4.1	1.2	0.0	4.1	31.6	4.7	0.0	1.8	1.2
150.50	0.0	1.6	0.0	1.6	18.8	1.6	0.0	0.0	0.0
154.75	1.5	1.5	0.0	5.9	8.9	1.0	0.0	1.0	0.0
157.75	1.8	5.3	7.1	23.6	10.7	1.3	0.9	3.1	2.2
159.63	3.6	0.0	1.6	4.1	13.9	0.0	1.1	0.0	0.0
160.85	0.0	0.4	0.0	3.1	2.2	0.6	0.0	0.0	0.0
163.35	0.0	1.7	0.9	5.5	4.3	0.0	0.0	0.0	0.0
164.85	5.4	0.0	0.0	2.4	31.1	0.3	0.0	0.0	0.0
165.84	2.8	0.9	0.9	6.1	37.6	0.0	0.0	1.9	2.4
166.85	6.1	0.5	0.5	3.3	26.3	1.9	0.0	0.5	0.9
169.55	5.7	1.4	0.5	2.8	49.1	0.9	0.0	0.9	1.9
169.55	12.2	1.4	0.9	17.8	14.1	1.9	1.4	1.9	0.5
174.85	16.8	1.8	0.9	7.1	3.5	3.5	0.0	1.8	3.5
176.55	0.0	0.5	1.0	7.1	10.4	0.0	0.0	1.4	1.0
179.63	4.8	6.2	3.8	10.0	32.4	1.4	0.5	0.5	0.5
180.85	0.0	0.0	0.0	3.4	8.6	0.4	0.0	0.0	0.0
183.55	0.0	1.5	1.0	1.0	4.4	0.0	0.0	0.0	0.0
185.70	1.9	5.7	2.9	10.5	34.8	0.0	0.5	0.5	1.0
187.75	0.0	0.0	1.0	1.5	7.4	0.0	0.0	0.0	0.0
193.40	0.0	1.2	0.6	10.7	10.1	6.0	0.0	3.0	0.6
194.40	2.8	0.9	6.5	9.3	31.9	0.0	0.5	2.3	0.0
197.60	0.0	0.5	0.5	10.0	9.5	1.0	0.0	1.0	0.5
199.70	0.0	0.0	0.5	2.0	2.9	0.0	0.0	0.0	0.0
200.05	0.5	0.5	2.4	0.5	0.0	1.0	0.0	0.5	1.0
203.35	0.0	0.0	0.0	0.5	1.4	0.0	0.0	0.5	0.0
206.55	0.0	0.0	1.2	3.6	13.6	0.0	0.0	0.6	0.6
212.65	6.1	0.0	2.8	5.2	34.3	0.0	0.5	0.5	0.9
218.35	0.5	1.0	1.0	1.9	11.9	0.0	0.0	1.0	0.5
221.75	0.0	0.0	0.0	5.7	15.2	0.5	0.0	0.0	0.0
225.95	5.0	0.0	1.2	5.6	21.1	0.6	0.0	0.0	0.0
228.50	1.9	0.5	0.5	2.8	4.3	0.0	0.0	0.5	0.5
231.70	0.6	0.0	0.6	2.4	5.9	0.0	0.0	0.6	0.0
235.97	0.5	0.0	0.0	3.3	12.3	1.4	0.0	0.0	0.0
241.22	1.0	0.0	0.0	2.4	9.8	1.0	0.0	0.0	0.0
242.66	6.6	0.9	0.9	7.0	18.8	1.9	0.0	0.0	0.0
246.65	3.2	0.0	2.7	3.2	37.9	0.0	0.0	1.8	1.4
249.25	5.9	0.7	14.7	27.9	2.2	1.5	2.2	16.2	0.7
253.50	13.7	0.9	0.0	8.7	33.3	1.4	0.0	1.8	1.4

Appendix 5-1. Cont.
(KAS09 core depth 113.50-253.50).

Core depth [m]	Prehnite	Pumpellyite	Hematite	Pyrite	Primary quartz	K-feldspar/ perthite	Plagioclase	Biotite	Amphibole
113.50	0.4	0.0	0.0	0.0	11.1	13.3	15.1	5.3	3.6
114.86	0.4	0.0	0.0	0.0	13.2	7.1	26.4	16.7	2.6
117.85	0.0	0.0	0.0	0.0	14.3	13.8	19.4	15.7	4.6
118.25	0.5	0.0	0.0	0.0	10.3	13.6	32.2	4.2	3.3
120.09	0.0	0.0	0.0	0.0	14.7	3.6	21.0	25.0	1.8
122.65	0.0	0.0	0.0	0.0	27.9	20.3	24.5	0.8	0.0
123.80	0.0	0.0	0.0	0.0	15.7	6.8	18.3	19.6	0.0
130.60	0.0	0.0	0.0	0.0	27.2	6.6	21.8	11.9	2.1
133.30	0.4	0.0	0.0	0.0	13.0	4.3	34.2	12.1	2.2
135.75	0.0	0.0	0.0	0.0	43.8	14.5	17.4	1.2	0.0
140.20	0.0	0.0	0.0	0.0	36.3	14.5	21.8	1.3	0.0
145.26	0.0	0.0	2.2	0.0	30.0	47.1	12.1	0.0	0.0
146.70	0.0	0.0	0.8	0.0	37.8	15.1	15.6	0.8	0.0
150.50	0.0	0.0	0.0	0.0	9.9	4.5	6.2	0.0	0.0
154.75	0.0	0.0	0.0	0.0	6.2	6.5	3.8	0.0	0.0
157.75	0.0	1.3	0.0	1.3	13.0	2.2	9.1	3.5	0.0
159.63	0.5	0.0	0.0	1.4	16.6	16.6	10.3	13.0	1.8
160.85	0.0	0.0	8.7	0.0	7.6	3.8	8.7	2.3	0.0
163.35	0.0	0.0	0.0	1.0	17.6	16.7	27.6	19.5	4.8
164.85	0.0	0.0	1.7	0.0	5.7	9.6	14.8	0.9	0.0
165.84	0.0	0.0	0.0	0.5	9.0	10.0	10.0	3.3	2.4
166.85	0.0	0.0	0.0	0.0	29.0	8.4	31.3	11.2	2.8
169.55	0.0	0.0	1.0	0.0	47.1	20.4	8.3	0.0	0.0
169.55	0.0	0.0	1.8	0.0	48.0	9.2	7.0	0.0	0.0
174.85	3.2	0.0	0.0	0.0	13.9	8.8	4.2	0.9	0.5
176.55	0.5	0.0	0.0	0.0	10.3	19.3	6.6	0.9	0.0
179.63	0.0	0.0	0.0	0.0	18.6	17.2	25.1	7.9	1.4
180.85	0.0	0.0	2.4	0.0	37.1	20.0	10.5	0.0	0.0
183.55	0.0	0.0	3.2	0.0	45.2	16.1	8.3	1.4	0.0
185.70	0.0	0.0	1.4	0.0	12.9	9.1	15.8	16.8	13.9
187.75	0.0	0.0	0.0	0.0	24.3	6.4	20.6	12.8	5.1
193.40	0.0	0.0	3.7	0.0	24.2	16.3	4.7	0.5	0.0
194.40	0.0	0.0	3.7	0.0	16.7	7.4	4.2	1.9	4.2
197.60	2.4	0.0	0.0	0.0	5.6	5.2	9.6	0.6	1.4
199.70	0.0	0.0	0.0	0.0	22.9	7.6	19.5	11.4	13.3
200.05	0.0	0.0	0.0	0.0	18.1	14.0	18.1	10.0	9.2
203.35	0.0	0.0	0.0	0.0	14.4	7.0	21.4	8.8	10.2
206.55	0.0	0.0	9.5	0.0	6.0	13.5	21.5	1.0	0.0
212.65	0.0	0.0	1.4	0.0	9.3	6.9	4.2	0.0	2.3
218.35	0.0	0.0	0.0	0.0	12.3	7.4	24.1	8.4	5.4
221.75	0.0	0.0	1.4	0.0	14.0	8.4	13.5	4.7	5.6
225.95	0.0	0.0	0.0	0.0	29.3	12.7	27.3	9.3	0.0
228.50	0.0	0.0	0.0	0.0	17.5	22.3	20.4	13.1	3.9
231.70	6.7	0.0	0.0	0.0	10.9	7.6	13.9	1.7	3.4
235.97	17.7	0.0	0.0	0.0	4.4	6.1	15.5	0.0	2.2
241.22	1.8	0.0	0.0	0.0	15.9	10.9	19.6	0.9	4.6
242.66	0.0	0.0	0.0	0.0	10.6	12.6	12.6	4.5	6.5
246.65	0.0	0.0	0.0	0.0	8.6	14.8	37.1	0.0	0.0
249.25	0.0	0.0	0.0	0.0	9.5	9.0	6.6	0.8	1.9
253.50	0.0	0.0	2.0	0.0	18.1	39.0	9.3	0.0	0.0

Appendix 5-1. Cont.
(KAS09 core depth 113.50-253.50).

Core depth [m]	Muscovite	Magnetite	Titanite	Fluorite/ apatite	Voids/ fractures	Total %	Rock color	Alteration index
113.50	0.0	0.5	0.9	0.0	0.0	100	RG	1.1
114.86	0.0	0.4	0.9	0.9	0.0	100	GR	1.1
117.85	0.0	0.0	0.0	3.3	0.0	100	GR	2.0
118.25	0.0	0.0	0.0	0.0	0.0	100	R	0.3
120.09	0.0	0.0	0.5	0.0	0.0	100	G	0.8
122.65	0.0	0.0	0.0	0.0	0.0	100	R	0.3
123.80	0.0	0.0	0.0	0.0	0.0	100	R	0.3
130.60	1.4	0.0	0.0	0.0	0.0	100	R	0.3
133.30	0.0	0.0	0.0	0.0	0.0	100	R	0.3
135.75	0.0	0.5	0.0	0.0	0.0	100	R	0.5
140.20	4.7	0.0	0.0	0.0	0.0	100	RG	2.3
145.26	0.0	0.0	0.0	0.0	0.0	100	R	0.4
146.70	0.0	0.0	1.2	0.0	0.0	100	G	0.9
150.50	0.0	1.1	1.1	0.0	0.0	100	G	0.3
154.75	0.0	0.0	0.0	0.0	0.0	100	G	0.3
157.75	0.0	0.0	1.3	0.0	0.0	100	R	1.3
159.63	0.0	0.0	2.1	0.0	0.0	100	GR	0.3
160.85	0.0	13.5	3.8	4.6	0.0	100	GR	0.1
163.35	0.0	10.6	3.4	0.9	0.0	100	G	0.1
164.85	0.0	0.0	0.9	0.0	0.0	100	GR	0.7
165.84	0.0	0.0	0.0	0.5	0.0	100	RG	1.1
166.85	0.0	0.0	0.9	0.0	0.0	100	G	0.7
169.55	0.0	0.0	0.9	0.0	0.0	100	RG	1.8
169.55	0.0	0.0	0.0	0.0	0.0	100	GR	1.1
174.85	0.0	0.0	0.0	0.0	0.0	100	RG	0.7
176.55	0.0	1.0	1.0	1.0	0.0	100	G	0.3
179.63	0.0	0.5	0.5	1.0	0.0	100	RG	1.5
180.85	0.0	1.2	0.4	0.0	0.0	100	G	0.2
183.55	0.0	0.5	0.0	2.0	0.0	100	G	0.1
185.70	0.0	1.0	1.0	1.0	0.0	100	RG	1.4
187.75	0.0	0.5	1.5	0.0	0.0	100	G	0.1
193.40	0.0	0.0	1.8	0.0	0.0	100	G	0.5
194.40	0.0	0.5	2.3	0.0	0.0	100	R	1.3
197.60	0.0	0.5	1.0	1.4	0.0	100	G	0.3
199.70	0.0	0.0	0.0	1.0	0.0	100	R	0.1
200.05	0.0	1.0	0.0	0.0	0.0	100	R	0.1
203.35	5.6	0.0	0.0	0.0	0.0	100	GR	0.0
206.55	0.0	0.0	1.8	0.0	0.0	100	G	0.2
212.65	0.0	0.0	2.4	0.0	0.0	100	RG	1.2
218.35	1.4	0.0	0.5	0.0	0.0	100	R	0.2
221.75	0.0	0.0	3.8	0.5	0.0	100	RG	0.3
225.95	0.6	1.2	3.7	0.6	0.0	100	RG	0.5
228.50	0.0	1.9	1.4	0.0	0.0	100	G	0.1
231.70	0.0	1.8	1.8	0.0	0.0	100	G	0.1
235.97	0.0	1.0	1.4	1.4	0.0	100	G	0.2
241.22	0.0	1.0	0.5	0.0	0.0	100	G	0.2
242.66	0.0	3.3	0.9	0.0	0.0	100	RG	0.6
246.65	0.5	0.5	0.0	0.5	0.0	100	RG	1.1
249.25	0.0	0.0	0.7	0.0	0.0	100	GR	3.3
253.50	0.0	0.9	1.4	0.0	0.0	100	RG	1.7

Appendix 5-1. Cont.
(KAS09 core depth 256.80-439.96).

Core depth [m]	Chloritised biotite	Argillised grains	Secondary chlorite	Total epidote	Sauss./alb. plagioclase	Calcite	Altered titanite	Secondary quartz	K-feldspar
256.80	1.0	0.0	0.0	1.9	16.2	0.0	0.0	0.5	0.5
259.20	0.0	0.0	1.0	3.0	12.8	0.0	0.0	0.0	0.0
259.55	2.9	0.0	3.8	3.8	35.7	1.0	0.0	1.9	0.0
263.20	1.4	0.9	3.3	2.8	29.4	0.9	0.0	0.9	0.0
265.87	3.6	0.0	5.5	2.3	25.9	1.8	0.0	0.9	0.0
270.90	1.5	0.0	1.5	0.5	5.3	0.5	0.0	0.0	0.0
275.05	1.0	0.0	1.9	0.5	5.7	0.5	0.0	0.0	0.0
275.20	1.4	0.0	10.4	9.0	21.3	1.0	0.5	1.0	1.0
275.90	0.0	0.0	2.4	4.8	16.4	0.5	0.0	0.0	0.0
282.31	1.4	0.0	1.8	5.5	9.6	0.0	0.0	1.4	1.4
285.58	0.9	0.0	0.0	7.0	10.8	0.9	0.0	0.9	0.9
294.24	0.0	0.0	0.0	2.0	4.4	1.0	0.0	0.0	0.0
297.60	2.8	0.5	0.5	3.3	3.8	0.5	0.5	1.4	0.9
301.50	2.8	0.5	0.9	1.4	14.6	0.5	0.0	0.0	0.0
307.46	2.3	0.5	0.5	1.4	14.6	0.0	0.5	0.9	0.5
311.17	6.4	0.5	1.4	8.3	38.1	1.8	0.5	1.4	0.9
312.45	4.6	0.5	1.4	3.7	11.1	0.0	0.0	0.9	0.5
315.45	8.1	0.5	0.5	6.2	42.2	1.0	0.5	1.0	0.5
316.65	1.0	0.0	1.0	2.4	6.8	0.0	0.0	0.0	0.0
318.80	1.4	0.5	6.2	1.9	20.0	0.0	0.0	1.0	1.0
319.83	0.5	0.0	1.0	1.0	2.0	0.0	0.0	0.0	0.0
323.17	1.9	0.0	2.4	3.4	15.8	0.0	0.0	1.0	1.0
324.30	0.5	0.5	0.5	1.4	9.9	0.0	0.0	0.5	0.9
328.42	3.1	0.5	2.7	8.0	25.0	0.0	0.9	0.9	2.7
332.85	3.6	0.5	2.7	3.6	33.8	2.3	0.0	1.4	2.3
335.44	1.9	0.5	0.0	1.9	15.6	0.0	0.5	1.4	0.9
340.30	1.8	0.5	0.5	3.2	6.9	0.0	2.3	0.5	0.5
344.34	0.5	0.5	0.5	0.9	10.8	0.0	0.5	0.9	0.5
348.20	0.0	0.5	0.5	1.4	18.6	0.5	0.0	1.0	0.5
350.60	7.4	0.5	0.9	6.5	14.0	0.0	1.4	0.5	0.9
353.34	5.5	0.5	0.5	5.5	11.9	0.0	0.5	1.0	0.5
357.63	6.5	1.7	3.5	3.0	36.4	0.0	0.9	1.3	2.6
361.08	1.8	0.9	0.9	3.6	17.1	0.0	0.9	0.9	0.9
363.26	0.5	0.0	0.0	1.5	5.9	0.0	0.0	1.0	1.5
370.16	4.4	0.0	6.3	7.3	38.7	0.0	0.0	0.5	1.0
379.79	1.4	0.0	4.2	4.2	32.4	0.0	0.0	1.4	1.4
388.40	1.0	0.0	1.9	1.0	13.0	0.0	0.0	1.0	1.0
390.16	1.4	0.0	4.7	1.4	30.8	0.0	1.4	0.9	0.9
397.06	0.9	0.9	5.3	6.2	41.6	2.2	1.3	1.3	1.3
397.60	1.5	0.0	1.9	3.4	11.1	0.0	0.0	1.0	1.0
398.75	0.5	3.8	3.3	4.2	26.3	0.0	0.5	1.4	1.4
403.27	0.0	0.0	7.0	4.2	39.9	0.9	0.5	0.9	1.4
404.34	1.0	0.0	2.0	1.5	15.1	0.5	0.0	1.0	0.5
410.05	0.5	2.8	0.9	3.7	24.9	0.0	0.0	0.0	0.0
412.40	0.0	0.0	3.7	1.9	23.6	0.5	0.0	0.9	0.9
417.80	0.0	2.6	4.2	0.0	7.3	10.9	0.0	1.0	1.0
421.73	2.0	0.5	1.0	3.9	24.9	0.0	0.0	0.0	0.0
429.44	0.0	0.0	12.2	14.0	39.6	0.5	1.4	1.8	2.7
433.75	1.0	0.0	0.5	5.2	10.9	0.0	0.0	0.0	0.0
439.96	2.4	0.0	0.5	0.5	24.3	0.0	1.0	0.0	0.0

Appendix 5-1. Cont.
(KAS09 core depth 256.80-439.96).

Core depth [m]	Prehnite	Pumpellyite	Hematite	Pyrite	Primary quartz	K-feldspar/ perthite	Plagioclase	Biotite	Amphibole
256.80	1.0	0.0	0.0	0.0	29.1	18.6	21.9	6.7	0.5
259.20	0.0	0.0	0.0	0.0	40.4	16.3	17.2	7.9	0.0
259.55	0.0	0.0	0.5	0.0	31.0	14.8	2.4	1.0	0.0
263.20	2.8	0.0	0.0	0.0	27.1	22.4	6.1	0.9	0.0
265.87	0.9	0.0	0.0	0.0	30.0	21.8	1.8	0.0	0.0
270.90	0.0	0.0	0.0	0.0	34.5	29.6	24.3	0.0	0.0
275.05	0.0	0.0	0.0	0.0	37.8	34.5	11.5	2.9	0.0
275.20	0.0	0.0	1.0	0.5	9.5	33.7	9.0	0.5	0.0
275.90	0.0	0.0	0.0	0.0	22.7	8.2	23.7	18.4	0.0
282.31	0.0	0.0	0.0	0.0	11.8	9.1	18.2	30.0	2.7
285.58	0.0	0.0	0.0	0.0	12.7	35.2	11.7	13.6	1.9
294.24	0.0	0.0	0.0	0.0	26.3	26.8	16.6	13.7	5.9
297.60	0.5	0.0	0.9	0.0	17.4	48.4	4.2	1.4	12.7
301.50	0.0	0.0	1.9	0.0	37.1	29.1	7.0	0.9	0.0
307.46	1.8	0.0	0.9	0.0	35.5	34.6	3.6	0.5	0.0
311.17	0.5	0.0	0.0	0.0	18.4	20.2	0.5	0.0	0.0
312.45	0.9	0.0	0.0	0.0	35.0	13.8	8.3	14.8	1.4
315.45	1.0	0.0	0.0	0.0	18.0	10.0	8.5	0.0	0.0
316.65	0.0	0.0	0.0	0.0	32.2	27.8	19.0	7.3	0.0
318.80	0.0	0.0	1.9	0.0	27.6	33.3	4.3	0.0	0.0
319.83	0.0	0.0	0.0	0.0	35.2	33.2	24.3	2.0	0.0
323.17	0.0	0.0	0.0	0.0	20.6	11.5	29.7	6.7	3.8
324.30	0.0	0.0	0.0	0.0	32.9	21.1	18.8	9.4	0.0
328.42	1.3	0.0	0.0	0.0	16.1	29.5	4.9	0.0	0.0
332.85	1.8	0.0	0.0	0.0	23.0	20.3	3.6	0.9	0.0
335.44	1.4	0.0	0.0	0.0	20.3	33.5	15.1	5.7	0.0
340.30	0.9	0.0	0.0	0.0	14.8	23.0	24.4	10.6	7.8
344.34	1.4	0.0	0.0	0.0	30.5	23.0	19.7	8.5	0.0
348.20	0.5	0.0	0.0	0.0	37.1	28.1	7.6	2.4	0.0
350.60	1.4	0.0	0.0	0.0	14.0	9.8	31.2	9.8	0.0
353.34	0.0	0.0	0.0	0.0	26.9	12.9	23.9	9.0	1.0
357.63	2.2	0.0	0.0	0.0	26.4	10.8	1.7	0.0	0.0
361.08	2.3	0.0	0.0	0.0	17.6	9.0	35.1	5.9	0.0
363.26	0.0	0.0	0.0	0.0	29.7	22.3	26.7	10.4	0.0
370.16	0.0	0.0	0.0	0.0	19.8	7.7	12.1	0.5	0.0
379.79	2.8	0.0	1.4	0.0	22.7	17.6	10.2	0.0	0.0
388.40	0.0	0.0	0.0	0.0	43.0	22.2	14.5	0.0	0.0
390.16	0.0	0.0	0.0	0.0	22.0	26.2	7.0	0.0	0.0
397.06	2.2	0.0	2.2	0.0	19.9	10.6	2.2	0.0	0.0
397.60	0.0	0.0	0.0	0.0	27.1	23.7	15.9	12.1	0.0
398.75	0.0	0.0	0.0	0.0	28.6	19.3	8.0	0.0	0.0
403.27	0.0	0.0	0.0	0.0	20.2	18.8	3.8	0.0	0.0
404.34	0.0	0.0	0.0	0.0	29.8	25.9	18.1	4.4	0.0
410.05	2.3	0.0	2.3	0.0	28.1	12.9	12.0	6.5	0.0
412.40	0.0	0.0	2.3	0.0	19.4	33.3	10.7	0.0	0.0
417.80	0.0	0.0	1.6	0.0	32.1	15.0	10.9	0.5	0.0
421.73	0.0	0.0	0.0	0.0	35.6	12.2	11.7	5.9	0.0
429.44	0.0	0.5	0.0	0.0	14.0	3.6	6.8	0.0	0.0
433.75	1.0	0.0	0.0	0.0	0.5	1.4	35.6	33.7	6.2
439.96	0.0	0.0	0.0	0.0	19.1	7.1	24.8	13.8	2.9

Appendix 5-1. Cont.
(KAS09 core depth 256.80-439.96).

Core depth [m]	Muscovite	Magnetite	Titanite	Fluorite/ apatite	Voids/ fractures	Total %	Rock color	Alteration index
256.80	0.0	1.4	1.0	0.0	0.0	100	R	0.3
259.20	0.0	0.5	0.5	0.5	0.0	100	RG	0.2
259.55	0.0	0.0	1.0	0.5	0.0	100	R	1.0
263.20	0.0	0.0	0.9	0.0	0.0	100	R	0.7
265.87	0.0	1.4	2.7	1.4	0.0	100	RG	0.7
270.90	2.4	0.0	0.0	0.0	0.0	100	R	0.1
275.05	0.0	1.4	0.5	1.9	0.0	100	R	0.1
275.20	0.0	0.5	0.0	0.0	0.0	100	R	0.9
275.90	0.0	1.5	1.0	0.5	0.0	100	G	0.3
282.31	0.0	0.5	1.8	5.0	0.0	100	G	0.3
285.58	0.0	2.4	0.9	0.0	0.0	100	G	0.3
294.24	0.0	0.5	2.0	1.0	0.0	100	G	0.1
297.60	0.0	0.0	0.5	0.0	0.0	100	GR	0.2
301.50	1.4	0.0	1.9	0.0	0.0	100	R	0.3
307.46	1.4	0.0	0.9	0.0	0.0	100	R	0.3
311.17	0.0	0.0	1.4	0.0	0.0	100	R	1.5
312.45	0.0	1.4	1.8	0.0	0.0	100	G	0.3
315.45	0.0	1.0	1.4	0.0	0.0	100	R	1.6
316.65	0.0	1.5	1.0	0.0	0.0	100	G	0.1
318.80	0.0	0.0	1.0	0.0	0.0	100	R	0.5
319.83	1.0	0.0	0.0	0.0	0.0	100	G	0.1
323.17	0.0	1.0	0.5	1.0	0.0	100	R	0.3
324.30	0.9	1.4	1.4	0.0	0.0	100	G	0.2
328.42	1.8	1.3	1.3	0.0	0.0	100	R	0.8
332.85	0.0	0.0	0.5	0.0	0.0	100	R	1.1
335.44	0.0	0.9	0.5	0.0	0.0	100	G	0.3
340.30	0.0	1.4	0.9	0.0	0.0	100	G	0.2
344.34	0.0	0.9	0.9	0.0	0.0	100	G	0.2
348.20	1.0	0.5	0.0	0.0	0.0	100	R	0.3
350.60	0.0	0.9	0.9	0.0	0.0	100	G	0.5
353.34	0.0	0.0	0.5	0.0	0.0	100	G	0.4
357.63	0.0	2.2	0.9	0.0	0.0	100	R	1.4
361.08	0.0	1.8	1.4	0.0	0.0	100	G	0.4
363.26	0.0	0.0	0.5	0.0	0.0	100	G	0.1
370.16	0.0	1.0	1.0	0.0	0.0	100	R	1.4
379.79	0.0	0.0	0.5	0.0	0.0	100	R	1.0
388.40	0.0	1.0	0.5	0.0	0.0	100	G	0.2
390.16	0.0	0.0	0.9	2.3	0.0	100	R	0.7
397.06	0.0	0.0	1.3	0.4	0.0	100	R	1.9
397.60	0.0	1.5	0.0	0.0	0.0	100	G	0.3
398.75	0.0	0.5	1.4	0.9	0.0	100	R	0.7
403.27	0.0	0.5	1.4	0.5	0.0	100	R	1.2
404.34	0.0	0.0	0.5	0.0	0.0	100	G	0.3
410.05	0.0	1.4	1.4	0.5	0.0	100	RG	0.6
412.40	0.9	0.5	1.4	0.0	0.0	100	R	0.5
417.80	7.3	0.5	0.0	0.0	5.2	100	G	0.4
421.73	0.0	1.0	1.5	0.0	0.0	100	GR	0.5
429.44	0.0	0.9	2.3	0.0	0.0	100	R	2.6
433.75	0.0	1.4	2.8	0.0	0.0	100	G	0.2
439.96	0.0	1.9	1.9	0.0	0.0	100	R	0.4

Appendix 5-2. Modal analyses of the sampled rocks from KAS 14 based on counting of 400 points in each thin section.
(KAS14 core depth 1.05-211.83).

Core depth [m]	Chloritised biotite	Argillised grains	Secondary chlorite	Total epidote	Sauss./alb. plagioclase	Calcite	Altered titanite	Secondary quartz	K-feldspar
1.05	4.1	1.4	0.9	3.7	35.6	0.9	0.5	0.5	1.8
2.65	3.6	0.5	0.9	1.4	30.0	0.0	1.4	0.9	2.7
11.55	6.4	0.4	0.9	1.7	32.6	0.0	1.3	0.9	3.4
18.65	1.4	0.9	0.9	0.5	12.3	0.0	1.4	3.2	1.8
27.35	4.1	0.4	6.6	7.8	36.2	2.9	0.8	5.8	6.6
35.98	1.4	0.5	0.9	7.8	13.8	0.0	0.5	0.9	1.4
46.20	0.0	0.0	1.9	0.0	6.6	0.0	0.5	0.0	0.0
54.55	0.0	0.0	10.3	6.8	19.7	0.0	0.0	1.3	0.9
63.63	1.4	0.0	1.4	2.3	17.7	0.9	0.0	0.9	0.5
70.28	0.0	0.0	1.4	1.9	6.5	0.0	0.0	2.3	1.4
76.23	1.6	3.6	6.9	9.3	11.7	0.4	1.2	2.0	2.0
98.32	1.3	4.4	13.7	13.7	32.7	2.7	0.4	0.9	0.9
102.45	0.0	9.9	11.3	12.6	13.5	2.7	0.0	1.4	0.9
110.70	0.0	3.1	10.5	3.5	21.0	7.4	0.0	0.4	0.4
113.30	0.0	0.0	0.0	1.0	16.7	0.0	0.0	0.0	0.0
121.40	0.0	6.5	15.3	8.3	31.9	0.5	2.8	0.9	0.9
123.05	0.0	8.4	18.1	4.9	33.9	0.4	0.9	0.9	0.9
131.10	1.8	2.7	1.4	6.8	25.5	5.5	0.0	0.9	0.9
143.36	0.0	0.9	15.4	13.0	27.0	0.0	0.9	1.4	0.5
144.83	0.5	0.0	1.4	8.6	23.3	0.0	0.5	0.5	0.5
153.30	0.0	3.8	9.5	10.0	50.0	0.5	0.5	1.0	1.0
159.95	3.7	2.7	3.7	9.6	26.5	0.0	0.5	1.4	1.8
165.80	0.9	3.7	16.1	6.9	20.7	1.8	1.4	3.2	1.4
169.10	1.0	2.9	1.9	3.4	16.8	0.0	0.0	0.0	0.0
176.75	1.9	0.0	2.9	8.7	35.4	0.0	0.0	0.0	0.0
178.08	4.3	2.9	2.4	11.9	30.0	0.0	0.0	0.5	0.5
192.30	4.4	1.8	4.9	12.8	30.5	0.0	0.0	2.7	1.8
198.00	0.9	2.3	22.3	20.5	30.9	0.9	0.9	1.8	1.4
207.10	6.1	1.4	7.1	7.6	33.0	2.4	0.0	1.9	1.4
211.83	1.0	5.7	1.4	4.7	21.3	0.0	0.0	2.4	2.4

Appendix 5-2 Cont.

(KAS14 core depth 1.05-211.83).

Core depth [m]	Prehnite	Pumpellyite	Hematite	Pyrite	Primary quartz	K-feldspar/ perthite	Plagioclase	Biotite	Amphibole
1.05	0.9	0.0	0.9	0.0	10.1	7.3	19.2	7.8	2.3
2.65	0.5	0.0	0.0	0.0	30.0	25.1	1.4	0.0	0.0
11.55	1.7	0.0	3.9	0.0	15.5	23.2	6.4	0.4	0.0
18.65	0.0	0.0	0.0	0.0	54.1	20.5	2.7	0.0	0.0
27.35	0.4	0.0	0.8	0.0	9.5	12.4	4.9	0.0	0.0
35.98	0.0	0.0	0.0	0.0	8.7	8.7	37.6	13.8	0.0
46.20	0.0	0.0	0.0	0.0	41.0	33.5	14.2	0.0	0.0
54.55	8.6	0.0	2.6	0.0	7.7	12.4	28.6	0.0	0.0
63.63	3.7	0.0	0.0	0.0	23.3	12.6	19.1	14.4	0.0
70.28	0.9	0.0	0.0	0.0	13.9	24.1	23.2	17.6	6.0
76.23	11.3	0.0	0.0	0.0	4.8	20.2	21.4	0.0	0.0
98.32	2.7	0.0	0.0	0.0	11.1	3.5	8.0	0.0	0.0
102.45	2.3	0.0	0.5	0.0	14.4	12.2	15.8	0.5	0.0
110.70	1.3	0.0	0.4	0.4	14.0	24.0	11.4	0.0	0.0
113.30	0.0	0.0	0.0	0.0	15.2	6.7	27.6	16.2	11.9
121.40	0.0	0.0	0.0	0.0	9.3	13.9	6.0	0.0	0.0
123.05	0.0	0.0	0.0	0.0	12.3	5.3	4.9	0.0	0.0
131.10	0.0	0.0	0.0	0.0	16.4	7.3	13.6	15.5	0.0
143.36	0.0	0.0	0.0	0.0	17.7	17.2	2.8	0.0	0.0
144.83	0.0	0.0	0.0	0.0	13.8	7.1	28.6	11.9	0.0
153.30	0.0	0.0	0.0	0.0	7.1	8.1	4.8	0.0	0.0
159.95	0.0	0.0	0.0	0.0	13.2	14.6	10.5	6.9	0.0
165.80	0.0	0.0	0.0	0.0	14.3	7.8	19.8	0.0	0.0
169.10	0.0	0.0	0.0	0.0	17.2	5.7	24.9	20.1	1.9
176.75	0.0	0.0	1.9	0.0	10.7	7.8	8.7	20.9	0.0
178.08	0.0	0.0	0.0	0.0	15.7	7.1	9.5	11.9	0.0
192.30	0.0	0.0	3.1	0.0	14.6	10.6	5.3	5.3	0.0
198.00	1.8	0.0	0.0	0.0	6.4	2.3	5.0	0.0	0.0
207.10	0.0	0.0	0.0	0.0	11.3	21.7	2.4	1.9	0.0
211.83	0.0	0.0	0.0	0.0	19.9	15.6	13.7	9.5	0.0

Appendix 5-2 Cont.

(KAS14 core depth 1.05-211.83).

Core depth [m]	Muscovite	Magnetite	Titanite	Fluorite/ apatite	Voids/ fractures	Total %	Rock color	Alteration index
1.05	0.0	0.9	1.4	0.0	0.0	100	G	1.1
2.65	0.0	0.9	0.9	0.0	0.0	100	R	0.7
11.55	0.0	0.0	1.3	0.0	0.0	100	R	1.1
18.65	0.0	0.0	0.5	0.0	0.0	100	R	0.3
27.35	0.0	0.8	0.0	0.0	0.0	100	R	2.6
35.98	0.0	2.3	1.8	0.0	0.0	100	RG	0.4
46.20	2.4	0.0	0.0	0.0	0.0	100	R	0.1
54.55	0.9	0.4	0.0	0.0	0.0	100	R	1.0
63.63	0.0	1.4	0.5	0.0	0.0	100	G	0.4
70.28	0.0	0.5	0.5	0.0	0.0	100	G	0.2
76.23	0.0	0.0	1.2	0.0	2.4	100	R	1.1
98.32	0.0	0.0	3.1	0.9	0.0	100	R	2.8
102.45	0.0	1.4	0.9	0.0	0.0	100	R	1.2
110.70	0.0	0.4	1.3	0.4	0.0	100	R	0.9
113.30	0.0	1.0	3.3	0.5	0.0	100	G	0.2
121.40	0.0	0.9	2.3	0.5	0.0	100	G	2.0
123.05	0.0	6.2	2.2	0.9	0.0	100	G	2.2
131.10	0.0	0.5	0.9	0.5	0.0	100	RG	0.8
143.36	0.0	0.9	1.9	0.5	0.0	100	R	1.4
144.83	0.0	1.9	1.4	0.0	0.0	100	G	0.5
153.30	0.0	1.4	1.4	1.0	0.0	100	R	3.2
159.95	0.0	1.8	1.8	1.4	0.0	100	R	1.0
165.80	0.0	0.0	1.8	0.0	0.0	100	R	1.3
169.10	0.0	1.0	2.4	1.0	0.0	100	G	0.4
176.75	0.0	0.0	1.0	0.0	0.0	100	GR	1.0
178.08	0.0	0.0	3.3	0.0	0.0	100	R	1.1
192.30	0.0	0.0	2.2	0.0	0.0	100	RG	1.6
198.00	0.0	0.5	2.3	0.0	0.0	100	R	5.1
207.10	0.0	1.4	0.5	0.0	0.0	100	GR	1.6
211.83	0.0	1.4	1.0	0.0	0.0	100	G	0.6

Appendix 5-3. KAS09 and KAS14. Electron microprobe analyses of primary and secondary feldspars based on eight oxygen atoms. nd = not detected.
(KAS09 core depth 0.40-23.55).

Core depth [m]	KAS09 0.40 B	KAS09 0.40 A	KAS09 11.87 B	KAS09 11.87 B	KAS09 11.87 B	KAS09 11.87 B	KAS09 11.87 C	KAS09 11.87 F	KAS09 23.55 C	KAS09 23.55 C	KAS09 23.55 C
Wt. %											
SiO_2	60.1	68.5	59.8	59.7	57.4	60.2	64	65	64	63.1	68.1
Al_2O_3	24.4	19.8	22.7	23.1	24.5	23.2	18.2	18.3	18.4	18.1	19.1
CaO	5.9	0.08	5.8	5.8	7.4	5.9	0.02	nd	nd	0.19	0.12
Na_2O	8.2	11.9	8.4	8.5	7.8	8.2	0.32	0.23	0.1	0.11	11.9
K_2O	0.02	0.04	0.14	0.11	0.16	0.18	15.6	15	16.2	15.6	0.09
BaO	nd	nd	nd	nd	0.65	nd	1	0.27	0.65	1.2	nd
SrO	nd	nd	0.27	0.3	0.14	nd	0.2	0.12	0.13	0.43	0.06
Total	98.62	100.32	97.3	97.8	99.5	98.0	99.5	100.2	99.5	98.0	99.5
Atom / Formula											
Si	2.71	2.98	2.74	2.73	2.64	2.84	3.00	3.02	2.99	2.98	3.00
Al	1.30	1.02	1.23	1.25	1.33	1.29	1.00	1.00	1.01	1.01	0.99
Ca	0.29	0.00	0.29	0.28	0.36	0.01	0.00	0.00	0.00	0.01	0.01
Na	0.72	1.01	0.75	0.75	0.70	0.75	0.03	0.02	0.01	0.01	1.02
K	0.00	0.00	0.01	0.01	0.01	0.01	0.93	0.98	0.97	0.94	0.01
Ba	0.00	0.00	0.00	0.00	0.01	0.00	0.02	0.01	0.01	0.02	0.00
Sr	0.00	0.00	0.01	0.01	0.00	0.00	0.01	0.00	0.00	0.01	0.00

A-Albitised plagioclase, B-magmatic plagioclase, C-K-feldpsar replacing plagioclase, D-magmatic K-feldspar, E-perthitic albite, F-Fracture-filling K-feldspar, G-Secondary K-feldspar in chloritised biotite

Appendix 5-3. Cont.
(KAS09 core depth 23.55-166.8).

Core depth [m]	KAS09 23.55 B	KAS09 23.55 C	KAS09 23.55 C	KAS09 77.70 A	KAS09 77.70 F	KAS09 77.70 A	KAS09 77.70 C	KAS09 97.71 B	KAS09 120.09 E	KAS09 140.2 B	KAS09 166.8 B
Wt. %											
SiO_2	65	62.3	61.3	68.5	64.2	68.9	64.3	59.6	68.6	60.4	61.8
Al_2O_3	21.9	19	19	19	17.7	19.3	18.2	24.8	20.8	24.6	23.8
CaO	4.2	nd	nd	0.03	0.01	0.06	0.03	6.5	1.5	6.2	5.4
Na_2O	8.7	0.34	0.26	11.6	0.06	11.9	0.19	7.8	9	8.0	8.7
K_2O	0.05	15.1	14.7	0.01	16.7	0.05	16.3	0.03	0.15	nd	0.06
BaO	nd	2.8	4.1	nd	0.06	0.03	0.16	0.04	nd	nd	nd
SrO		0.21	nd	nd	0.04	nd	0.06	nd	nd	nd	0.14
Total	101.3	99.6	99.1	99.3	99.2	100.3	99.8	98.77	99.6	99.2	99.1
Atom / Formula											
Si	2.86	2.94	2.93	3.01	3.01	3.00	3.00	2.69	2.98	2.70	2.75
Al	1.14	1.06	1.07	0.99	0.98	0.99	1.00	1.32	1.06	1.30	1.25
Ca	0.20	0.00	0.00	0.00	0.00	0.00	0.00	0.31	0.07	0.30	0.26
Na	0.74	0.03	0.02	0.99	0.01	1.01	0.02	0.68	0.76	0.69	0.75
K	0.00	0.91	0.90	0.00	1.00	0.00	0.97	0.00	0.01	0.00	0.00
Ba	0.00	0.05	0.08	0.00	0.00	0.00	0.00	0.00	0.00	0.00	0.00
Sr	0.00	0.01	0.00	0.00	0.00	0.00	0.00	0.00	0.00	0.00	0.00

A-Albitised plagioclase, B-magmatic plagioclase, C-K-feldpsar replacing plagioclase, D-magmatic K-feldspar, E-perthitic albite, F-Fracture-filling K-feldspar, G-Secondary K-feldspar in chloritised biotite

Appendix 5-3. Cont.
(KAS09 core depth 166.85-253.50).

Core depth [m]	KAS09 166.85 C	KAS09 166.85 C	KAS09 166.85 A	KAS09 166.85 A	KAS09 169.55 C	KAS09 169.55 B	KAS09 169.55 A	KAS09 246.65 C	KAS09 246.65 B	KAS09 246.65 A	KAS09 253.50 G
Wt. %											
SiO_2	64.3	63.6	68.1	68.8	68.3	60.7	68.6	65.0	59.7	69.1	65.1
Al_2O_3	18.4	18.6	20	20.7	29.1	24.5	19.6	19.9	25.0	19.9	18.8
CaO	0.06	nd	0.41	0.32	0.02	5.9	0.02	0.02	6.7	0.02	nd
Na_2O	0.24	0.29	11.9	11.2	0.09	8.3	11.4	0.03	8.0	11.9	nd
K_2O	16.4	15.4	0.08	0.22	16.7	nd	0.02	16.8	0.01	nd	16.8
BaO	0.64	1.7	nd	nd	0.08	nd	nd	0.84	0.02	nd	nd
SrO	nd	0.07	0.07	nd	0.05	nd	0.02	0.02	0.02	0.01	nd
Total	97.3	97.8	99.5	98	114.34	99.4	99.66	102.61	99.45	100.93	100.7
Atom / Formula											
Si	2.99	2.98	2.97	2.97	2.75	2.71	3.00	2.95	2.68	2.99	2.99
Al	1.01	1.03	1.03	1.05	1.38	1.29	1.01	1.06	1.32	1.02	1.02
Ca	0.00	0.00	0.02	0.02	0.00	0.28	0.00	0.00	0.32	0.00	0.00
Na	0.02	0.03	1.01	0.94	0.01	0.72	0.97	0.00	0.70	1.00	0.00
K	0.97	0.92	0.00	0.01	0.86	0.00	0.00	0.97	0.00	0.00	0.99
Ba	0.01	0.03	0.00	0.00	0.00	0.00	0.00	0.02	0.00	0.00	0.00
Sr	0.00	0.00	0.00	0.00	0.00	0.00	0.00	0.00	0.00	0.00	0.00

A-Albitised plagioclase, B-magmatic plagioclase, C-K-feldpsar replacing plagioclase, D-magmatic K-feldspar, E-perthitic albite, F-Fracture-filling K-feldspar, G-Secondary K-feldspar in chloritised biotite

Appendix 5-3. Cont.
(KAS09 core depth 285.58-397.06).

Core depth [m]	KAS09 285.58 B	KAS09 324.30 C	KAS09 324.30 B	KAS09 328.42 A	KAS09 328.42 B	KAS09 328.42 C	KAS09 328.42 C	KAS09 332.85 B	KAS09 332.85 C	KAS09 397.06 C	KAS09 397.06 D
Wt. %											
SiO_2	61.2	65.0	62.3	67.7	61.4	63.3	63.1	60.5	66.7	63.9	64.5
Al_2O_3	23.5	18.7	23.1	19.3	23.9	19.4	18.9	24.1	19.4	17.5	17.6
CaO	5.4	nd	4.8	0.11	5.7	nd	0.02	5.5	0.02	0.01	0.08
Na_2O	9.2	0.02	9.1	11.6	8.6	0.16	0.16	8.9	0.02	0.07	0.17
K_2O	nd	16.9	0.02	0.16	0.02	15.8	15.6	0.01	16.6	16.4	16.3
BaO	nd	0.3	0.02	nd	nd	0.14	1.7	nd	0.32	0.07	0.08
SrO	nd	0.02	0.01	0.03	0.01	0.23	0.08	0.01	0.01	nd	0.03
Total	99.3	100.94	99.35	99.6	99.1	97.3	97.8	99.02	103.07	99.5	100.2
Atom / Formula											
Si	2.74	2.99	2.78	2.99	2.74	2.96	2.96	2.72	2.99	3.02	3.02
Al	1.24	1.01	1.21	1.01	1.26	1.07	1.05	1.28	1.03	0.98	0.97
Ca	0.26	0.00	0.23	0.01	0.27	0.00	0.00	0.27	0.00	0.00	0.00
Na	0.80	0.00	0.79	0.99	0.74	0.02	0.02	0.78	0.00	0.01	0.02
K	0.00	0.99	0.00	0.01	0.00	0.94	0.93	0.00	0.95	0.99	0.97
Ba	0.00	0.01	0.00	0.00	0.00	0.00	0.03	0.00	0.01	0.00	0.00
Sr	0.00	0.00	0.00	0.00	0.00	0.01	0.00	0.00	0.00	0.00	0.00

A-Albitised plagioclase, B-magmatic plagioclase, C-K-feldpsar replacing plagioclase, D-magmatic K-feldspar, E-perthitic albite, F-Fracture-filling K-feldspar, G-Secondary K-feldspar in chloritised biotite

Appendix 5-3. Cont.
(KAS14 core depth 2.65-102.45).

Core depth [m]	KAS14 2.65 A	KAS14 2.65 C	KAS14 2.65 B	KAS14 11.55 C	KAS14 11.55 B	KAS14 682 A	KAS14 70.28 B	KAS14 102.45 B
Wt. %								
SiO_2	69.0	64.8	59.8	64.9	59.8	68.4	60.5	60.2
Al_2O_3	19.3	20.0	24.8	18.3	24.7	19.2	24.2	24.4
CaO	0.02	0.03	6.2	nd	6.0	0.06	5.8	5.6
Na_2O	11.4	0.02	8.1	0.09	0.03	11.2	8.7	9.1
K_2O	0.02	16.7	0.02	16.6	nd	nd	0.01	0.02
BaO	nd	0.02	0.01	0.02	nd	nd	nd	0.02
SrO	0.01	0.02	0.01	0.05	nd	nd	nd	0.01
Total	99.75	101.59	98.94	99.96	90.53	98.86	99.21	99.35
Atom / Formula								
Si	3.01	2.95	2.69	3.00	2.82	3.01	2.71	2.70
Al	0.99	1.07	1.31	1.00	1.37	1.00	1.28	1.29
Ca	0.00	0.00	0.30	0.00	0.30	0.00	0.28	0.27
Na	0.97	0.00	0.71	0.01	0.00	0.96	0.76	0.79
K	0.00	0.97	0.00	0.98	0.00	0.00	0.00	0.00
Ba	0.00	0.00	0.00	0.00	0.00	0.00	0.00	0.00
Sr	0.00	0.00	0.00	0.00	0.00	0.00	0.00	0.00

A-Albitised plagioclase, B=magmatic plagioclase, C-K-feldpsar replacing plagioclase, D-magmatic K-feldspar, E-perthitic albite, F-Fracture-filling K-feldspar, G-Secondary K-feldspar in chloritised biotite

Appendix 5-4. KAS09. Electron microprobe analyses of biotite and amphibole. The chemical formula of biotite is based on 24 (O, OH), and that of amphibole is based on 23 (O, OH). All iron is assumed to be as FeO. nd = not detected. (KAS09 core depth 11.87-439.96).

Core depth [m]	**KAS09 11.87** biotite	**KAS09 11.87** amphibole	**KAS09 11.87** amphibole	**KAS09 20.67** amphibole	**KAS09 20.67** amphibole	**KAS09 74.40** biotite	**KAS09 163.35** amphibole	**KAS09 163.35** amphibole	**KAS09 221.75** biotite	**KAS09 297.60** amphibole	**KAS09 297.60** amphibole	**KAS09 439.96** biotite
Wt. %												
SiO_2	36.5	55.2	45.5	45.7	54.8	36.1	45.2	54.1	36.3	55.2	45.9	36.8
TiO_2	1.5	Nd	1.2	0.90	0.03	1.8	1.6	nd	2.3	0.05	1.4	1.9
Al_2O_3	14.5	4.8	7.6	7.9	4.6	13.9	7.7	5.3	14.8	4.6	7.6	14.2
FeO	17.7	10.5	16.4	16.8	10.6	18.0	15.9	10.8	18.3	10.2	16.6	19.1
MnO	0.34	0.17	0.22	0.47	0.19	0.32	0.34	0.24	0.26	0.21	0.45	0.03
MgO	13.5	14.7	11.6	11.9	14.7	13.7	12.1	14.7	13.1	14.9	11.5	13.0
CaO	nd	11.8	12.1	12.1	11.8	0.01	11.9	11.8	0.02	11.7	11.8	nd
Na_2O	nd	1.8	1.1	0.84	2.0	0.01	1.2	1.6	nd	1.9	1.1	0.02
K_2O	9.8	0.35	0.78	1.0	0.31	9.9	0.69	0.41	9.9	0.23	1.0	9.8
BaO	0.21	nd	0.04	0.04	0.01	0.15	0.06	0.03	0.08	0.01	0.07	0.13
Total	94.05	99.32	96.54	97.65	99.04	93.89	96.69	98.98	95.06	99	97.42	94.98
Atom / Formula												
Si	5.64	7.73	6.89	6.86	7.71	5.61	6.82	7.63	5.56	7.74	6.90	5.65
Al^{iv}	2.36	0.27	1.11	1.15	0.29	2.39	1.18	0.38	2.44	0.26	1.11	2.35
∑Z	8.00	8.00	8.00	8.00	8.00	8.00	8.00	8.00	8.00	8.00	8.00	8.00
Al^{vi}	0.28	0.52	0.24	0.25	0.47	0.15	0.19	0.51	0.23	0.50	0.24	0.22
Ti	0.17	0.00	0.14	0.10	0.00	0.21	0.18	0.00	0.27	0.01	0.16	0.22
Fe^{2+}	2.29	1.23	2.08	2.11	1.25	2.34	2.01	1.27	2.34	1.20	2.09	2.45
Mn	0.05	0.02	0.03	0.06	0.02	0.04	0.04	0.03	0.03	0.03	0.06	0.00
Mg	3.11	3.07	2.62	2.66	3.08	3.17	2.72	3.09	2.99	3.11	2.58	2.98
∑X,Y	5.89	4.83	5.10	5.18	4.83	5.92	5.15	4.90	5.87	4.84	5.12	5.87
Ca	0.00	1.77	1.96	1.95	1.78	0.00	1.92	1.78	0.00	1.76	1.90	0.00
Na	0.00	0.49	0.32	0.24	0.55	0.00	0.35	0.44	0.00	0.52	0.32	0.01
K	1.93	0.06	0.15	0.19	0.06	1.96	0.13	0.07	1.93	0.04	0.19	1.92
Ba	0.01	0.00	0.00	0.00	0.00	0.01	0.00	0.00	0.01	0.00	0.00	0.01
∑W	1.94	2.32	2.44	2.38	2.38	1.98	2.41	2.30	1.94	2.32	2.42	1.93

Appendix 5-5. KAS09 and KAS14. Electron microprobe analyses of muscovite and sericite. The chemical formulae of sericite and muscovite are based on 24 (O, OH). All iron is assumed to be as Fe_2O_3. nd = not detected.
(KAS09 core depth 7.42-335.44. KAS14 depth 102.45-165.80).

Core depth [m]	**KAS09 7.42** sericite	**KAS09 20.77** muscovite	**KAS09 39.70** sericite	**KAS09 97.75** sericite	**KAS09 130.60** muscovite	**KAS09 140.20** muscovite	**KAS09 166.85** sericite	**KAS09 203.35** muscovite	**KAS09 253.50** sericite	**KAS09 335.44** sericite	**KAS14 102.45** sericite	**KAS14 165.80** sericite
Wt. %												
SiO_2	48.7	47.3	48.6	47.4	47.0	47.6	48.9	47.2	48.8	49.0	48.7	47.4
TiO_2	0.02	0.45	0.02	nd	0.37	0.18	0.01	0.22	0.02	0.03	0.03	0.01
Al_2O_3	32.9	31.6	32.7	32.9	31.9	31.3	33.0	31.5	32.8	32.5	32.8	33.1
Fe_2O_3	5.2	4.2	5.4	5.5	4.1	3.9	5.4	4.1	5.7	6.1	6.0	5.5
MnO	0.01	nd	0.01	0.02	0.02	0.02	nd	nd	0.01	0.02	0.01	nd
MgO	1.2	1.8	0.82	1.0	1.9	2.1	0.70	1.3	1.1	0.91	1.2	1.3
CaO	0.01	nd	0.01	0.01	nd	0.01	0.02	nd	0.01	0.01	0.01	nd
Na_2O	0.32	0.18	0.33	0.31	0.08	0.04	0.34	0.05	0.35	0.30	0.33	0.35
K_2O	9.7	10.4	9.6	9.7	10.5	10.3	9.8	10.6	9.6	9.7	9.7	9.6
BaO	0.21	0.18	0.22	0.25	0.14	0.27	0.55	0.23	0.17	0.16	0.24	0.22
SrO	0.01	0.05	0.01	0.01	0.03	nd	nd	0.03	0.01	nd	nd	0.02
Total	98.28	96.16	97.72	97.1	96.04	95.72	98.72	95.23	98.57	98.73	99.02	97.5
Atom / Formula												
Si	6.31	6.29	6.33	6.23	6.26	6.34	6.32	6.34	6.31	6.33	6.28	6.21
Al^{iv}	1.69	1.71	1.67	1.77	1.74	1.66	1.68	1.66	1.69	1.67	1.72	1.79
∑Z	8.00	8.00	8.00	8.00	8.00	8.00	8.00	8.00	8.00	8.00	8.00	8.00
Al^{vi}	3.33	3.24	3.35	3.33	3.26	3.26	3.35	3.32	3.30	3.28	3.27	3.31
Ti	0.00	0.05	0.00	0.00	0.04	0.02	0.00	0.02	0.00	0.00	0.00	0.00
Fe^{3+}	0.51	0.42	0.53	0.54	0.41	0.39	0.53	0.41	0.55	0.59	0.58	0.54
Mn	0.00	0.00	0.00	0.00	0.00	0.00	0.00	0.00	0.00	0.00	0.00	0.00
Mg	0.23	0.36	0.16	0.20	0.38	0.42	0.14	0.26	0.21	0.18	0.23	0.25
Ca	0.00	0.00	0.00	0.00	0.00	0.00	0.00	0.00	0.00	0.00	0.00	0.00
Na	0.08	0.05	0.08	0.08	0.02	0.01	0.09	0.01	0.09	0.08	0.08	0.09
K	1.60	1.76	1.60	1.63	1.78	1.75	1.62	1.82	1.58	1.60	1.60	1.60
Ba	0.01	0.01	0.01	0.01	0.01	0.01	0.03	0.01	0.01	0.01	0.01	0.01
Sr	0.00	0.00	0.00	0.00	0.00	0.00	0.00	0.00	0.00	0.00	0.00	0.00
∑W,X,Y	5.77	5.89	5.73	5.80	5.90	5.86	5.75	5.86	5.75	5.73	5.77	5.82

Appendix 5-6. KAS09 and KAS14. Electron microprobe analyses of primary and secondary titanite (all iron is assumed to be as Fe_2O_3). The chemical formula is calculated based on five oxygen atoms. nd = not detected.
(KAS09 core depth 20.67-23.55).

Core depth [m]	KAS09 20.67 E	KAS09 20.67 D	KAS09 21.01 E	KAS 09 21.01 D	KAS 09 21.01 D	KAS 09 21.01 A	KAS09 21.01 A	KAS09 23.55 E	KAS09 23.55 D
Wt. %									
SiO_2	30.8	30.1	31.2	30.4	30.4	30.6	27.8	30.7	30
TiO_2	27.3	35.5	28.2	36.5	35.9	27.7	37	27.7	34.9
Al_2O_3	6.0	1.4	5.9	1.2	1.6	6.4	1.2	6.1	1.3
Fe_2O_3	2.5	1.6	2.6	1.5	1.3	2.6	1.5	2.1	1.6
MnO	0.02	0.01	0.06	0.08	0.03	0.02	0.1	nd	0.12
MgO	0.01	nd	0.43	nd	0.13	nd	nd	nd	0.03
CaO	28.6	28.2	28.1	28.2	27.4	28.8	28	28.7	26.9
Na_2O	0.06	nd	0.12	nd	0.03	0.08	0.09	nd	0.02
K_2O	0.01	nd	0.02	0.01	nd	0.01	nd	nd	nd
BaO	0.17	0.42	0.41	0.37	0.39	0.24	0.35	0.35	0.45
SrO	0.01								
Total	95.48	97.3	96.9	98.1	96.9	96.5	96.1	94.4	95.2
Atom / Formula									
Si	1.05	1.02	1.05	1.01	1.02	1.03	0.96	1.04	1.03
Al	0.24	0.06	0.23	0.05	0.06	0.26	0.05	0.24	0.05
Ti	0.70	0.90	0.71	0.92	0.91	0.70	0.96	0.71	0.90
Fe^{3+}	0.06	0.04	0.07	0.04	0.03	0.07	0.04	0.05	0.04
Mn	0.00	0.00	0.00	0.00	0.00	0.00	0.00	0.00	0.00
Mg	0.00	0.00	0.02	0.00	0.01	0.00	0.00	0.00	0.00
Ca	1.04	1.02	1.01	1.01	0.99	1.04	1.03	1.05	0.99
Na	0.00	0.00	0.01	0.00	0.00	0.01	0.01	0.00	0.00
K	0.00	0.00	0.00	0.00	0.00	0.00	0.00	0.00	0.00
Ba	0.00	0.01	0.01	0.01	0.01	0.00	0.01	0.01	0.01
Sr	0.00								

A-Euhedral crystals in chloritised biotite, B- Remnants of dissolved magmatic titanite, C-Titanite overgrowth, D-Magmatic titanite, E- Small lenticular and sheet-like crystals with diffused boundary in chloritised biotite.

Appendix 5-6 – cont.
(KAS09 core depth 39.70-253.50).

Core depth [m]	KAS09 39.70 C	KAS09 39.70 D	KAS09 39.70 D	KAS09 56.20 E	KAS09 97.71 E	KAS09 120.09 E	KAS09 253.50 E	KAS09 253.50 C
Wt. %								
SiO_2	26.6	29	29.2	29.5	30.1	29.6	30.2	29.5
TiO_2	38.7	35	35.4	27.9	26.7	28.0	27.6	27.8
Al_2O_3	5.2	1	1	5.4	7.5	6.1	5.7	4.2
Fe_2O_3	1.4	1.7	1.4	3.0	1.9	2.8	2.6	2.9
MnO	0.01	0.08	0.09	nd	0.01	nd	0.01	nd
MgO	nd	nd	nd	0.01	0.01	0.01	0.01	nd
CaO	24.4	26.5	27	28.7	28.8	28.4	28.1	28.9
Na_2O	0.02	nd	nd	0.09	0.07	0.03	0.06	0.09
K_2O	0.02	nd	nd	nd	nd	0.01	0.01	0.01
BaO	0.42	0.4	0.38	0.13	0.21	0.12	0.09	0.05
SrO				nd	0.01	0.02	0.01	nd
Total	96.2	93.4	94.3	94.73	95.31	95.09	94.39	93.45
Atom / Formula								
Si	0.90	1.01	1.01	1.02	1.03	1.02	1.04	1.04
Al	0.21	0.04	0.04	0.22	0.30	0.25	0.23	0.17
Ti	0.98	0.92	0.92	0.73	0.68	0.72	0.72	0.73
Fe^{3+}	0.04	0.05	0.04	0.08	0.05	0.07	0.07	0.08
Mn	0.00	0.00	0.00	0.00	0.00	0.00	0.00	0.00
Mg	0.00	0.00	0.00	0.00	0.00	0.00	0.00	0.00
Ca	0.88	0.99	1.00	1.06	1.05	1.04	1.04	1.09
Na	0.00	0.00	0.00	0.01	0.01	0.00	0.00	0.01
K	0.00	0.00	0.00	0.00	0.00	0.00	0.00	0.00
Ba	0.01	0.01	0.01	0.00	0.00	0.00	0.00	0.00
Sr	0.00	0.00	0.00	0.00	0.00	0.00	0.00	0.00

A-Euhedral crystals in chloritised biotite, B- Remnants of dissolved magmatic titanite, C-Titanite overgrowth, D-Magmatic titanite, E- Small lenticular and sheet-like crystals with diffused boundary in chloritised biotite.

Appendix 5-6 – cont.
(KAS09 core depth 253.50-429.44. KAS14 core depth 165.80).

Core depth [m]	KAS09 253.50 D	KAS09 328.42 D	KAS09 340.30 D	KAS09 397.06 E	KAS09 429.44 D	KAS14 165.80 D	KAS14 165.80 C	KAS14 165.80 E
Wt. %								
SiO_2	30.3	29.5	30.4	31.1	30.1	30.5	30.8	29.9
TiO_2	34.8	33.6	35.7	24.1	37.2	35.8	31.9	28.3
Al_2O_3	1.5	2.8	1.7	8.4	1.6	1.9	4.2	5.7
Fe_2O_3	1.9	1.7	1.6	2.9	1.9	1.2	1.3	2.6
MnO	nd	0.04	nd	0.02	0.01	0.07	0.04	nd
MgO	nd	nd	0.01	0.51	0.01	nd	0.05	0.51
CaO	28.7	28.2	28.5	28.8	28.2	28.6	28.6	27.7
Na_2O	0.04	0.05	0.05	0.03	0.04	0.09	0.17	nd
K_2O	nd	nd	nd	0.04	nd	0.05	nd	nd
BaO	0.06	0.34	0.08	0.29	0.05	0.35	0.33	0.29
SrO	0.01		nd		0.01			
Total	97.31	96.23	98.04	96.5	99.12	96.9	98.1	96.9
Atom / Formula								
Si	1.02	1.01	1.01	1.05	0.99	1.01	1.03	1.03
Al	0.06	0.11	0.07	0.33	0.06	0.07	0.17	0.23
Ti	0.88	0.86	0.90	0.61	0.92	0.89	0.80	0.73
Fe^{3+}	0.05	0.04	0.04	0.07	0.05	0.03	0.03	0.07
Mn	0.00	0.00	0.00	0.00	0.00	0.00	0.00	0.00
Mg	0.00	0.00	0.00	0.03	0.00	0.00	0.00	0.03
Ca	1.04	1.03	1.02	1.04	1.00	1.02	1.03	1.02
Na	0.00	0.00	0.00	0.00	0.00	0.01	0.01	0.00
K	0.00	0.00	0.00	0.00	0.00	0.00	0.00	0.00
Ba	0.00	0.01	0.00	0.00	0.00	0.01	0.00	0.00
Sr	0.00		0.00		0.00			

A-Euhedral crystals in chloritised biotite, B- Remnants of dissolved magmatic titanite, C-Titanite overgrowth, D-Magmatic titanite, E- Small lenticular and sheet-like crystals with diffused boundary in chloritised biotite.

Appendix 5-7. KAS09. Electron microprobe analyses of primary and secondary epidote (all iron is assumed to be as Fe_2O_3). The chemical formula is calculated based on 12.5 oxygen atoms. nd = not detected.
(KAS09 core depth 0.40-140.20).

Core depth [m]	KAS09 0.40 B	KAS09 0.40 B	KAS09 11.87 B	KAS09 21.01 A	KAS09 21.01 A	KAS09 39.70 B	KAS09 77.70 B	KAS09 120.09 C	KAS09 120.09 B	KAS09 140.20 B
Wt. %										
SiO_2	37.2	36.7	39.9	37.1	34.2	37.3	37.6	37.6	37.8	37.2
TiO_2	0.14	0.04	nd	0.08	0.52	0.09	0.12	nd	0.05	0.10
Al_2O_3	22.4	22.3	21.3	22.3	9.1	22.1	22.3	22.8	22.4	22.6
Fe_2O_3	14.1	17.6	13.8	13.9	17.9	13.9	13.6	13.6	14.1	18.2
MnO	0.24	0.13	0.1	0.28	0.12	0.21	0.26	0.27	0.36	0.27
MgO	nd	0.01	nd	nd	nd	nd	nd	nd	nd	0.01
CaO	22.9	22.2	20.6	23.2	34	23.1	22.8	22.5	22.4	18.1
Na_2O	nd	0.01	0.87	nd	0.01	nd	0.03	nd	0.03	0.03
K_2O	nd	nd	0.08	nd	nd	0.01	nd	nd	0.02	0.02
BaO	nd	nd	nd	nd	nd	nd	nd	nd	nd	nd
SrO	0.35	0.49	0.11	0.1	0.1	0.41	0.34	0.46	0.78	0.13
Total	97.33	99.48	96.6	95.8	94.7	98.2	95.8	98	95.84	96.66
Atom/ Formula										
Si	3.00	2.92	3.19	3.00	3.01	3.02	3.03	3.02	3.03	3.00
Al^{iv}	0.00	0.08	0.00	0.00	0.00	0.00	0.00	0.00	0.00	0.00
∑Z	3.00	3.00	3.19	3.00	3.01	3.02	3.03	3.02	3.03	3.00
Al^{vi}	2.13	2.02	2.01	2.13	0.94	2.11	2.12	2.16	2.12	2.15
Ti	0.01	0.00	0.00	0.01	0.03	0.01	0.01	0.00	0.00	0.01
Fe^{3+}	0.86	1.06	0.83	0.85	1.19	0.85	0.83	0.82	0.85	1.11
∑Y	2.99	3.07	2.84	2.98	2.16	2.96	2.95	2.98	2.97	3.26
Mn	0.02	0.01	0.01	0.02	0.01	0.01	0.02	0.02	0.02	0.02
Mg	0.00	0.00	0.00	0.00	0.00	0.00	0.00	0.00	0.00	0.00
Ca	1.98	1.89	1.77	2.01	3.21	2.00	1.97	1.94	1.92	1.57
Na	0.00	0.00	0.14	0.00	0.00	0.00	0.01	0.00	0.01	0.01
K	0.00	0.00	0.01	0.00	0.00	0.00	0.00	0.00	0.00	0.00
Ba	0.00	0.00	0.00	0.00	0.00	0.00	0.00	0.00	0.00	0.00
Sr	0.02	0.02	0.01	0.01	0.01	0.02	0.02	0.02	0.04	0.01
∑X	2.01	1.93	1.92	2.03	3.22	2.03	2.01	1.98	1.99	1.60

A-in chloritised biotite, B-Magmatic, C-in saussuritised plagioclase

Appendix 5-7. Cont.
(KAS09 core depth 166.85-439.96).

Core depth [m]	KAS09 166.85 C	KAS09 187.75 A	KAS09 212.65 D	KAS09 241.22 D	KAS09 263.20 B	KAS09 263.20 B	KAS09 328.42 B	KAS09 340.30 B	KAS09 439.96 B
Wt. %									
SiO_2	38.6	37.2	36.4	36.8	37.6	36.9	37.2	37.0	36.6
TiO_2	nd	0.12	nd	0.04	0.06	0.04	0.07	0.13	0.07
Al_2O_3	23.4	23.0	21.6	22.2	23.1	22.6	23.9	22.5	22.8
Fe_2O_3	13.4	16.3	15.2	14.6	12.4	18.1	12.6	13.9	14.5
MnO	0.19	0.07	0.26	0.02	0.14	0.03	0.23	0.21	0.02
MgO	nd	0.01	nd	nd	nd	0.01	nd	0.01	nd
CaO	22.3	22.5	23.0	22.3	23.1	22.8	23.2	22.7	22.3
Na_2O	0.04	nd	0.02	0.01	0.01	nd	0.03	0.02	nd
K_2O	0.13	0.02	nd	nd	0.01	nd	0.05	0.01	nd
BaO		0.01	0.01	0.01	nd	nd		nd	0.01
SrO	0.31	nd	0.52	0.01	0.07	nd	0.31	0.01	nd
Total	96.8	99.23	97.01	95.99	96.49	100.48	96.14	96.49	96.3
Atom / Formula									
Si	3.05	2.95	2.97	3.00	3.03	2.91	2.98	3.00	2.97
Al^{iv}	0.00	0.05	0.03	0.00	0.00	0.09	0.02	0.00	0.03
∑Z	3.05	3.00	3.00	3.00	3.03	3.00	3.00	3.00	3.00
Al^{vi}	2.18	2.09	2.04	2.13	2.20	2.00	2.23	2.15	2.16
Ti	0.00	0.01	0.00	0.00	0.00	0.00	0.00	0.01	0.00
Fe^{3+}	0.80	0.97	0.93	0.90	0.75	1.07	0.76	0.85	0.89
∑Y	2.98	3.07	2.98	3.03	2.95	3.08	2.99	3.01	3.05
Mn	0.01	0.01	0.02	0.00	0.01	0.00	0.02	0.01	0.00
Mg	0.00	0.00	0.00	0.00	0.00	0.00	0.00	0.00	0.00
Ca	1.89	1.91	2.01	1.95	2.00	1.92	1.99	1.97	1.94
Na	0.01	0.00	0.00	0.00	0.00	0.00	0.01	0.00	0.00
K	0.01	0.00	0.00	0.00	0.00	0.00	0.01	0.00	0.00
Ba	0.00	0.00	0.00	0.00	0.00	0.00	0.00	0.00	0.00
Sr	0.01	0.00	0.03	0.00	0.00	0.00	0.01	0.00	0.00
∑X	1.94	1.92	2.06	1.95	2.01	1.93	2.03	1.99	1.94

A-in chloritised biotite, B-Magmatic, C-in saussuritised plagioclase

Appendix 5-8. KAS09 and KAS14. Electron microprobe analyses of prehnite (all iron is assumed to be as Fe_2O_3). The chemical formula is calculated based on 22 oxygen atoms. nd = not detected.
(KAS09 core depth 13.95-397.06, KAS14 core depth 76.23).

Core depth [m]	KAS09 13.95 A	KAS09 13.95 A	KAS09 77.70 A	KAS09 77.70 A	KAS09 332.85 A	KAS09 332.85 A	KAS09 397.06 C	KAS14 76.23 A	KAS14 76.23 A
Wt. %									
SiO_2	42.5	43.0	42.6	41.6	43.6	43.5	44.8	43.4	42.3
TiO_2	nd	0.12	nd	0.05	nd	0.02	0.01	0.02	0.07
Al_2O_3	23.7	20.6	22.4	20.0	23.8	19.1	23.6	22.1	19.7
Fe_2O_3	2.4	4.2	3.8	5.2	1.8	7.7	2.5	3.1	6.6
MnO	0.01	nd	nd	0.02	0.01	0.03	0.02	0.01	0.09
CaO	27.5	27.1	27.1	26.3	26.7	26.8	26.9	26.4	27.0
Na_2O	0.01	nd	0.05	0.10	nd	0.01	0.07	nd	0.03
K_2O	0.01	0.01	0.04	0.02	0.02	0.02	0.09	0.05	0.06
Total	96.13	95.03	95.99	93.29	95.93	97.18	97.99	95.08	95.85
Atom / Formula									
Si	5.88	6.05	5.92	5.99	6.00	6.05	6.04	6.05	5.96
Al^{iv}	0.12	0.00	0.08	0.01	0.00	0.00	0.00	0.00	0.04
∑Z	6.00	6.05	6.00	6.00	6.00	6.05	6.04	6.05	6.00
Al^{vi}	3.74	3.42	3.60	3.38	3.86	3.13	3.75	3.63	3.24
Ti	0.00	0.01	0.00	0.01	0.00	0.00	0.00	0.00	0.01
Fe^{3+}	0.25	0.45	0.40	0.56	0.19	0.81	0.25	0.33	0.70
Mn	0.00	0.00	0.00	0.00	0.00	0.00	0.00	0.00	0.01
∑Y	3.99	3.87	3.99	3.95	4.04	3.94	4.01	3.96	3.95
Ca	4.07	4.09	4.04	4.06	3.94	3.99	3.89	3.95	4.08
Na	0.00	0.00	0.01	0.03	0.00	0.00	0.02	0.00	0.01
K	0.00	0.00	0.01	0.00	0.00	0.00	0.02	0.01	0.01
∑X	4.08	4.09	4.06	4.09	3.94	4.00	3.92	3.95	4.10

A-Fracture-filling, B-In chloritised biotite, C- In K-feldspar

Appendix 5-9. KAS09, KAS14 and KA1131B. Electron microprobe analyses of pumpellyite (all iron is assumed to be as Fe_2O_3). The chemical formula is calculated based on 24.5 (O, OH). nd = not detected.
(KAS09 core depth 21.01-163.35).

Core depth [m]	KAS09 21.01	KAS09 21.01	KAS09 21.01	KAS09 21.01	KAS09 21.01	KAS09 44.85	KAS09 44.85	KAS09 94.6	KAS09 94.6	KAS09 94.6	KAS09 163.35
Wt. %											
SiO_2	36	36	36.1	35.1	35.8	36.0	36.1	36.0	36.2	35.4	35.6
TiO_2	0.17	0.19	0.11	0.1	0.15	0.18	0.14	0.12	0.10	0.13	0.14
Al_2O_3	15.1	17.8	15.9	12.3	16.3	13.6	17.0	14.2	16.2	11.8	12.6
Fe_2O_3	17.2	12.5	17	20.7	14.9	18.7	14.2	17.9	16.7	21.6	20.2
MnO	0.1	0.07	0.01	0.32	0.08	0.11	0.03	0.07	0.05	0.24	0.32
MgO	2.4	2.6	2.4	2.6	2.9	2.7	2.5	2.6	2.3	2.6	2.4
CaO	22.2	22.4	22	22	21.8	22.2	22.4	22.2	22.5	22.1	22.0
Na_2O	nd	0.11	0.01	0.08	0.04	0.02	nd	nd	0.01	nd	0.01
K_2O	nd	0.01	nd	0.03	7.5	nd	nd	nd	0.02	nd	nd
BaO	nd	nd	nd	nd	nd	nd	nd	nd	nd	nd	nd
SrO	0.11	nd	0.12	nd	nd	0.02	nd	nd	0.02	nd	0.01
Total	91.7	90.6	92.1	91	90.7	93.53	92.37	93.09	94.1	93.87	93.28
Atom / Formula											
Si	6.05	6.05	6.02	6.00	5.85	6.07	6.05	6.07	6.01	6.02	6.06
Al^{iv}	0.00	0.00	0.00	0.00	0.15	0.00	0.00	0.00	0.00	0.00	0.00
∑Z	6.05	6.05	6.02	6.00	6.00	6.07	6.05	6.07	6.01	6.02	6.06
Al^{vi}	2.99	3.52	3.13	2.48	2.98	2.70	3.36	2.82	3.17	2.37	2.53
Ti	0.02	0.02	0.01	0.01	0.02	0.02	0.02	0.02	0.01	0.02	0.02
Fe^{3+}	2.17	1.58	2.13	2.66	1.83	2.37	1.79	2.27	2.09	2.77	2.59
∑Y	5.19	5.13	5.27	5.16	4.83	5.10	5.17	5.11	5.27	5.15	5.13
Mn	0.01	0.01	0.00	0.05	0.01	0.02	0.00	0.01	0.01	0.04	0.05
Mg	0.60	0.65	0.60	0.66	0.71	0.68	0.62	0.65	0.57	0.66	0.61
Ca	4.00	4.03	3.93	4.03	3.81	4.01	4.02	4.01	4.00	4.03	4.01
Na	0.00	0.04	0.00	0.03	0.01	0.01	0.00	0.00	0.00	0.00	0.00
K	0.00	0.00	0.00	0.01	1.56	0.00	0.00	0.00	0.00	0.00	0.00
Ba	0.00	0.00	0.00	0.00	0.00	0.00	0.00	0.00	0.00	0.00	0.00
Sr	0.01	0.00	0.01	0.00	0.00	0.00	0.00	0.00	0.00	0.00	0.00
∑X	4.62	4.73	4.54	4.77	6.11	4.71	4.65	4.68	4.59	4.72	4.67

Appendix 5-9. Cont.
(KAS09 core depth 163.35-397.06).

Core depth [m]	KAS09 163.35	KAS09 163.35	KAS09 253.5	KAS09 253.5	KAS09 311.17	KAS09 311.17	KAS09 357.63	KAS09 357.63	KAS09 357.63	KAS09 397.06
Wt. %										
SiO_2	36.1	36.2	35.7	36.1	36.2	36.1	35.6	36.1	36.0	35.2
TiO_2	0.15	0.11	0.20	0.12	0.13	0.16	0.14	0.14	0.12	0.11
Al_2O_3	18.0	15.7	13.1	18.2	15.2	17.9	15.3	13.7	17.5	12.4
Fe_2O_3	12.9	17.2	19.7	13.0	17.4	14.8	16.8	19.2	12.3	19.6
MnO	0.03	0.04	0.23	0.04	0.10	0.09	0.11	0.28	0.02	0.21
MgO	2.6	2.4	2.6	2.6	2.6	2.3	2.5	2.5	2.6	2.5
CaO	22.1	22.4	22.0	22.3	22.0	22.3	22.1	22.0	22.4	22.4
Na_2O	nd	0.02	0.01	nd	0.01	0.02	nd	0.07	0.03	0.03
K_2O	nd	nd	0.01	0.03	nd	0.01	nd	0.04	0.03	0.02
BaO	nd	nd	0.01	nd	nd	nd	nd	nd	0.02	nd
SrO	0.03	nd	nd	nd	0.01	0.02	0.07	nd	0.02	nd
Total	91.91	94.07	93.56	92.39	93.65	93.7	92.62	94.03	91.04	92.47
Atom / Formula										
Si	6.04	6.02	6.04	6.02	6.05	5.97	6.02	6.06	6.08	6.05
Al^{iv}	0.00	0.00	0.00	0.00	0.00	0.03	0.00	0.00	0.00	0.00
∑Z	6.04	6.02	6.04	6.02	6.05	6.00	6.02	6.06	6.08	6.05
Al^{vi}	3.55	3.08	2.61	3.57	2.99	3.45	3.05	2.71	3.49	2.51
Ti	0.02	0.01	0.03	0.02	0.02	0.02	0.02	0.02	0.02	0.01
Fe^{3+}	1.63	2.15	2.51	1.63	2.19	1.84	2.14	2.43	1.56	2.54
∑Y	5.19	5.24	5.15	5.22	5.20	5.32	5.20	5.16	5.07	5.06
Mn	0.00	0.01	0.03	0.01	0.01	0.01	0.02	0.04	0.00	0.03
Mg	0.65	0.60	0.66	0.65	0.65	0.57	0.63	0.63	0.66	0.64
Ca	3.96	3.99	3.99	3.98	3.94	3.95	4.00	3.96	4.06	4.13
Na	0.00	0.01	0.00	0.00	0.00	0.01	0.00	0.02	0.01	0.01
K	0.00	0.00	0.00	0.01	0.00	0.00	0.00	0.01	0.01	0.00
Ba	0.00	0.00	0.00	0.00	0.00	0.00	0.00	0.00	0.00	0.00
Sr	0.00	0.00	0.00	0.00	0.00	0.00	0.01	0.00	0.00	0.00
∑X	4.62	4.60	4.68	4.64	4.60	4.54	4.66	4.66	4.73	4.81

Appendix 5-9. Cont.
(KAS09 core depth 397.06-429.44, KAS14 core depth 153.3, KA1131B core depth 29.55).

Core depth [m]	KAS09 397.06	KAS09 397.06	KAS09 397.06	KAS09 417.8	KAS09 417.8	KAS09 429.44	KAS09 429.44	KAS14 153.3	KAS14 153.3	KA1131B 29.55
Wt. %										
SiO_2	36.0	36.9	36.2	35.8	36.1	36.0	35.9	35.9	36.0	52.2
TiO_2	0.15	nd	0.03	0.11	0.14	0.13	0.09	0.17	0.19	nd
Al_2O_3	17.5	22.7	16.8	17.4	14.9	18.1	12.6	16.2	19.1	25.1
Fe_2O_3	12.3	6.5	15.0	14.2	17.3	12.6	20.7	14.8	11.7	3.6
MnO	0.02	0.15	0.07	0.03	0.16	0.02	0.03	0.04	0.02	nd
MgO	2.6	3.3	2.5	2.6	2.4	2.5	2.6	2.5	2.8	2.9
CaO	22.3	23.3	22.3	22.4	22.3	22.1	22.0	22.1	22.2	1.2
Na_2O	nd	0.03	0.01	0.04	nd	0.02	nd	0.02	nd	nd
K_2O	nd	nd	0.01	nd	nd	0.01	0.01	nd	0.02	6.6
BaO	nd	nd	0.02	nd	nd	0.03	0.02	0.04	nd	nd
SrO	nd	nd	nd	0.02	nd	0.01	nd	nd	nd	0.09
Total	90.87	92.88	92.94	92.6	93.3	91.52	93.95	91.77	92.03	91.7
Atom / Formula										
Si	6.09	5.98	6.04	5.99	6.06	6.05	6.06	6.07	5.99	7.86
Al^{iv}	0.00	0.03	0.00	0.01	0.00	0.00	0.00	0.00	0.01	0.00
∑Z	6.09	6.00	6.04	6.00	6.06	6.05	6.06	6.07	6.00	7.86
Al^{vi}	3.49	4.31	3.31	3.42	2.95	3.58	2.51	3.23	3.74	4.45
Ti	0.02	0.00	0.00	0.01	0.02	0.02	0.01	0.02	0.02	0.00
Fe^{3+}	1.57	0.79	1.88	1.79	2.19	1.59	2.63	1.88	1.47	0.41
∑Y	5.07	5.10	5.19	5.22	5.15	5.19	5.15	5.13	5.23	4.86
Mn	0.00	0.02	0.01	0.00	0.02	0.00	0.00	0.01	0.00	0.00
Mg	0.66	0.80	0.62	0.65	0.60	0.63	0.66	0.63	0.70	0.65
Ca	4.04	4.04	3.99	4.01	4.01	3.98	3.98	4.00	3.96	0.19
Na	0.00	0.01	0.00	0.01	0.00	0.01	0.00	0.01	0.00	0.00
K	0.00	0.00	0.00	0.00	0.00	0.00	0.00	0.00	0.00	1.27
Ba	0.00	0.00	0.00	0.00	0.00	0.00	0.00	0.00	0.00	0.00
Sr	0.00	0.00	0.00	0.00	0.00	0.00	0.00	0.00	0.00	0.01
∑X	4.70	4.87	4.63	4.68	4.64	4.62	4.64	4.65	4.66	2.12

Appendix 5-10. KAS09 and KAS14. Electron microprobe analyses of the various types of chlorite and berthierine (all iron is assumed to be as FeO). The chemical formula is calculated based on 28 (O, OH). We are aware though of the fact that berthierine is a 7Å-clay mineral. Assuming 28 (O, OH) for both berthierine and chlorite allows a direct comparison of their chemical composition, and display better the chemical transition of Fe-chlorite into berthierine. nd = not detected.
(KAS09 core depth 20.67-23.55).

Core depth [m]	KAS09 20.67 A	KAS09 21.01 A	KAS09 21.01 A	KAS09 21.01 A	KAS09 21.01 A	KAS09 21.01 A	KAS09 23.55 C	KAS09 23.55 BER	KAS09 23.55 BER	KAS09 23.55 BER
Wt. %										
SiO_2	30.4	30.4	28.2	27.9	29.9	30.1	28.4	27.2	28.6	29.4
TiO_2	0.38	0.08	nd	0.03	0.11	0.04	nd	0.02	0.04	0.02
Al_2O_3	15	15.5	17.2	16.8	14.8	15.2	15.1	11.3	10.9	11.7
FeO	21.4	21.6	23.2	23.4	21.7	22.4	27.8	46.1	44.2	41.4
MnO	0.4	0.38	0.47	0.49	0.43	0.4	0.82	0.48	0.5	0.41
MgO	18.1	19.7	18.2	18.2	18.8	15.2	13.8	1.9	2.7	3.4
CaO	0.06	0.15	0.11	0.07	0.15	0.09	0.23	0.35	0.39	1.1
Na_2O	nd	nd	nd	0.09	nd	nd	0.05	0.1	0.09	0.1
K_2O	0.66	0.11	0.08	nd	0.08	0.09	0.01	0.04	0.09	0.11
Total	86.8	87.9	87.6	86.8	86	87.1	86.1	87.4	87.5	87.4
Atom / Formula										
Si	6.37	6.25	5.90	5.88	6.30	6.53	6.20	6.53	6.76	6.81
Al^{iv}	1.63	1.76	2.10	2.12	1.70	1.47	1.80	1.47	1.24	1.19
∑Z	8.00	8.00	8.00	8.00	8.00	8.00	8.00	8.00	8.00	8.00
Al^{iv}	2.08	2.00	2.14	2.06	1.98	2.42	2.08	1.72	1.79	2.00
Ti	0.06	0.01	0.00	0.01	0.02	0.01	0.00	0.00	0.01	0.00
Fe^{2+}	3.75	3.71	4.06	4.13	3.82	4.07	5.07	9.25	8.73	8.02
Mn	0.07	0.07	0.08	0.09	0.08	0.07	0.15	0.10	0.10	0.08
Mg	5.66	6.03	5.67	5.72	5.91	4.92	4.49	0.68	0.95	1.17
Ca	0.01	0.03	0.03	0.02	0.03	0.02	0.05	0.09	0.10	0.27
Na	0.00	0.00	0.00	0.04	0.00	0.00	0.02	0.05	0.04	0.05
K	0.18	0.03	0.02	0.00	0.02	0.03	0.00	0.01	0.03	0.03
∑W,X,Y	11.81	11.88	12.00	12.05	11.86	11.53	11.87	11.90	11.75	11.63

A-Psuedomorphically chloritised biotite, B-Microcrystalline chlorite replacing biotite, C-Microcrystalline void/fracture-filling, BER-Berthierine replacing biotite and magnetite

Appendix 5-10. Cont.
(KAS09 core depth 77.70-123.80).

Core depth [m]	KAS09 77.70 A	KAS09 120.09 B	KAS09 120.09 A	KAS09 120.09 A	KAS09 120.09 A	KAS09 120.09 C	KAS09 120.09 A	KAS09 120.09 BER	KAS09 123.80 BER	KAS09 123.80 C
Wt. %										
SiO_2	31.4	35.7	30.9	29	28.8	30.8	33.1	29.4	25.5	28.6
TiO_2	0.03	0.03	nd	0.03	0.12	0.17	0.01	0.02	nd	0.08
Al_2O_3	15.6	16.5	16.7	16.7	16.3	16.2	17	11.7	14.8	15.4
FeO	17.2	15.5	22.1	23.2	23.1	28.4	23.1	44.4	41.1	30.8
MnO	0.41	0.64	0.48	0.52	0.51	0.96	0.91	0.41	0.32	0.36
MgO	17.6	17.9	17.9	17.8	17.4	13.6	18.1	3.4	4.4	9.1
CaO	0.22	0.86	0.29	0.11	0.21	0.43	0.47	1.1	0.37	0.56
Na_2O	nd	nd	nd	nd	nd	nd	0.09	0.11	nd	0.05
K_2O	0.09	0.73	0.09	nd	0.12	0.04	0.08	0.12	0.01	0.21
Total	85.6	88.2	88.5	87.3	86.5	89.8	86.8	86	87.1	89.8
Atom / Formula										
Si	6.68	7.03	6.30	6.06	6.08	6.35	6.44	6.67	6.01	6.41
Al^{iv}	1.32	0.97	1.70	1.94	1.92	1.65	1.56	1.33	1.99	1.59
∑Z	8.00	8.00	8.00	8.00	8.00	8.00	8.00	8.00	8.00	8.00
Al^{iv}	2.59	2.86	2.32	2.17	2.14	2.29	2.33	1.80	2.12	2.48
Ti	0.01	0.00	0.00	0.01	0.02	0.03	0.00	0.00	0.00	0.01
Fe^{2+}	3.06	2.55	3.77	4.05	4.08	4.90	3.76	8.42	8.10	5.77
Mn	0.07	0.11	0.08	0.09	0.09	0.17	0.15	0.08	0.06	0.07
Mg	5.58	5.26	5.44	5.54	5.48	4.18	5.25	1.15	1.55	3.04
Ca	0.05	0.18	0.06	0.03	0.05	0.10	0.10	0.27	0.09	0.13
Na	0.00	0.00	0.00	0.00	0.00	0.00	0.03	0.05	0.00	0.02
K	0.02	0.18	0.02	0.00	0.03	0.01	0.02	0.04	0.00	0.06
∑W,X,Y	11.38	11.14	11.70	11.88	11.89	11.66	11.64	11.80	11.93	11.59

A-Psuedomorphically chloritised biotite, B-Microcrystalline chlorite replacing biotite, C-Microcrystalline void/fracture-filling, BER-Berthierine replacing biotite and magnetite

Appendix 5-10. Cont.
(KAS09 core depth 123.80-397.06, KAS14 core depth 11.55-165.80).

Core depth [m]	KAS09 123.80 C	KAS09 328.42 A	KAS09 397.06 A	KAS09 397.06 A	KAS09 397.06 A	KAS14 11.55 B	KAS14 165.80 A	KAS14 165.80 A	KAS14 165.80 A	KAS14 165.80 A
Wt. %										
SiO_2	25.7	29.7	29.5	28.8	28.5	33.2	31.8	28.8	29.3	27.1
TiO_2	0.01	0.03	0.03	0.01	0.06	0.05	0.01	0.07	0.11	0.26
Al_2O_3	17.6	16.4	17.1	16.4	16	16.4	13.8	16.8	17.9	17.8
FeO	30.6	22.2	22.6	21.9	22.7	17.4	22.5	23.4	22.9	24.3
MnO	0.67	0.6	0.58	0.63	0.57	0.41	0.36	0.43	0.36	0.41
MgO	11.7	19	19	18.4	18.4	21.9	17.2	18.3	18.6	17.2
CaO	nd	0.1	0.09	0.15	0.07	0.21	0.58	0.13	0.39	0.19
Na_2O	0.04	nd	0.06	nd	nd	nd	nd	nd	0.05	nd
K_2O	nd	0.01	nd	0.03	0.03	0.03	0.02	0.01	0.23	0.01
Total	87.5	89.1	86.1	86.8	87.4	89.1	86.27	89.8	87.5	86.1
Atom / Formula										
Si	5.70	6.12	6.02	6.06	6.03	6.49	6.67	5.98	5.94	5.72
Al^{iv}	2.30	1.88	1.98	1.94	1.97	1.51	1.33	2.02	2.06	2.28
∑Z	8.00	8.00	8.00	8.00	8.00	8.00	8.00	8.00	8.00	8.00
Al^{iv}	2.31	2.10	2.14	2.13	2.02	2.27	2.09	2.10	2.21	2.15
Ti	0.00	0.01	0.01	0.00	0.01	0.01	0.00	0.01	0.02	0.04
Fe^{2+}	5.68	3.82	3.86	3.85	4.02	2.84	3.95	4.07	3.88	4.29
Mn	0.13	0.11	0.10	0.11	0.10	0.07	0.06	0.08	0.06	0.07
Mg	3.87	5.83	5.78	5.77	5.80	6.38	5.38	5.67	5.62	5.42
Ca	0.00	0.02	0.02	0.03	0.02	0.04	0.13	0.03	0.09	0.04
Na	0.02	0.00	0.02	0.00	0.00	0.00	0.00	0.00	0.02	0.00
K	0.00	0.00	0.00	0.01	0.01	0.01	0.01	0.00	0.06	0.00
∑W,X,Y	12.00	11.89	11.93	11.91	11.97	11.62	11.62	11.95	11.95	12.02

A-Psuedomorphically chloritised biotite, B-Microcrystalline chlorite replacing biotite, C-Microcrystalline void/fracture-filling, BER-Berthierine replacing biotite and magnetite

Appendix 5-11. KAS09. Electron microprobe analyses of illite/vermiculite (all iron is assumed to be as Fe_2O_3). The chemical formula is calculated based on 24 (O, OH). nd = not detected. (KAS09 core depth 21.01-397.06).

Core depth [m]	KAS09 21.01	KAS09 21.01	KAS09 23.55	KAS09 39.70	KAS09 120.09	KAS09 397.06	KAS09 397.06	KAS09 397.06	KAS09 397.06	KAS09 397.06
Wt. %										
SiO_2	45.6	42.9	38.2	39.9	43.6	48.8	52.9	48.7	47.6	45.6
TiO_2	0.07	0.06	0.19	nd	0.01	0.04	0.01	0.09	0.04	0.03
Al_2O_3	19.8	18.9	15.3	14	19	22.6	21.7	21.6	22.5	20
Fe_2O_3	12	13.3	22.4	15.6	14.9	6.8	3.3	6.7	6.6	6.3
MnO	0.3	0.34	0.29	0.55	0.5	0.23	0.09	0.2	0.31	0.28
MgO	11.5	12.8	12.3	18	10	12.7	6.2	11.4	11.8	10.2
CaO	0.93	0.91	0.83	0.91	0.79	1.2	0.34	0.91	0.86	1.2
Na_2O	0.02	nd	0.09	0.09	nd	0.04	nd	0.02	0.07	nd
K_2O	2.9	2.5	2.8	1.6	3.3	3.5	7.4	4.4	3.9	4.1
Total	92.2	90.6	91.8	92.4	90.8	91.7	90.8	92.2	90.6	91.8
Atom / Formula										
Si	6.27	6.04	5.59	5.79	6.15	6.39	7.17	6.52	6.39	6.55
Al^{iv}	1.74	1.96	2.41	2.21	1.85	1.61	0.83	1.48	1.61	1.45
∑Z	8.00	8.00	8.00	8.00	8.00	8.00	8.00	8.00	8.00	8.00
Al^{vi}	1.47	1.18	0.23	0.19	1.31	1.88	2.64	1.93	1.95	1.94
Ti	0.01	0.01	0.02	0.00	0.00	0.00	0.00	0.01	0.00	0.00
Fe^{3+}	1.24	1.41	2.47	1.70	1.58	0.67	0.34	0.68	0.67	0.68
Mn	0.04	0.04	0.04	0.07	0.06	0.03	0.01	0.02	0.04	0.03
Mg	2.36	2.69	2.68	3.90	2.10	2.48	1.25	2.28	2.36	2.19
∑X,Y	5.11	5.32	5.43	5.86	5.06	5.06	4.24	4.92	5.02	4.85
Ca	0.14	0.14	0.13	0.14	0.12	0.17	0.05	0.13	0.12	0.19
Na	0.01	0.00	0.03	0.03	0.00	0.01	0.00	0.01	0.02	0.00
K	0.51	0.45	0.52	0.30	0.59	0.59	1.28	0.75	0.67	0.75
∑W	0.65	0.59	0.68	0.46	0.71	0.76	1.33	0.89	0.81	0.94

Appendix 6-1. Correlation matrix for minerals from KAS-09. Argillised grains include mainly fine-crystalline chlorite completely replacing biotite.

	Chloritised biotite	Argillised grains	Secondary chlorite	Total epidote	Sauss./alb. plagioc.	Calcite	Titanite	Altered titanite	Secondary quartz	K-feldspar	Prehnite	Pumpellyite	Primary quartz	K-feld./perthite	Plagioclase	Biotite	Amphibole	Muscovite	Magnetite	Hematite	Pyrite	Fluorite/apatite	Voids/fractures
Chloritised biotite	1.00																						
Argillised grains	0.09	1.00																					
Secondary chlorite	0.02	0.33	1.00																				
Total epidote	0.17	0.16	0.27	1.00																			
Sauss./alb. plagioc.	0.40	0.03	0.21	-0.06	1.00																		
Calcite	0.10	0.10	0.14	0.21	0.01	1.00																	
Titanite	-0.05	-0.02	-0.03	-0.01	0.09	-0.11	1.00																
Altered titanite	0.12	0.21	0.50	0.22	0.17	0.00	-0.17	1.00															
Secondary quartz	0.06	0.01	0.43	0.32	-0.03	0.15	0.02	0.24	1.00														
K-feldspar	0.00	-0.08	0.13	0.17	-0.10	0.17	-0.21	0.07	0.46	1.00													
Prehnite	0.09	0.09	-0.03	0.27	0.03	0.24	-0.07	0.07	0.07	0.34	1.00												
Pumpellyite	0.03	-0.04	-0.07	-0.01	-0.04	0.04	-0.03	-0.06	-0.08	-0.07	-0.04	1.00											
Primary quartz	-0.38	-0.26	-0.27	-0.41	-0.31	-0.22	-0.35	-0.24	-0.17	0.07	-0.17	-0.15	1.00										
K-feld./perthite	-0.26	-0.21	-0.22	-0.25	-0.29	-0.15	-0.39	-0.21	-0.28	-0.06	-0.11	-0.01	0.45	1.00									
Plagioclase	-0.23	-0.07	-0.22	-0.13	-0.47	-0.14	0.22	-0.10	-0.06	-0.07	-0.05	-0.01	-0.12	-0.29	1.00								
Biotite	-0.11	-0.15	-0.38	-0.05	-0.24	-0.09	0.46	-0.21	-0.13	-0.19	-0.13	-0.06	-0.27	-0.38	0.43	1.00							
Amphibole	0.03	0.11	-0.15	-0.05	-0.22	-0.12	0.37	-0.04	-0.13	-0.20	-0.03	-0.06	-0.32	-0.18	0.19	0.43	1.00						
Muscovite	-0.07	-0.06	0.22	-0.12	-0.03	0.57	-0.13	-0.05	0.16	0.07	-0.08	0.12	0.08	0.02	-0.15	-0.20	-0.15	1.00					
Magnetite	-0.15	0.06	-0.08	-0.04	-0.16	-0.05	0.40	-0.04	-0.13	-0.12	-0.03	-0.06	-0.20	-0.17	0.10	0.35	0.60	-0.04	1.00				
Hematite	0.08	0.06	0.22	0.00	0.10	0.21	-0.19	0.30	0.22	0.02	-0.07	-0.05	-0.03	-0.01	-0.18	-0.25	-0.10	0.07	-0.12	1.00			
Pyrite	0.06	0.00	0.07	0.01	0.08	0.02	0.07	-0.01	0.09	-0.02	-0.04	0.00	-0.12	-0.05	-0.02	0.06	0.00	-0.01	-0.04	-0.05	1.00		
Fluorite/apatite	-0.10	-0.09	-0.10	-0.03	-0.03	-0.10	0.18	0.01	-0.14	-0.12	-0.08	-0.05	-0.09	-0.05	-0.05	0.28	0.31	-0.11	0.40	-0.11	-0.07	1.00	
Voids/fractures	0.11	0.11	0.10	-0.06	0.05	0.43	-0.04	0.11	0.11	-0.01	0.00	-0.02	-0.10	-0.10	-0.04	-0.12	-0.07	0.23	-0.06	0.51	-0.03	-0.06	1.00

Appendix 6-2. Correlation matrix for minerals from KAS-14. Argillised grains include mainly fine-crystalline chlorite completely replacing biotite.

	Chloritised biotite	Argillised grains	Secondary chlorite	Total epidote	Sauss./alb. plagioc.	Calcite	Titanite	Altered titanite	Secondary quartz	K-feldspar	Prehnite	Pumpellyite	Primary quartz	K-feld./perthite	Plagioclase	Biotite	Amphibole	Muscovite	Magnetite	Hematite	Pyrite	Fluorite/apatite	Voids/fractures
Chloritised biotite	1.00																						
Argillised grains	-0.27	1.00																					
Secondary chlorite	-0.35	0.52	1.00																				
Total epidote	0.00	0.31	0.61	1.00																			
Sauss./alb. plagioc.	0.40	0.13	0.29	0.38	1.00																		
Calcite	-0.04	0.23	0.22	0.06	0.07	1.00																	
Titanite	-0.05	0.29	0.26	0.39	0.24	-0.13	1.00																
Altered titanite	-0.01	0.17	0.37	0.01	0.16	-0.19	0.09	1.00															
Secondary quartz	0.21	0.00	0.17	0.14	0.02	0.09	-0.34	0.22	1.00														
K-feldspar	0.54	-0.10	-0.08	-0.03	0.25	0.05	-0.34	0.29	0.77	1.00													
Prehnite	-0.11	0.00	0.13	0.10	-0.27	-0.01	-0.23	0.01	0.05	0.04	1.00												
Pumpellyite	-0.17	0.30	0.27	0.05	0.13	-0.06	0.18	0.65	-0.07	-0.06	-0.09	1.00											
Primary quartz	-0.06	-0.20	-0.36	-0.54	-0.41	-0.16	-0.30	0.16	0.02	-0.07	-0.28	-0.04	1.00										
K-feld./perthite	0.15	-0.31	-0.33	-0.52	-0.41	0.03	-0.61	0.03	0.09	0.18	0.12	-0.17	0.51	1.00									
Plagioclase	-0.32	-0.24	-0.36	-0.23	-0.59	-0.12	-0.01	-0.40	-0.24	-0.28	0.29	-0.25	-0.22	-0.14	1.00								
Biotite	-0.03	-0.31	-0.60	-0.21	-0.23	-0.17	0.14	-0.54	-0.35	-0.34	-0.24	-0.15	-0.09	-0.28	0.52	1.00							
Amphibole	-0.20	-0.24	-0.29	-0.35	-0.28	-0.16	0.28	-0.24	-0.18	-0.19	-0.10	-0.06	-0.04	-0.07	0.39	0.44	1.00						
Muscovite	-0.27	-0.11	0.01	-0.24	-0.29	-0.15	-0.29	0.16	-0.22	-0.22	0.06	0.31	0.36	0.38	0.02	-0.24	-0.09	1.00					
Magnetite	-0.17	0.36	0.17	-0.07	0.14	-0.09	0.08	-0.09	-0.11	-0.05	-0.19	-0.14	-0.16	-0.22	0.07	0.02	-0.02	-0.20	1.00				
Hematite	0.44	-0.25	-0.13	-0.01	0.23	-0.12	-0.15	-0.08	0.05	0.26	0.19	-0.09	-0.17	0.08	-0.07	-0.07	-0.12	0.02	-0.26	1.00			
Pyrite	-0.24	0.26	0.28	-0.06	0.05	0.44	0.11	0.37	-0.15	-0.14	-0.06	0.71	-0.05	0.06	-0.21	-0.22	-0.08	0.19	-0.15	-0.07	1.00		
Fluorite/apatite	-0.18	0.28	0.17	0.09	0.26	0.10	0.41	-0.14	-0.27	-0.23	-0.18	-0.11	-0.16	-0.26	-0.10	0.04	0.09	-0.17	0.39	-0.26	-0.01	1.00	
Voids/fractures	-0.01	0.09	0.01	0.09	-0.25	-0.06	-0.05	0.19	0.10	0.10	0.74	-0.03	-0.21	0.17	0.16	-0.15	-0.06	-0.06	-0.14	-0.09	-0.05	-0.11	1.00

Appendix 8-9A. KAS09 and KAS14. Carbon, oxygen and strontium isotopic values of calcite obtained at various depths from the two drill cores studied. The precipitation temperatures of calcite are calculated based on the fractionation equation of Friedman and O'Neil (1977) and assuming that the $\delta^{18}O_{SMOW}$ value of water varied between -6‰ and -1‰.

Borehole	Depth [m]	$\delta^{13}C_{PDB}$ [‰]	$\delta^{18}O_{PDB}$ [‰]	T°C [$\delta^{18}O_{SMOW}$ =-1‰]	T°C [$\delta^{18}O_{SMOW}$ =-6‰]	$^{87}Sr/^{86}Sr$
KAS-09	9.54	-5.2	-7.1	45	19	0.714421
	99.72	-20.1	-7.6	48	22	0.715361
	112.70	-12.9	-12.8	85	50	0.715850
	137.40	-7.1	-13.8	94	57	0.714975
	141.10	-20.8	-8.8	56	28	0.716136
	146.10	1.4	-7.9	50	23	0.713821
	164.84	-6.4	-7.9	50	23	0.717004
	254.45	-4.3	-18.2	143	90	0.716766
	268.10	-6.4	-9.4	60	31	0.717091
	410.90	-4	-15.3	109	67	0.716558
KAS-14	92.64	-6	-8.2	51	24	0.715437
	99.23	-30.1	-8.1	51	24	0.714763
	144.35	-8.5	-7	45	19	0.716170
	155.00	-14.4	-7.3	46	19	0.716105
	204.50	-4.7	-8	50	23	0.716901